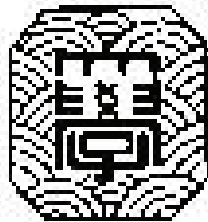


**A STUDY ON PERFORMANCE EVALUATION OF LOCALLY
CORRODED STEEL PLATE GIRDER BRIDGE ENDS**

局部腐食した鋼プレートガーダー端部の性能評価に関する研究

NAUMAN KHURRAM

A Dissertation Submitted in Partial Fulfillment of the
Requirements for the Degree of
Doctor of Philosophy



Department of Civil Engineering
YOKOHAMA NATIONAL UNIVERSITY, JAPAN
September, 2012

ABSTRACT

Many field inspections and steel bridge surveys report that steel plate girder bridges are more susceptible to corrode at the end due to the accumulation of the water at bearing region. This water pools at the bearing is the result of rain shower and water leakage from the construction joints, which cause the corrosion of bearing stiffener and nearby web. The statistical data shows that only in Japan in more than 70% corroded steel bridges, corrosion was found near the girder ends, which is primarily due to very aggressive environmental and severe topographical conditions of Japan (Chapter 2). Corrosion at plate girder ends damages the bearing stiffener and nearby web locally and in most of the cases rest of the girder part remains intact. Bearing stiffeners have a very important role in resisting the compressive load. Moreover, besides resisting the compressive load bearing stiffeners are also designed as anchor to balance the horizontal component of tension field action developed in the exterior web and resist the moment transferred by the in plane bending. Thus, any significant damage on bearing stiffener and nearby web may cause the buckling/crushing near the bearing and may also cause a significant loss in the bearing and shear capacity. Further, some field inspection data regarding the steel bridge damages was also collected from the Pakistan (Chapter 3) to assess the feasibility of required action to deal with these steel bridges. The inspection data also depicts the similar plate girder ends damages as reported in Japan.

As number old of steel bridges are increasing day by day in Japan and all around the world and it is very difficult to replace the all old bridges at the same time along with the construction of the new bridges due to many constraints, *i.e.* economy of the country, traffic switching problem, lack of expertise and resources, manpower and machinery etc. Moreover, many bridges may have the adequate capacity to be used (Chapter 1). Therefore, all the corroded and old bridges demand the proper evaluation to assess their current performance level *e.g.* residual bearing and shear capacity so that suitable measure regarding the repair, retrofitting or replacement of these steel bridges can be adopted. The present study focuses

on the experimental and analytical evaluation of bearing and shear capacity of corroded bridges affected by the end panel corrosion.

The chapter 4 discusses the experimental program conducted on the large scale plate girder ends specimens, simulated with local corrosion damage on the bearing stiffener. In all, total five plate girder end specimens were used. On one specimen no damage is considered and regarded as the healthy specimen and on the rest of two pair, 50% thickness of the bearing stiffener is reduced within the damage height " D_h " of 20mm and 60mm uniformly and non-uniformly starting from the top face of the bottom flange near the weld seam. The study reported that 20mm damage height does not change either the ultimate capacity or buckling failure mode. However, a relatively large damage of 60mm shift the buckling of the stiffener within the damage zones along with the normal buckling within the normal web buckling.

The chapter 5 deals with the extension of study to evaluate the bearing capacity of the plate girder ends analytically. For this purpose the test results obtained through the experimental program (conducted and mention in chapter 4) are modeled in a powerful finite element (FE) software ABAQUS. The comparison of the experimental and analytical results are made in term of the load-displacement relationships and deformed buckling modes and analytical results show the good agreement. Four various damage groups, Stiffener damage only, stiffener damage plus the free web end damage, stiffener damage plus interior web damage and stiffener damage plus the web damage at both side of the bearing stiffener were considered in the analytical program. Various residual thicknesses *i.e.* 75%, 50% and 25 etc. were assumed within the different damage heights zones. As the study is targeted to study the effect of the local damage, the maximum damage height is considered as 100mm (10% of girder height). True stress-strain relationships are determined by performing the tension test on the coupon cut from the used specimens with isotropic strain hardening rule are utilized in the analytical study. Initial deflections and welding residual stresses are also considered in the finite element (FE) study. Many trial analyses with different damage shapes and forms suggest that a simple uniform rectangular type of the damage with minimum thickness can be utilized in the FE simulation. Further, analytical results conclude that bearing stiffener has very important role in resisting the bearing load and any severe damage may reduce its radius

of gyration along the weak axis which may give rise to the stability problem by causing the buckling/ crippling failure at bearing. The results also revealed that the web damage alone does not affect the load carrying capacity significantly however; it reduces the load carrying capacity substantially when web damage is combined with the stiffener damage.

The Chapter 6 describes the effect of local corrosion damages at the girder end on its shear capacity. An extensive analytical study is conducted on a four panel plate girder model and similar damage cases are assumed as considered (in Chapter 5) for the bearing capacity analysis. A mild steel with yield stresses equal to 345Mpa with elastics perfectly plastics (EPP) characteristics under kinematics plasticity rule is used. A small initial out-of-plane deflection is also incorporated while; no residual stresses are considered in the study as they have no effect on the shear capacity. Analytical results indicate that a loss of the bearing stiffener more than 50% can be fatal for the plate girder and it reduces the anchorage for the tension field action and thus refrains the girder to achieve its full post buckling strength. Also, complete loss of stiffener thickness shifts the failure mode of the girder from shear to buckling.

The Chapter 7 comprises of some proposed empirical relationships to estimate ultimate capacity under the shear and compressive loads application. This section also discusses a proposed damage parameter named the “*Reduced Thickness Ratio*” to assess the buckling failure mode of the plate girder specimen under compressive load

Finally, Chapter 8 consists of a summary of conclusions and recommendations that are drawn from the above mentioned work. Subsequently some recommendations are also made for future research.

ACKNOWLEDGEMENT

All thanks and gratitude to almighty Allah, the most gracious, most merciful and most beneficent, Who enabled me to complete this thesis.

I would like to express sincere and heartiest thanks to my thesis supervisors; Prof. Dr. Katsuchi HIROSHI, Assoc. Prof. Dr Eiichi SASAKI and Prof. Dr. Hitoshi YAMADA for their encouragement, kind guidance, valuable suggestions and keen supervision throughout this project. Great appreciation is expressed for the members of examination committee, Prof. Tatsuya TSUBAKI and Assoc. Prof. Nishio MAYUKO for their contribution in reviewing this research work.

I am also very thankful to the faculty members of the Department of Civil Engineering, Yokohama National University for giving me this opportunity to pursue my doctoral study in the most amiable environment, and Mrs. Yurie HONJO, Japanese language teacher, for her undaunted effort in helping me to get acquainted with the life in Japan.

I would also like to extend my heartiest gratitude to Dr. Kazuhiko HAYASHI, Concrete Laboratory, Yokohama National University his kind help and guidance during the experimental phase of this work. The author also acknowledges the friends and lab colleagues for their devoted cooperation and help at every practical phase of this research work.

And last but not the least; I would like to thank Ministry of Education, Culture and Sports Science and Technology, JAPAN for providing me the opportunity to come to Japan and conduct this research work. This work would not have been possible without their support and cooperation.

Acknowledgements are incomplete without mentioning the immense motivation, sacrifices and the prayers of my parents that enabled me to reach the completion stage of this study.

*To my beloved parents and respectable teachers and
especially to my grandmother*

TABLE OF CONTENTS

ABSTRACT	I
ACKNOWLEDGEMENT	IV
LIST OF FIGURES	XI
LIST OF TABLES	XV
LIST OF NOTATIONS	XVI
1 INTRODUCTION	1
1.1 GENERAL.....	1
1.2 BACK GROUND.....	1
1.3 STRUCTURAL EFFECT OF CORROSION	3
1.3.1 <i>Effect on Bearing Capacity</i>	3
1.3.2 <i>Effect on Shear Capacity</i>	4
1.4 PROBLEM STATEMENT	5
1.5 AIMS AND OBJECTIVES.....	6
1.6 STRATEGY AND FLOW OF STUDY	6
1.7 UTILIZATION OF RESEARCH.....	6
1.8 OUTLINE OF DISSERTATION	7
2 LITERATURE REVIEW	9
2.1 GENERAL.....	9
2.2 TYPES OF THE CORROSION DAMAGES ON STEEL BRIDGES	9
2.2.1 <i>Uniform Corrosion</i>	9
2.2.2 <i>Local Corrosion</i>	10
2.2.3 <i>Crevice Corrosion</i>	10
2.2.4 <i>Galvanic Corrosion</i>	10
2.2.5 <i>Stress Corrosion</i>	11

2.3	EFFECT OF ENVIRONMENTAL EXPOSURE ON CORROSION RATE	11
2.4	RELIABILITY STUDY BY KAYSER (1989)	13
2.5	BRIDGE DAMAGES IN JAPAN BY TAMAKOSHI.....	14
2.5.1	<i>Reason of Corrosion Damages in Japan</i>	15
2.5.2	<i>Damage Location and Causes</i>	16
2.5.3	<i>Corrosion Damages at Girder Ends</i>	16
2.5.4	<i>Corrosion other than the End of Girder</i>	18
2.5.5	<i>Corrosion on Exterior and Interior Girders of Bridges</i>	18
2.5.6	<i>Corrosion Inside the Sections of Girders</i>	18
2.6	RESEARCH REPORT BY MICHIGAN DEPARTMENT OF TRANSPORTATION (MDOT).....	19
2.7	SHEAR CAPACITY OF GIRDER WITH LOCAL WEB DAMAGE.....	20
3	CORROSION DAMAGES OF STEEL BRIDGES IN PAKISTAN.....	22
3.1	GENERAL.....	22
3.2	OBJECTIVES OF THE SURVEY	23
3.3	BRIDGES IN PAKISTAN.....	23
3.3.1	<i>Type of Steel Used in Bridges</i>	25
3.3.2	<i>Inspection and Maintenance Schedule of Bridges in Pakistan</i>	25
3.3.3	<i>Current Damage Repairing Method</i>	26
3.4	USE OF THE DIGITAL INSTRUMENTATION IN FIELD INSPECTION	27
3.5	TYPES OF THE DAMAGES OBSERVED IN STEEL BRIDGES.....	28
3.5.1	<i>Uniform Corrosion Damages</i>	29
3.5.2	<i>Local or Pitted Corrosion Damages</i>	30
3.5.3	<i>Atmospheric Corrosion</i>	30
3.6	CONCLUSIONS.....	31
4	EXPERIMENTAL METHODOLOGY.....	32
4.1	GENERAL.....	32
4.2	DESIGN PHILOSOPHY	33

4.2.1	<i>Types of Test Specimens</i>	33
4.3	MATERIAL PROPERTIES	36
4.4	TESTING ARRANGEMENT.....	37
4.4.1	<i>Load and Displacement Measurement</i>	38
4.5	EXPERIMENTAL RESULTS.....	40
4.5.1	<i>Load and Displacement Curves of Test Specimens</i>	40
4.5.2	<i>Deformed Buckling Shapes of Test Specimens</i>	41
4.6	CONCLUSIONS.....	44
5	ANALYTICAL EVALUATION OF CORRODED PLATE GIRDER ENDS	
	UNDER COMPRESSIVE LOADING.....	45
5.1	GENERAL.....	45
5.2	OBJECTIVES OF THE STUDY	46
5.3	FINITE ELEMENT MODELLING STRATEGY	47
5.3.1	<i>Shell Element Model</i>	47
5.3.2	<i>Shell-Solid Coupling Model</i>	47
5.4	BOUNDARY CONDITIONS AND MATERIAL PROPERTIES	49
5.5	INITIAL IMPERFECTIONS.....	49
5.5.1	<i>Initial Deflections</i>	49
5.5.2	<i>Residual Stresses</i>	53
5.6	MODEL VERIFICATION.....	56
5.6.1	<i>Verification of Healthy Specimen</i>	56
5.6.2	<i>Verification of Specimens with 20mm Damage</i>	57
5.6.3	<i>Verification of Specimens with 60mm Damage</i>	60
5.7	EXTENSION OF ANALYTICAL STUDY	62
5.7.1	<i>Number of Analytical Cases</i>	62
5.7.2	<i>Idealization of Damage Shape</i>	63
5.7.3	<i>Effect of Corrosion Damage Form</i>	65
5.8	ANALYTICAL RESULTS.....	67
5.8.1	<i>Load-Displacement Curves</i>	67

5.8.2	<i>Buckling Failure Modes</i>	69
5.8.3	<i>Comparison of Shell and Shell-Solid Coupling Results</i>	71
5.9	SERIES OF FE ANALYSIS	72
5.10	EFFECT OF WEB CORROSION ON LOAD CARRYING CAPACITY	74
5.10.1	<i>Effect of Exterior Web Corrosion</i>	74
5.10.2	<i>Effect of Interior Web Corrosion</i>	75
5.10.3	<i>Effect of Web Corrosion at Both Side of the Stiffener</i>	76
5.11	BUCKLING FAILURE MODE.....	76
5.12	ANALYSIS OF THE RESULTS	79
5.13	CONCLUSIONS.....	82
6	ANALYTICAL EVALUATION OF CORRODED PLATE GIRDER END UNDER SHEAR LOADING	83
6.1	GENERAL.....	83
6.2	FE MODEL CHARACTERISTICS.....	85
6.2.1	<i>Model Geometry and Boundary Conditions</i>	85
6.2.2	<i>FE Mesh and Material Properties</i>	88
6.2.3	<i>Initial Imperfections</i>	88
6.3	VALIDATION OF FINITE ELEMENT MODEL.....	89
6.3.1	<i>Method of Study</i>	90
6.4	RESULTS AND DISCUSSION	92
6.4.1	<i>Stiffener Damage only</i>	93
6.4.2	<i>Stiffener Damage plus Free Web End</i>	94
6.4.3	<i>Stiffener Damage plus Inner Web</i>	96
6.4.4	<i>Stiffener Damage plus Web on Both Sides</i>	97
6.5	DISCUSSION ON RESULTS	99
6.6	CONCLUSIONS.....	103
7	EMPERICAL RELATIONSHIPS	104
7.1	GENERAL.....	104

7.2	PREDICTION OF BUCKLING MODE	104
7.3	EMPIRICAL RELATIONSHIPS FOR BEARING CAPACITY	107
7.3.1	<i>Relationships for Bearing Capacity with Stiffener Damage</i>	107
7.3.2	<i>Relationships for Bearing Capacity with Stiffener plus Web Damage</i>	110
7.4	EMPIRICAL RELATIONSHIPS FOR SHEAR CAPACITY	112
7.4.1	<i>Relationships for Shear Capacity with Stiffener Damage</i>	112
7.4.2	<i>Relationship for Shear Capacity with Stiffener plus Web Damage</i>	114
8	CONCLUSIONS AND FUTURE RECOMMENDATIONS	116
8.1	CONCLUSIONS AND SUMMARY	116
8.2	FUTURE RECOMMENDATION.....	117
	REFERENCES.....	118
	APENIX A RULES FOR THE REGRESSION MODEL.. ERROR! BOOKMARK NOT DEFINED.	
A.1	SELECTION OF THE MODEL	122
A.1.1	<i>Types of the Basic Model</i>	122
A.1.2	<i>Types of the Logistic Model</i>	123
A.2	CALCULATION OF CORRELATION COEFFICIENT	124
A.3	CALCULATION OF COEFFICIENT OF DETERMINATION	124
A.4	EXAMINATION OF RESIDUAL.....	124

LIST OF FIGURES

Figure 1.1: Types of the bridges in Japan	2
Figure 1.2: Corrosion damages at plate girder end	3
Figure 1.3: Buckling failure of girder due to excessive section lost at bearings	3
Figure 1.4: Effective cross-sectional area of bearing stiffener (Japan Road Association)	4
Figure 1.5: Horizontal reaction produced by tension field action	4
Figure 2.1: Different corrosion types on the steel plate girder	10
Figure 2.2: Environmental effect on steel bridges corrosion (Kayser 1989).....	11
Figure 2.3: Typical corrosion map of steel bridges	13
Figure 2.4: Reliability versus time for short Span (12 m) steel bridge.....	14
Figure 2.5: Environmental and geographical features of Japan (Murakoshi 2006).....	15
Figure 2.6: Subdivision of plate girder for damage identification.....	16
Figure 2.7: Actual corrosion damage cases on plate girder end (Tamakoshi 2006b).....	17
Figure 2.8: Corrosion damages at non-composite steel bridges end	17
Figure 2.9: Corrosion damages at composite steel bridges end.....	17
Figure 2.10: Locations of corrosion in the steel bridges in Japan	19
Figure 2.11: Dimensions of the plate girder used by Liu (2011).....	20
Figure 2.12: Residual capacity of different Damage cases by Liu (2011).....	21
Figure 3.1: Attock Bridge as constructed in 1883	24
Figure 3.2: Sukker Bridge across Indus River	24
Figure 3.3: Some short span steel bridged across the canals in Pakistan	24
Figure 3.4: The corrosion on the girder due to non-painting.....	25
Figure 3.5: The replaced bridged in the yard.....	26
Figure 3.6: Use of the digital instruments.....	28
Figure 3.7: Uniform corrosion on steel bridges near sea line areas.....	29
Figure 3.8: Uniform corrosion on the lower portion of web and bottom flanges.....	29
Figure 3.9: Damages at plate girder end due to rain and drainage water accumulation	30

Figure 3.10: Damages at plate girder end due to deposited corrosion.....	31
Figure 4.1: Detail dimensions of the test specimen in mm.....	33
Figure 4.2: Sketch of bearing stiffener damage type in test specimens.....	35
Figure 4.3: Pictures of uniform and non-uniform damage with 20mm damage height.....	35
Figure 4.4: Pictures of uniform and non-uniform damage with 60mm damage height.....	36
Figure 4.5: True Stress-strain data of SS400 steel used in test specimens	37
Figure 4.6: Sketch of test set-up	37
Figure 4.7: Experimental Set-up.....	38
Figure 4.8: Detail of instruments used in the experimental program	39
Figure 4.9: Detail of instruments used in the experimental program	41
Figure 4.10: Failure mode of Healthy specimen.....	41
Figure 4.11: Failure mode of specimen S20U50	42
Figure 4.12: Failure mode of specimen S20N50	42
Figure 4.13: Failure mode of specimen S60U50	43
Figure 4.14: Failure mode of specimen S60N50	43
Figure 5.1: Bearing stiffener damage due to corrosion.....	46
Figure 5.2: Buckling of bearing stiffener caused by section loss (Murakoshi, 2006)	46
Figure 5.3: Meshing details of the Shell-Solid coupling model	48
Figure 5.4: Buckling behavior of plates with initial out-of-plane deviation.....	51
Figure 5.5: Typical initial imperfections of stiffened panels: (a) out-of-flatness of a subpanel; (b) out-of-straightness of a stiffener; (c) stiffener camber deflection. (IDM, 1987)	51
Figure 5.6: Buckling mode corresponding to first eignvalue	52
Figure 5.7: Residual stress distribution in the stiffened Panel (SCC-399, 1997).	53
Figure 5.8: Behaviour of plates in compression, with and without welding residual stress. Plate with (a) stable post-buckling behaviour, (b) unstable post-buckling behaviour....	54
Figure 5.9: Typical welding residual stresses in the plate girder end.....	55
Figure 5.10: Verification of load-displacement curve of healthy specimen.....	56
Figure 5.11: Verification of deformed shapes of healthy specimen	57
Figure 5.12: Verification of load-displacement curves of specimens with $D_h = 20\text{mm}$	58
Figure 5.13: Verification of uniformly damaged (S20U50) specimens with $D_h = 20\text{mm}$	59

Figure 5.14: Verification of non-uniformly damaged (S20N50) specimens with $D_h = 20\text{mm}$	59
Figure 5.15: Verification of uniformly damaged (S60U50) specimens with $D_h = 60\text{mm}$	60
Figure 5.16: Verification of non-uniformly damaged (S60N50) specimens with $D_h = 60\text{mm}$	61
Figure 5.17: Verification of load-displacement curves of specimens with $D_h = 60\text{mm}$	62
Figure 5.18: Different trail damage shapes.....	63
Figure 5.19: Mesh of triangular type of damage.....	64
Figure 5.20: Load-displacement curves of different damage shapes for $D_h = 20\text{mm}$ with 50% section loss.....	64
Figure 5.21: Various damage forms considered in the study.....	65
Figure 5.22: Effect of various corrosion forms for different damage heights with 50% residual thickness.....	66
Figure 5.23: Buckling of different stiffener damage forms for 20mm damage height.....	67
Figure 5.24: Buckling of different stiffener damage forms for 100mm damage height.....	67
Figure 5.25: Load capacity curves for different damage heights.....	68
Figure 5.26: Deformed Buckling Modes.....	70
Figure 5.27: Various damage cases considered in the study.....	74
Figure 5.28: Effect of exterior web damage on bearing capacity.....	75
Figure 5.29: Effect of interior web damage on bearing capacity.....	75
Figure 5.30: Effect of web damage at both side of stiffener on bearing capacity.....	76
Figure 5.31: Various deformed shapes.....	77
Figure 5.32: Ultimate load comparison of damage groups WES and IWS.....	79
Figure 5.33: Relationships between residual strength and residual thickness.....	81
Figure 6.1: Typical corrosion damages at plate girder end by Tamakoshi (2006b).....	84
Figure 6.2: Complete loss of bearing stiffener by Khurram (2012).....	85
Figure 6.3: Phases in behaviour up to collapse of a typical panel in shear.....	85
Figure 6.4: Detail dimensions of the girder model (Dimensions are in mm).....	86
Figure 6.5: Correlation between plate girders with different panels.....	87
Figure 6.6: Meshing detail of FE model.....	88

Figure 6.7: First buckling eignvalue mode shape of plate girder	88
Figure 6.8: Verification of load-displacement curves with results of Real (2007).....	89
Figure 6.9: Verification of load-displacement curves with results of Alinia (2009)	89
Figure 6.10: Deformed buckling shape.....	90
Figure 6.11: Different damage cases for shear capacity analysis	92
Figure 6.12: Load-displacement curves for the cases with stiffener damage only	93
Figure 6.13: Deformed modes for the cases with stiffener damage only	94
Figure 6.14: Load-displacement for the cases with stiffener plus exterior web damage.....	95
Figure 6.15: Deformed modes for the cases with stiffener plus exterior web damage.....	96
Figure 6.16: Load-displacement for the cases with stiffener plus interior web damage	96
Figure 6.17: Deformed modes for the cases with stiffener plus interior web damage	97
Figure 6.18: Load-displacement for the case with stiffener plus both sides web damage.....	98
Figure 6.19: Deformed modes for the case with stiffener plus both sides web damage.....	99
Figure 6.20: Remaining capacity of specimen with stiffener damage.....	100
Figure 6.21: Remaining capacity of specimen with stiffener plus exterior web damage	100
Figure 6.22: Remaining capacity of specimen with stiffener plus interior web damage.....	101
Figure 6.23: Remaining capacity of specimen with stiffener plus both sides web damage .	101
Figure 7.1: Remaining capacity versus reduced thickness ratio	106
Figure 7.2: Comparison of ultimate shear capacities determined analytically and by empirical formula with stiffener damage	108
Figure 7.3: Correlation between evaluated and predicted capacities for different damage heights with stiffener damage	109
Figure 7.4: Comparison of ultimate bearing capacities determined analytically and by empirical formula with stiffener plus web damage.....	110
Figure 7.5: Correlation between analytically evaluated and predicted capacities for different damage heights with stiffener plus web damage	111
Figure 7.6: Comparison of ultimate shear capacities determined analytically and by empirical formula with stiffener damage	113
Figure 7.7: Comparison of ultimate shear capacities determined analytically and by empirical formula with stiffener plus web damage.....	115

LIST OF TABLES

Table 2.1: Average values of corrosion parameters, A and B (Kayser 1989).....	12
Table 4.1: Description of various experimental test specimens	34
Table 4.2: Material properties of SS400 steel used in the test specimens	36
Table 4.3: Detail of the instruments used in the experimental program.....	39
Table 4.4: Ultimate capacity of experimental test specimens.....	40
Table 5.1: Imperfections and residual stresses values by Smith <i>et al.</i> 1988.....	53
Table 5.2: Analytical cases used in the study	62
Table 5.3: Comparison of ultimate capacity of shell and shell-solid models	71
Table 5.4: Various analytical cases for bearing capacity analysis.....	73
Table 5.5: Ultimate bearing capacity and deformed shape for various analytical cases	78
Table 6.1: ASSHTO classification for flange types.....	87
Table 6.2: Analytical cases for shear capacity evaluation	91
Table 6.3: Remaining shear capacity for different damage cases.....	102

LIST OF NOTATIONS

b_f	flange width
D_h	corrosion damage height
d	depth of the plate girder
E	young's modulus of elasticity
e	width of web free end
N	non-uniform damage
$P_{H,ult}$	ultimate load for the healthy specimen
P_{ult}	ultimate load
S	straggle damage
t	steel plate thickness
t_0	original thickness of the steel plate
t_f	flange thickness
t_s	stiffener thickness
t_w	web thickness
U	uniform damage
w_0	initial imperfection value
β	slenderness parameter
σ_{cr}	critical buckling stresses
σ_R	compressive residual stresses
σ_u	ultimate stresses
σ_y	yield stresses
ν	poison ratio

INTRODUCTION

1.1 GENERAL

Due to the ease in manufacturing and rapid construction, Steel plate girders are the most common type of steel bridges all around the world. Corrosion and live load (Fatigue) are the two major aging problems, which gradually reduce the life of these steel bridges by degrading their load carrying capacity. Fatigue is purely depends upon the traffic intensity and number of loading cycles but on the other hand, corrosion is much unpredictable phenomenon and entirely based on the environmental and exposure conditions. Corrosion may either damage the steel bridges uniformly or locally which may cause the reduction in the ultimate capacity gradually with the increase in the damage in the structure. The deterioration by corrosion usually consists of thinning sections in the web and stiffener or irregularly shaped holes in the web just above the flange that may decrease the load carrying capacity in shear, bearing, and sometimes in bending. The following contents represent the history of corrosion behaviour on the steel bridges and its possible effect on its load carrying characteristics and stability.

1.2 BACK GROUND

The total number of bridges on road highways and railway networks in Japan is as high as 670,000 (Tamakoshi 2006b). A large part of these bridges, around 39% is comprised of the steel bridges. Further, plate girders are the most common among these steel bridges, which possess a total share of 51% as illustrated in Figure 1.1. Statistical reports indicate that more than half of steel brides in Japan are above age 60 and some bridges are aged above 100 years (Ichikawa 1994). Like many other countries steel bridges in Japan are also facing a very severe corrosion problem due to its aggressive topographic and environmental condition (Murakoshi 2005). Some main causes of corrosion are describes as following.

- Water leakage from cracks of concrete slab or pavements
- Water leakage at girder ends
- Water puddle (accumulation of rain water) near bearing region
- Airborne Salt
- Splashing water, sand or salt
- Others causes *i.e.* deposited and stress corrosion

Statistical surveys and field inspection illustrate that most of the plate girder bridges tend to corrode at the end of the girder and cause the reduction of excessive material from the bottom of bearing stiffener and adjacent web as exhibited in Figure 1.2 where in one case complete loss of bearing stiffener thickness can also be noticed. Mainly, such types of the corrosion are the result of first three corrosion factors as mentioned above. Such types of the damage may cause the buckling/crushing at bearing which may further elevate the stability problem to structure as whole. Figure 1.3 demonstrates a typical buckling at the plate girder end due to excessive material lost by corrosions. In the recent time, corrosion induced damages are the most common issues in repairing and replacement of steel bridges in Japan (Natori 2001, Kitada 2006).

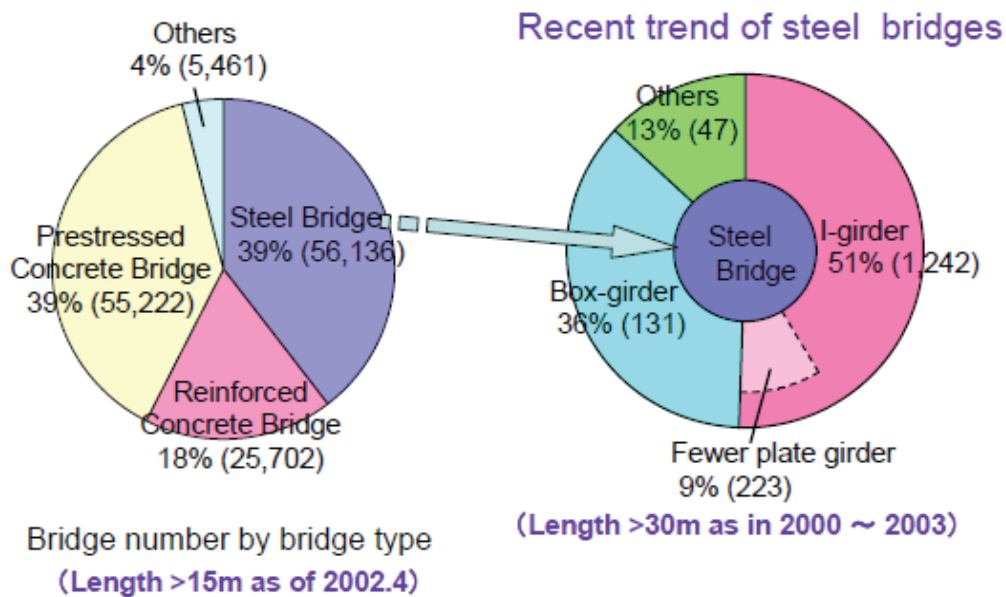


Figure 1.1: Types of the bridges in Japan



(a) Damage case in Japan (Tamakoshi 2006a)



(b) Damage case in Pakistan

Figure 1.2: Corrosion damages at plate girder end

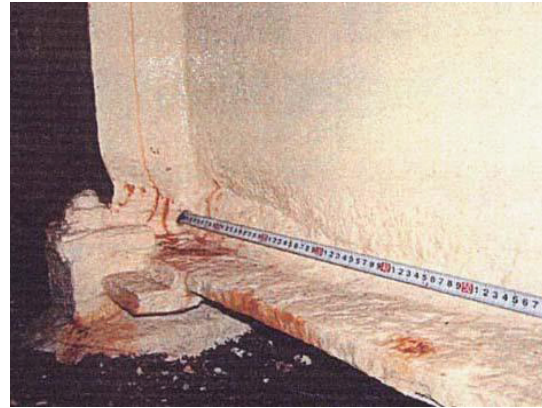


Figure 1.3: Buckling failure of girder due to excessive section lost at bearings

1.3 STRUCTURAL EFFECT OF CORROSION

1.3.1 Effect on Bearing Capacity

Normally, bearing stiffeners are designed as a column to resist the bearing load at the girder support and the effective area of the column is calculated as the cross section area of the bearing stiffener along with some portion of the web to calculate the radius of gyration, which is used to evaluate its stability against buckling as shown in Figure 1.4. Any significant corrosion on the bearing stiffener and web may reduce the radius of gyration and thus, the resistance against the bulking under compression load.

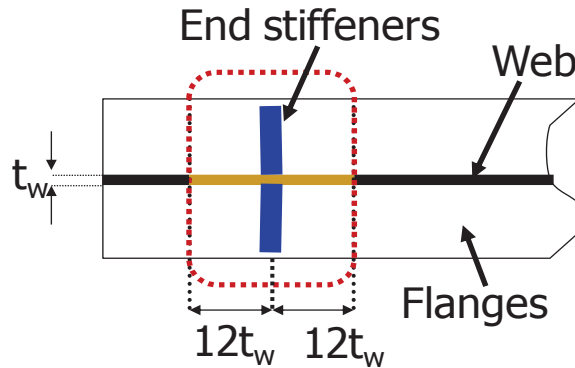


Figure 1.4: Effective cross-sectional area of bearing stiffener (Japan Road Association)

1.3.2 Effect on Shear Capacity

Transverse stiffeners play an important role in allowing the full ultimate load resistance of a plate girder. Firstly, they prevent the web from out-of-plane deflections and thus increase the critical shear buckling resistance of the web; secondly they prevent the flanges from coming closer to each other and continue to remain effective after the web buckles, to provide anchorage for the tension field (Hoguland 1997).

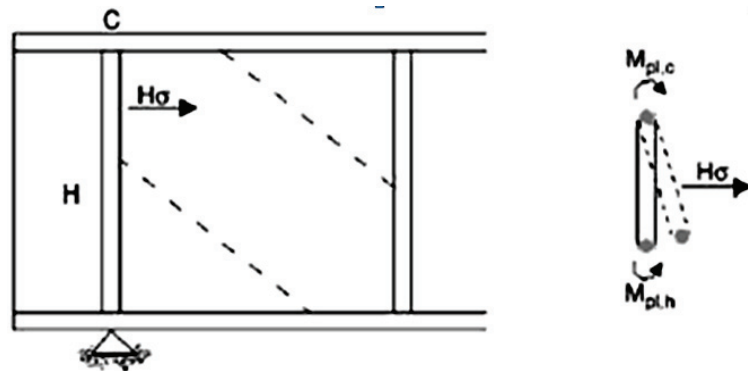


Figure 1.5: Horizontal reaction produced by tension field action

Beside the design for the bearing reaction the bearing stiffener are also designed to resist the in plane bending moment (M_{pl}) due to the anchor force (H_Q) as shown in Figure 1.5. Usually tension filed action increases the ultimate strength by three to four times more than the critical strength and any critical damage in the bearing stiffener at the support may reduce the anchorage force (H_Q) to develop the tension filed action which may further cause the bearing

failure instead of shear collapse mechanism before developing the tension field action in the web. So any damage within the bearing stiffener may reduce the bearing and shear strength rapidly due to the possibility of buckling.

1.4 PROBLEM STATEMENT

As the number of old and corroded bridges is increasing day by day. Thus, replacement of all these bridges along with the construction of new bridges is not possible due to many constraints *i.e.* economic barrier, traffic switching and lack of the manpower and technical resources. So the most feasible option is to evaluate the remaining capacity of these bridges and repairing/retrofitting can be carried out where it is required and only unusable and severely damaged bridges can be replaced gradually.

However, corroded steel bridges need the proper evaluation due to the following reasons

1. Many bridges may have adequate load carrying capacity and may be used without any significant repairing.
2. If required then repairing/retrofitting decision can be taken for the proper maintenance.
3. To carry out the replacement to avoid any casualty and serious damage.

In order to evaluate the remaining capacity of corroded steel bridges and to select the appropriate solution as mentioned above one must have the knowledge of the following questions.

- Where corrosion is likely to occur on the steel bridges?
- When it starts and governing causes?
- Extent and rate of corrosion on the steel bridges?

The bearing stiffeners have the vital role in resisting the bearing and shear capacity of steel plate girder bridges. However, any significant loss in the thickness of the stiffener may affect its bearing strength.

1.5 AIMS AND OBJECTIVES

The present study has the following main objectives.

1. Investigation of corrosion damage cases in actual structure (Relationship between inspection data and failure mode)
2. Evaluation of remaining capacities and failure modes of plate girder ends in compression and shear keeping in mind the most frequent corrosion damages in the real cases considering various damage levels.
3. Development of empirical relationships to determine the remaining life and failure pattern of corroded bridges.

1.6 STRATEGY AND FLOW OF STUDY

The evaluation procedure for corrosion effects on bridges can be divided into three stages.

Stage 1: Conducting the damaged bridge inspection and collecting data regarding the types of corrosion damages on the steel bridges.

Stage 2: Identifying the severity of the damage conditions produced by corrosion and necessity of required actions. It includes the addressing damage locations, nature of damage, amount and geometry of damage, extent of damage and environment conditions.

Stage 3: Conducting quantitative evaluation to determine the residual capacity of a deteriorated bridge and to propose the simple method to evaluate the remaining capacity.

1.7 UTILIZATION OF RESEARCH

The research work will be help full for the following purposes.

1. Simple parameter can be used to judge the performance level and expected failure mode.

-
2. Results will be useful to determine the effect of local damage on bearing and shear capacity and over all stability of system can also be assessed.
 3. Monitoring and inspection interval can be decided.
 4. Suitable retrofitting and repairing measures can be suggested

1.8 OUTLINE OF DISSERTATION

The dissertation comprises eight chapters that have been organized in following sequence.

Chapter 1, Introduction, includes the introduction of the research, problem statement, research objective, scope and its significance.

Chapter 2: Literature Review, presents the detail literature on all the topics related to the research work including the different studies conducted on the corroded bridges.

Chapter 3: Bridge Damages of Steel Bridges in Pakistan, includes the current condition of the steel bridges in Pakistan and nature of the damage suffered by these steel bridges

Chapter 4: Experimental Methodology, deals with the experimental evaluation and comparison of various plate girder specimens simulated with different corrosion damages at the bearing stiffener.

Chapter 5: Analytical Evolution of the Plate Girder End under the Compressive Loading is discussed in this chapter.

Chapter 6: Analytical Evolution of the Plate Girder End under the Shear Loading, the effect of local corrosion damage at the girder end on its ultimate and post buckling shear capacity is evaluated analytical in this section

Chapter 7: Empirical Relationship, some empirical relationships to calculate the ultimate bearing and shear capacity of the steel bridge girders affected by the end panel corrosion damage are proposed in this chapter.

Chapter 8, Conclusions and Future Recommendations, some salient conclusion are drawn in this chapter and further, some suggestions regarding future work are also made in this chapter.

LITERATURE REVIEW

2.1 GENERAL

Corrosion is one of the severe problems that steel bridges are suffering, which deteriorate their life by reducing the load carrying capacity. Corrosion in a steel girder may affect the capacity in bending, shear, and bearing (buckling, crippling, and crushing). In order to evaluate the remaining capacity of corroded steel bridges, it is essential to have the proper knowledge regarding the most common types of corrosion damages in the steel bridges. This chapter comprises of some field surveys regarding the most susceptible types of the corrosion damages and some earlier attempt to access the residual capacity of corroded bridges.

2.2 TYPES OF THE CORROSION DAMAGES ON STEEL BRIDGES

Generally, there are five common forms of corrosion which can affect a steel girder bridge (Kayser 1989). The each corrosion form is due to the various environmental exposures, stress condition and other structural damage conditions. These corrosion forms are categorized as following.

2.2.1 *Uniform Corrosion*

It is the most common form of general corrosion, which is uniformly distributed on the surface. This type of the corrosion is often found on the whole web and especially at the bottom portion of webs. The loss in web material may reduce the shear capacity due to section loss and web buckling.

2.2.2 Local Corrosion

While pitting corrosion is restricted to a small area; it usually begins with an anomaly on the surface. This type is dangerous because it may cause local stress concentrations and is difficult to check.

2.2.3 Crevice Corrosion

Crevice corrosion occurs where different components of the structure are close, leading to narrow spaces. Normally, this type of the corrosion is observed at the top flanges of plate girders as shown in the Figure 2.1. In such cases water leaks through the cracks in the slab and gather within the cracks above the top surface of the flanges

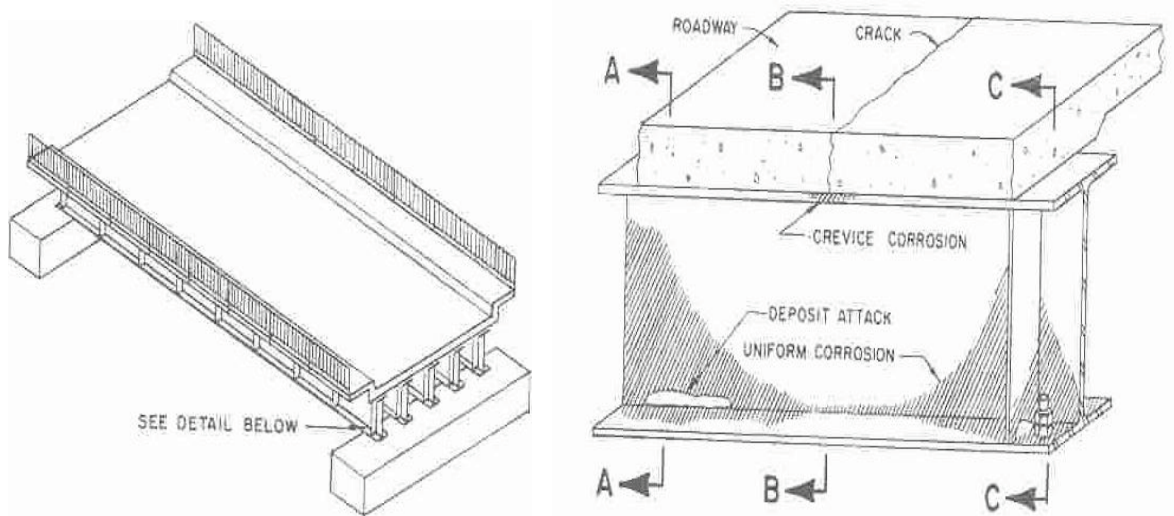


Figure 2.1: Different corrosion types on the steel plate girder

2.2.4 Galvanic Corrosion

Galvanic corrosion takes place when two different metals are placed in an electrolyte and are electrically connected, as is possible at bolted or welded connections.

2.2.5 Stress Corrosion

The amount of capacity reduction caused by loss of section depends whether the component is in compression or tension. Tensile stress will increase the rate of corrosion because paint is detached from highly stressed places and expose the steel to corrosion and this type of corrosion is called stress corrosion.

A combination of different forms of corrosion can often occur, and the combination of pitting, crevice, and stress corrosion under cyclic loading is called corrosion fatigue.

2.3 EFFECT OF ENVIRONMENTAL EXPOSURE ON CORROSION RATE

Corrosion rate is highly influenced by the environment, *i.e.* the amount of moisture in the air and the presence of salt thus, the geographic location play a vital role in planning the maintenance of steel bridges. Figure 2.2 shows that steel bridges near marine environment have more probability to corrode with the years of exposure as compared to the rural and urban environment. It has also been observed that the rate of corrosion can be different for different girders. For example, in highway overpasses, girders are exposed to a mixture of salt, snow, and water splashed by trucks. The highest concentration of this aggressive medium is on the exterior girder, and the concentration of salt and/or water decreases in the direction of traffic.

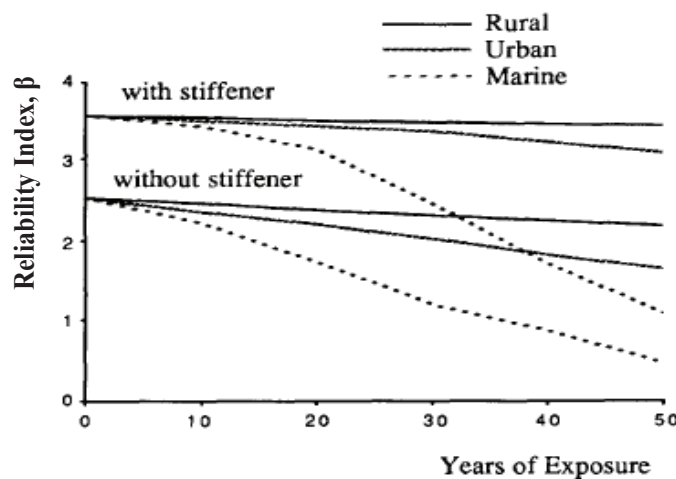


Figure 2.2: Environmental effect on steel bridges corrosion (Kayser 1989)

Komp (1987) showed that the corrosion propagation can be modeled, with a good approximation, by an exponential function as shown in equation (2.1).

$$C(t) = At^B \quad (2.1)$$

Where,

$C(t)$ = the average corrosion penetration in micrometers (10^{-6} m)

t = the time in years

And A and B = parameter determined from regression analysis of experimental data

The parameters A and B are random variables therefore, actual corrosion loss, C , is also a random variable and has been determined based on field tests by Albrecht and Naeemi (1984). Table 2.1 illustrates the mean values, the coefficients of variation, and the coefficients of correlation for A and B . As corrosion develops at much slower rate in weathering steel after the first year therefore, the parameters are smaller for the weathering steel as compared to the carbon steel. Further, in most cases the parameters are the lowest in rural environments and highest in urban environments. It was stated that values of A and B involve a considerable uncertainty as these values were determined from tests of small metal specimens. In the extrapolation to full-size bridges, some error may occur due to variations in component size, orientation, and local environment as more data become available on the corrosion of actual steel bridges, parameters A and B can be revised.

Table 2.1: Average values of corrosion parameters, A and B (Kayser 1989)

Environment	Carbon steel		Weathering steel	
	A	B	A	B
Rural	34.0	0.65	33.3	0.50
Urban	80.2	0.59	50.7	0.57
Marine	70.6	0.79	40.2	0.56

2.4 RELIABILITY STUDY BY KAYSER (1989)

Kayser (1989) conducted some field surveys to identify the most common type of the corrosion damages in the steel bridges. From his surveys it was observed that corrosion is likely to occur along the top surface of the bottom flange due to traffic spray accumulation and over the entire web near the supports due to deck leakage. The typical corrosion pattern on the steel girder is illustrated in Figure 2.3.

According to Kayser (1989) loss of material may affect any one of three modes of resistance in a girder, bending, shear, and bearing. Loss of flange material will cause a reduction in the net area available to resist bending. The moment of inertia will be reduced, causing an increase in deflection. Also, the ultimate bending strength will be reduced, causing a reduction in maximum carrying capacity.

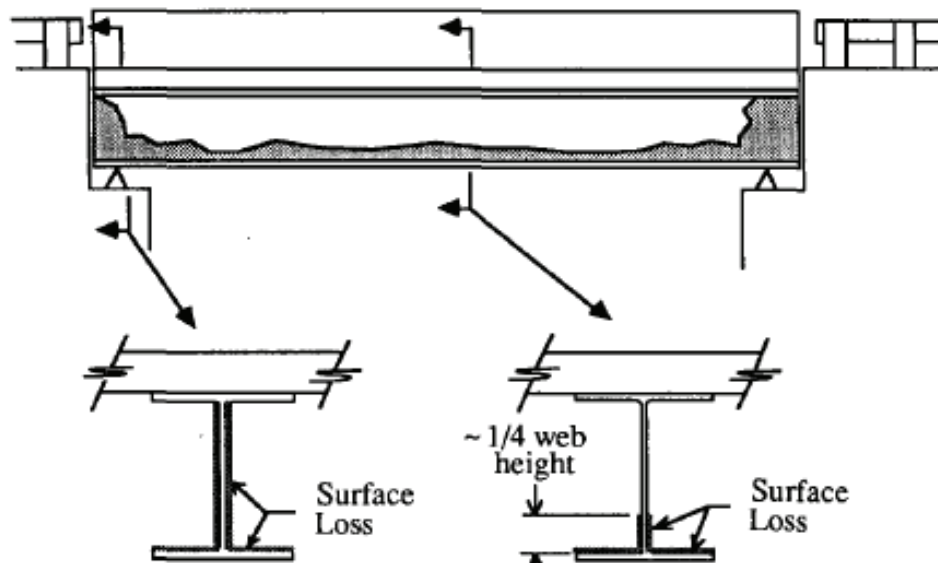


Figure 2.3: Typical corrosion map of steel bridges

He also pointed out that the performance reliability of steel plate girder bridges highly depends upon the presence of bearing stiffeners as it governs the controlling failure mode in the bridges. For the new bridges provided with the bearing stiffeners, the controlling parameter is the bending. But with the passage of time, considerable loss of the material from

the bearings and in the end panels may shift the controlling mode from bending to bearing failure.

The loss of girder material due to corrosion has more effect on the web than on the flange as clear from the Figure 2.4. This causes a larger percentage decrease in shear and bearing reliability than in bending reliability. He concluded that a surface loss of 2 mm on both sides of the web and on the top of the flange will reduce the web area by 27%, and the flange area by 10%. The web will further be affected by the fact that it acts in compression, subject to buckling, while the flange is in tension. Further, the web being a compression element is the component most susceptible to corrosion loss. This variation in safety loss from one component to another, or from one mode of resistance to another means that resistance criterion which governs when a bridge is new may not governs when a bridge becomes corroded.

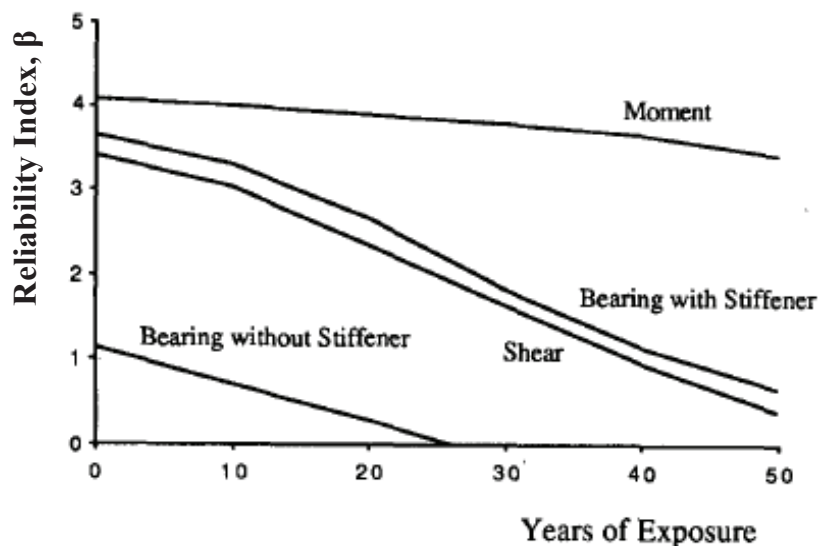


Figure 2.4: Reliability versus time for short Span (12 m) steel bridge

2.5 BRIDGE DAMAGES IN JAPAN BY TAMAKOSHI

There are more than 670,000 highway and railways bridges in Japan which comprised of around 40% steel bridges. Most of these steel bridges were constructed in between 1955 and 2000 during the economic growth time (Tamakoshi 2006). Among these steel bridges mostly

non-composite and composite steel plate girder are the most common types of the steel bridges. Corrosion is one of the aging deterioration problem suffered by these steel bridges which reduce the load carrying capacity and life of these steel bridges.

2.5.1 Reason of Corrosion Damages in Japan

Japan is situated in severe geographical and environmental conditions which highly favour the aggressive and corrosive environment for the steel structures and bridges. As shown in Figure 2.5 Japan is a long and slender island country, its geographical feature comprised of large coastal and mountainous area. Its meteorological conditions are also very severe which include much rain, seasonal wind in winter, and frequent typhoon. Moreover, about 60% area is snowy and cold. All these are the some main favourable factors for the corrosion. Further, airborne salt in air and usage of deicing agents also play a vital role in the corrosion of steel bridges in Japan (Murakoshi 2006).



Figure 2.5: Environmental and geographical features of Japan (Murakoshi 2006)

2.5.2 Damage Location and Causes

Tamakoshi (2006) studied the locations of corrosion damages on non-composite and composite steel plate girder bridges by partitioning the bridge in various divisions longitudinally, included middle support point of continuous girders. He categorized these divisions as, end of girders, one-fourth of span and center of girder as highlighted in Figure 2.6.

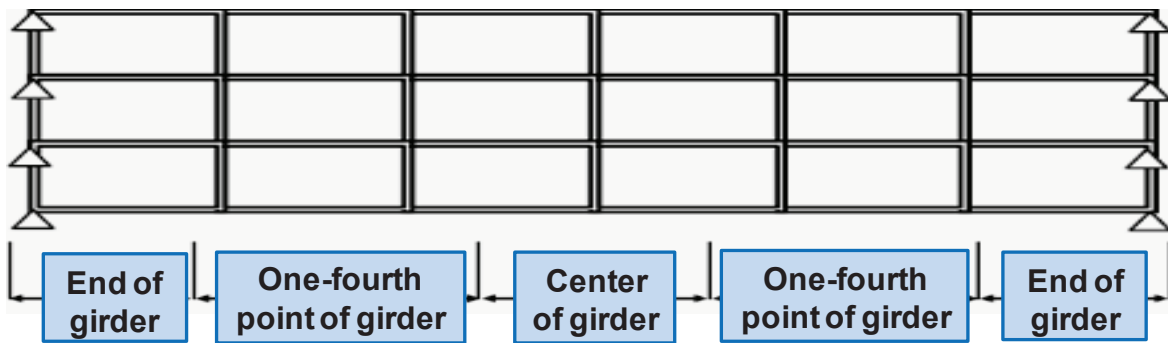


Figure 2.6: Subdivision of plate girder for damage identification

2.5.3 Corrosion Damages at Girder Ends

Tamakoshi (2006a) in his field surveys analyzed the damage types and conditions of 1717 non-composite and 1351 composite steel bridges in his bridges survey. He reported corrosion damage cases of 38 non-composite and 43 composite steel bridges in his survey. Among the 38 non-composite bridges 35 bridges were corroded at the end of girder near bearings. The rate was 92.1% of all the corroded bridges.

This rate was 88.4%, (38 bridges out of 43) among the composite steel bridges. In most of the cases, cause of the corrosion damage was the water leakage from the expansion joints. Also, water pool and moisture around bearings which made girder ends to corrode rapidly. Some actual corrosion damages at plate girder ends are illustrated in Figure 2.7. The Figure 2.8 and 2.9 shows the statistical data regarding the location of the corrosion damages of all researched non-composite and composite steel bridged respectively.



Figure 2.7: Actual corrosion damage cases on plate girder end (Tamakoshi 2006b)

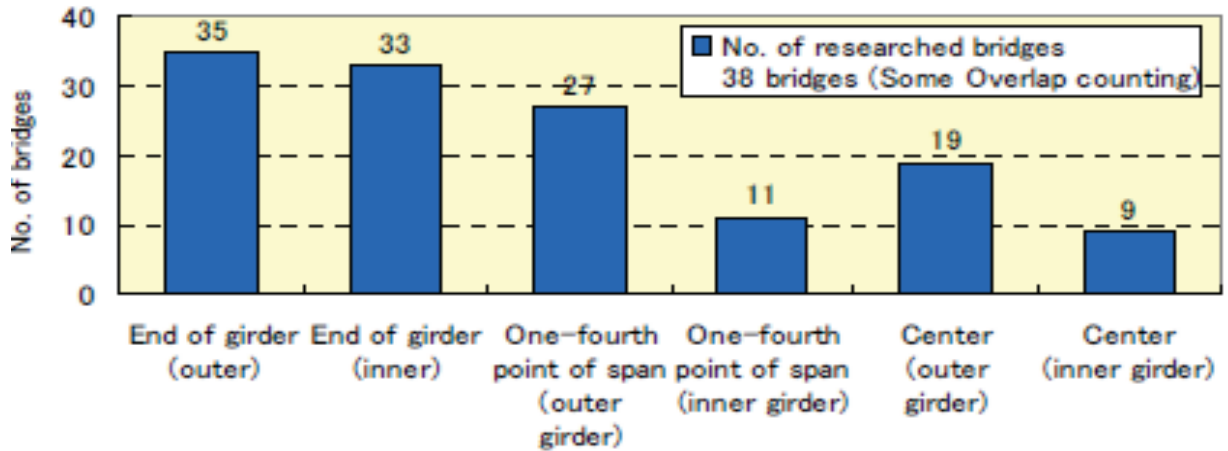


Figure 2.8: Corrosion damages at non-composite steel bridges end

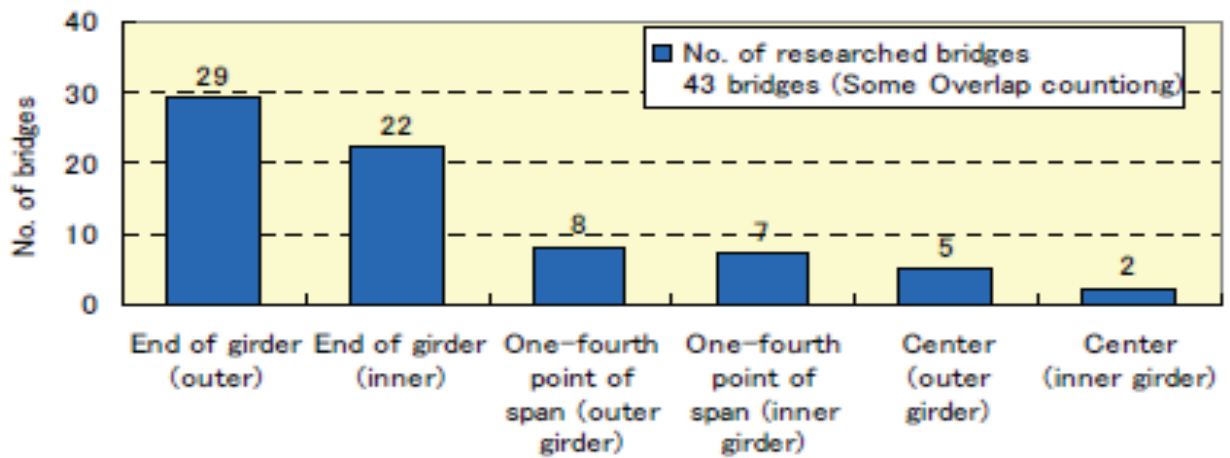


Figure 2.9: Corrosion damages at composite steel bridges end

2.5.4 Corrosion other than the End of Girder

There were also some bridges that were corroded at the middle part of interior girders, along flanges cross-section on outer girders and webs and at splice plates. These are examples of corrosion other than that at the end of girders. The reason of such is that some bridges held water on its members and the corrosion progresses due to the chocking of drainage hole. Also, water leakage through cracks in the deck causes corrosion at upper flanges in main girders. Tamakoshi (2006a) reported that only in two non-composite bridges (5.6%) corrosion was not found at the end of girders, but at other points. However, among the composite type steel bridges this ratio was little high, 11.6 % of all the bridges

2.5.5 Corrosion on Exterior and Interior Girders of Bridges

Among the non-composite type, many bridges were corroded at both the exterior and interior girders. The rate was 86.8% of the bridges studied, and only there were only few cases where excessive corrosion was found only at exterior or interior girders. On the other hand, among the composite type, in many cases of corrosion was found only on exterior girders, 76.8 % of all those studied and rate of corrosion for interior girders was 55.9 %.

2.5.6 Corrosion Inside the Sections of Girders

Besides the corrosions on the web and top flange a significant corrosion was also observed at lower flanges in sections of composite-type plate girder. The rate of lower flange corrosions was 65.1 % of the bridges studied. Further, field observations indicate that newly built bridges, particularly those built using corrosion-resistant steel and/or painted with freeze-resistant coatings tends to corrode locally and thus, comparatively older bridges are likely to corrode as a whole on the span. Figure 2.10 shows the some common locations of the steel bridges suffered by the corrosion.

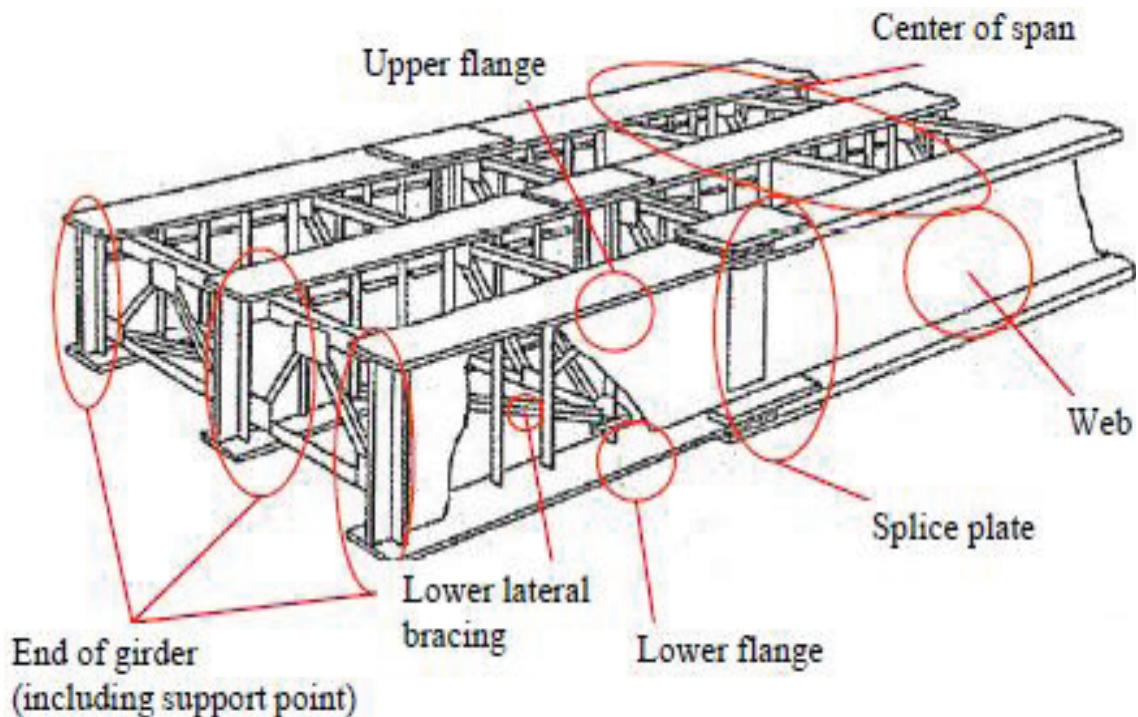


Figure 2.10: Locations of corrosion in the steel bridges in Japan

2.6 RESEARCH REPORT BY MICHIGAN DEPARTMENT OF TRANSPORTATION (MDOT)

According to the 2003 Michigan state bridge inventory, 40% of state-owned bridges built in the last decade are steel girder bridges. This number is even greater if one considers all the existing bridges in the state. Corrosion of steel beams primarily due to deicing media made of salt and water is a very common problem in the state of Michigan. This generally takes the form of localized deterioration of steel beam ends usually from deck joint leakage and occasional spray from passing vehicles. The deterioration usually consists of thinning sections in the web or irregularly shaped holes in the web just above the flange and may decrease the load carrying capacity in shear, bearing, and sometimes bending. The evaluation procedure for corrosion effects on bridges has three phases. Phase 1 includes collecting bridge data, understanding the structure behavior and coordinating the purpose of inspection with the bridge inspector. Phase 2 identifies the criticality of the conditions created by corrosion and urgency of required actions. It includes examining the inspection report and

addressing the location of damage, nature of damage, amount and geometry of damage, extent of damage and environment conditions. Phase 3 includes quantitative evaluation, which determines the residual capacity of a deteriorated bridge. (MDOT)

2.7 SHEAR CAPACITY OF GIRDER WITH LOCAL WEB DAMAGE

In a recent attempt, Liu et al. (2011) consider four different types of the local damage cases named as damage case C, T, U and V to evaluate the shear capacity of the steel plate girder with the local damages in web. The geometrical dimensions, loading and boundary conditions of the plate girder model used in the study are given in the Figure 2.11. The remaining ultimate capacity versus residual thickness plots for various damage cases are presented in the Figure 2.12. The study concludes that local web damage C, T and V have a little effect on the ultimate shear capacity as can be seen in the Figure 2.12 (a, b & C) and only the damage case U has the significant role in the ultimate strength reduction of the girder.

The study did not consider the effect of corrosion damage on the shear capacity along with the web damage, that can be more significant factor in the ultimate strength and post-buckling shear strength of the girder as bearing stiffener strength provides the anchorage to balance the horizontal reaction of the tension field action developed in the adjacent web panel. The study indicates that damage group V is more susceptible to strength reduction however; usually such type of damage is not occur in the actual field conditions.

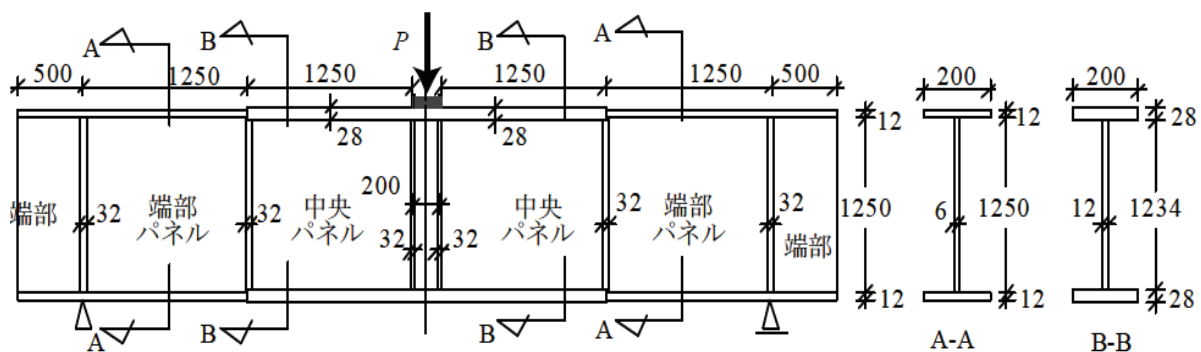
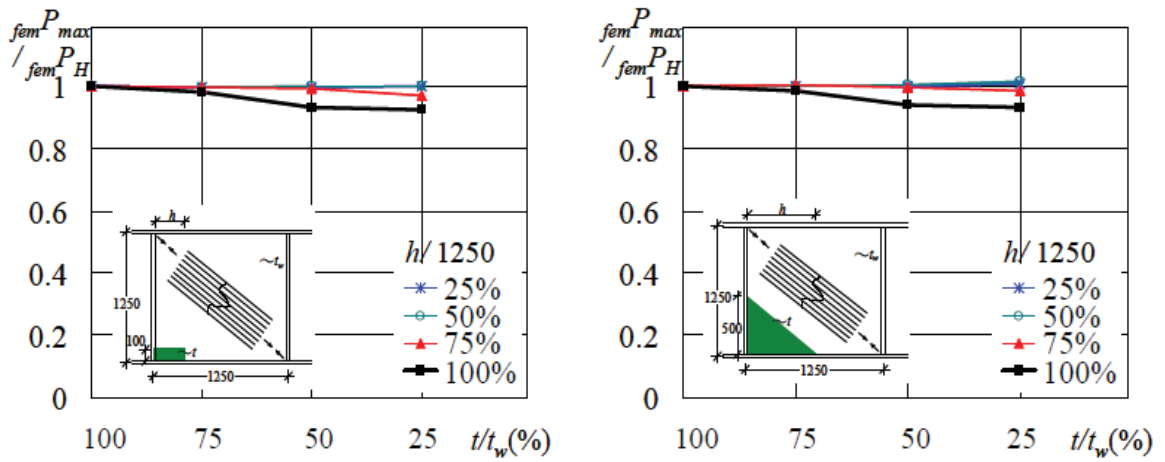
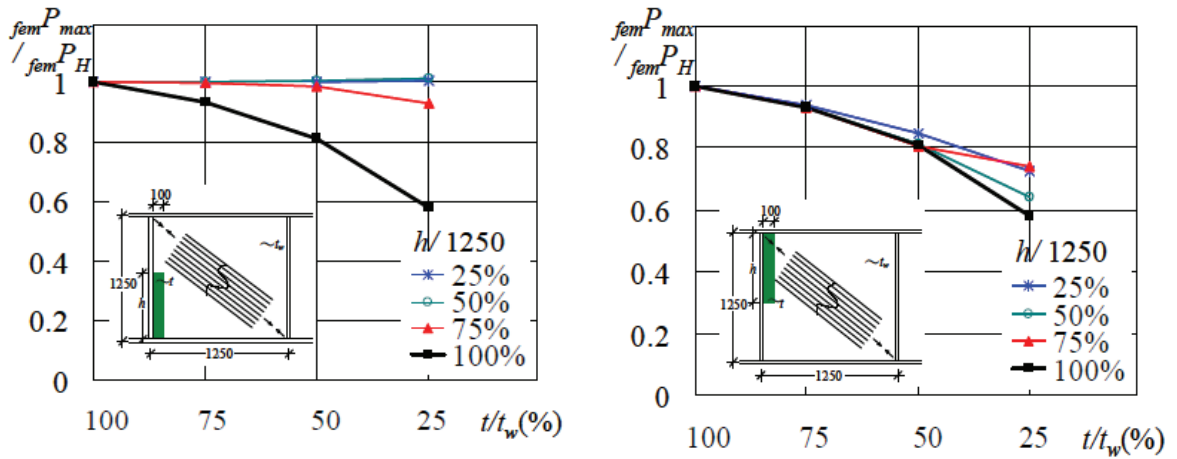


Figure 2.11: Dimensions of the plate girder used by Liu (2011)



(a) Damage group, C

(b) Damage group, T



(a) Damage group, V

(b) Damage group, U

Figure 2.12: Residual capacity of different Damage cases by Liu (2011)

CORROSION DAMAGES OF STEEL BRIDGES IN PAKISTAN

3.1 GENERAL

There are 14570 various kinds of bridges over the Pakistan Railways. Most of the railway bridges are the short to medium span steel bridges which were constructed under the British authority before the independence of the Pakistan. The struggling economy is the main constraint for the constructions of new bridges so it has been become inevitable to maintain and repair the existing bridges to extend their life. Corrosion and fatigue are the two main threats to these steel bridges, which disintegrate their capacity and life gradually. Many constraints like economic and switching off traffic problem demand the proper health monitoring of the structure system to assess the damage level and remaining capacity to take necessary measure. Furthermore, undamaged bridges also need proper evaluation for their fitness and suitability for the current traffic load and intensity. For the evaluation of the remaining capacity to take the suitable measures like replacement or retrofitting of the steel bridges some knowledge regarding the general and common types of damages to these steel bridges is essentially required. As a part of research program the effort was made to collect some real field data regarding the damages to the steel bridges from some developing country (*i-e.* Pakistan), as due to the less maintenance by virtue of financial constraint more severe damage may be observed. Later these damages may be simulated to determine the effect and extent of the damage to the capacity of the steel bridges. This technical report contains the information about the types of steel bridges and related aging damages in Pakistan.

3.2 OBJECTIVES OF THE SURVEY

There are following objectives of this report.

1. To collect the data related with the number and types of the steel bridges in Pakistan
2. To assess the types of damages to steel bridges in Pakistan
3. Current inspections and maintenance measures of steel bridges.

3.3 BRIDGES IN PAKISTAN

In the last six decades, Pakistan has not built a bridge of any aesthetic or architectural value. Most of the new major bridges are of the economic variety built for the roads out of pre-cast concrete boxes or beams, or of plate girders that any one hardly notices driving over. Since rivers spans in Pakistan are not very wide or deep therefore, rivers are not used for the navigation purpose like in some developed and industrialized countries. Thus, no high super structure like Golden Gate Bridge in San Francisco and other structures all over the world have been constructed. The most of the bridges in Pakistan are short to medium span bridges which are built across the five major rivers and extensively large canal network system. Many of the railways bridges are more than 100 years old, constructed before the independence of Pakistan in 1947 by the British Government.

The British government constructed most of the truss type of the bridges like Attock Bridge as shown in Figure 3.1. The bridge was first opened in 1883 and then reconstructed from 1926 to 1929. The *Khushal Garh Bridge* over *River Indus* having the longest truss type span at 459 feet (140m). Similarly, Jhelum Bridge across River Jhelum is 4745 feet (1450 m). Figure 3.2 shows the single span suspension bridge of 874 feet (266 m) located at Sukkur across *River Indus* constructed in 1889, which is an engineering marvel. Pakistan has world largest and extensive canals network throughout the country so most of the small span truss and plate girder bridges are located on the canals. Figure 3.3 shows two short span, truss and plate girder bridges across the canal system in Pakistan.



Figure 3.1: Attock Bridge as constructed in 1883



Figure 3.2: Sukker Bridge across Indus River



Figure 3.3: Some short span steel bridged across the canals in Pakistan

3.3.1 Type of Steel Used in Bridges

As stated above most of the steel bridges are more than 100 years old and constructed under the British government before the partition of subcontinent therefore, in most of the bridge cast Iron, wrought iron aluminum alloy and mild steel were used in most of the steel bridges. Cast iron and wrought are now obsolete as bridge material, except for specialized use. Aluminium bridges are still in experimental stage and presently not competitive with the steel bridges in cost.

3.3.2 Inspection and Maintenance Schedule of Bridges in Pakistan

The steel bridges are inspected by Bridge Division of Pakistan Railway as per following schedule

- Normal steel bridges after each 5 years
- Reversed camber steel bridges after each 3 years
- Highly stressed bridges after each 2 years



Figure 3.4: The corrosion on the girder due to non-painting

As per painting schedule followed on Pakistan Railways, the bridges are required to be painted very year to prevent it from corrosion which develops rapidly in costal environment. The inspection of the most of the bridges depicted that during certain periods the painting

schedule was not adhered to, which resulted in severe development of corrosion. Figure 3.4 shows the corrossions on the girders due to non-painting.

3.3.3 Current Damage Repairing Method

Due to the lack of the expertise, maintenance funds and instruments for the inspection of bridge health and condition, it is very difficult to assess the strength and remaining life of the steel bridge. Therefore, bridge section of Pakistan railways has abandoned most of the bridge and replacing only some of them where location is more important. Many of replaced bridges may have sufficient strength and some of them may be retrofitted and repair properly to reduced the economic and traffic constraints. Most of the replaced bridges have been replaced due to the non-availability of remaining life assessment and retrofitting techniques and expertise. All the replaced bridges are kept in Bridge yard at Bridge Manufacturing Division of Pakistan Railways in city Jhelum of Pakistan. The pictures in Figure 3.5 shows that most of the bridge may have the sufficient capacity and life but have been replaced due to the non availability of technical and financial resources to evaluate the bridge health.



Figure 3.5: The replaced bridged in the yard

In normal practice the damages are repaired without assessing the capacity by some computational method using some thumb rule. In case of the plate girder bridges temporary flanges are welded to the girder to carry sufficient dead load where flanges are buckled locally, while the damages portion is cut-out and replaced by welding a new section of same

dimension which may later cause the fatigue problem. In some cases where there is some doubt regarding the repairing the bridge is either replaced or discarded.

3.4 USE OF THE DIGITAL INSTRUMENTATION IN FIELD INSPECTION

The new modern instruments are very useful in the field of health monitoring of steel bridges. For the inspection and measuring of actual bridge condition two pocket size field instruments *Coating Thickness Gauge* and *Ultrasonic Thickness Gauge* were used to measure the coating of paint and remaining thickness or residual loss of the metal as shown in the Figure 3.6(a & b) respectively. Later on the base of measured data and material properties these bridges may be simulated in some finite element (FE) program to evaluate the remaining capacity and compare the results with the filed damages cases. On the bases of using these instruments two bridges were recommended to use after repainting rather than discarding and also damage level in most of the bridges was determined.



(a) Measurement of paint coating thickness



(b) Measurement of residual thickness of section



(c) Plate Girder Bridge after retrofitting and repainting

Figure 3.6: Use of the digital instruments

3.5 TYPES OF THE DAMAGES OBSERVED IN STEEL BRIDGES

There are following two type of the corrosion damages are found in the bridges

- Uniform corrosion Damages
- Local or pitted corrosion Damages
- Deposited corrosion

3.5.1 Uniform Corrosion Damages

Uniform corrosion pattern were generally observed in Karachi city which is near the sea line area and where plate girder are submerged in the water due to high flood level in the river and canals. Near the sea line area usually uniform corrosion was observed on whole bridge surface as shown in Figure 3.7. But in case of the submerged and other plate girder bridges that are exposed to high humidity and elevated temperature are found to be uniformly corroded from the top surface of bottom flange and up to the 1/4 to the 1/6 portion of web from the bottom flange as shown in the Figure 3.8. It is generally accumulation and sticking of the water vapours at the lower web surface in humid and rainy season.



Figure 3.7: Uniform corrosion on steel bridges near sea line areas



Figure 3.8: Uniform corrosion on the lower portion of web and bottom flanges

3.5.2 Local or Pitted Corrosion Damages

In many cases local corrosion and pitted corrosion damage were also observed in the field. Usually these types of the damages are more commonly found at bridge ends. Primarily these damages are due to the leakage and accumulation of the water at bearing region in cases of the non through bridges. But in case of through bridges the damages at the end may be due the deposited corrosion and accumulation of the rain water at bridge ends due to the poor drainage conditions. Figure 3.9 shows the typical damages at plate girder end due deposited corrosion and corrosion due to the rain and drainage water respectively. The corrosion damage at plate girder end reduces the thickness of the bearing stiffener and web that may subsequently reduce the bearing and shear capacity of the plate girder.



Figure 3.9: Damages at plate girder end due to rain and drainage water accumulation

3.5.3 Atmospheric Corrosion

This type of the corrosion occurs when dissimilar metals are connected in the presence of an electrolyte a galvanic corrosion reaction occurs. Electrolytes are electrically conductive solutions such as sea water or road salt spray which contain chloride or rain, mist or dew containing sulfur or nitrogen compounds. The most common sources of chloride contamination are marine and coastal environments as well as winter road salting spray. Sulfur and nitrogen compounds are more ubiquitous being the product of air pollution and industrial fallout. Figure 3.10 shows the some deposited corrosion cases.



Figure 3.10: Damages at plate girder end due to deposited corrosion

3.6 CONCLUSIONS

1. For the effective maintenance of the steel bridge the knowledge of the general types and pattern of damages is inevitable.
2. By assessing the damage level the proper evaluation of the steel bridges can be carried out for the retrofitting or replacement of the bridges.
3. The actual field damage condition may be incorporated and simulated to check the stability problem to the structure in case of the failure.

EXPERIMENTAL METHODOLOGY

4.1 GENERAL

Many field surveys (Chapter 2) have reported that steel plate girder ends tend to corrode more frequently, due to the leakage of water from construction joints and/or detention of rain water near bearing regions. Such type of corrosion at the plate girder end damages the stiffener and web portion severely, and may cause a buckling failure and overall stability problem to the bridge structure. In some actual cases, buckling failures of plate girder (Figure 1.3) has also been observed due to the excessive loss of material at the bottom portion of bearing stiffeners. (A typical buckling failure due to material loss at bearings is shown in Figure 4.1)

Generally, bearing stiffeners are designed as a column to resist the bearing load at the girder support and the effective area of the column is calculated as the cross section area of the bearing stiffener plus some portion of the web, which is used to evaluate its stability against buckling. Thus, any local corrosion damage may reduce the effective area so the radius of gyration which may also increase the sensitivity of the plate girder to buckle under the compressive load. Further, corruptions may penetrate into the bearing stiffener either from one side or both side of the thickness, uniformly or non-uniformly. Therefore, the proper assessment of the effect of the both types of corrosion on the ultimate bearing capacity is required. So that some simple parameter *i.e.* average or minimum thickness can be determined for the simple finite element simulation of local corrosion damage in the bridge structures.

The following contents describe the types of the test specimens and complete experimental strategy for the evaluation of plate girder ends with the local corrosion damage.

4.2 DESIGN PHILOSOPHY

In the present study, five identical steel plate girder end specimens but with different types of corrosion damage in the bearing stiffener, were utilized in the experimental program. All specimens were designed similar to the actual plate girder from the field used by Hung *et al.* (2002), by picking a reduced scale ratio of two-third ($2/3$). As the primary objective of the study is to investigate the corrosion effect on bearing capacity, thickness of bearing stiffener was set to 12mm and thickness of web and intermittent stiffener were fixed to 6mm. A relatively large thickness, 16 mm was chosen for the flanges to reduce the punching effect during the load application of concentrated compressive load. In all welds a leg length of 5mm was applied. The detail dimensions of the test specimen are illustrated in Figure 4.1.

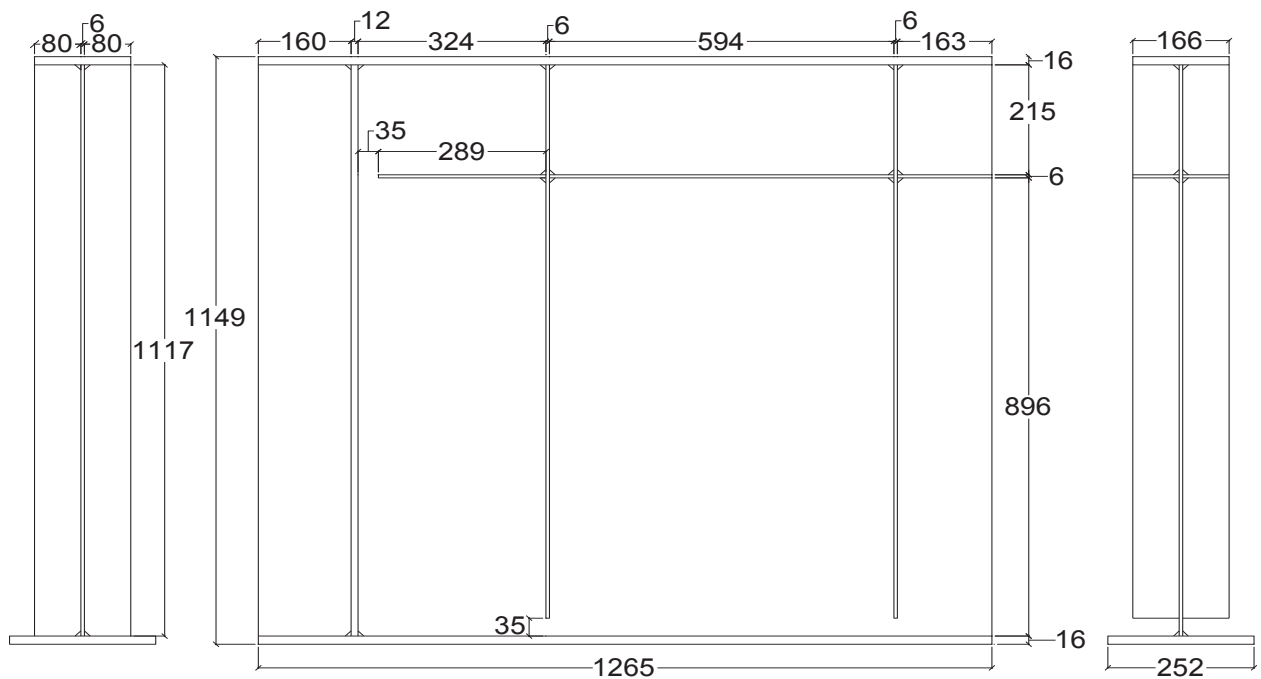


Figure 4.1: Detail dimensions of the test specimen in mm

4.2.1 Types of Test Specimens

In all, total five plate girder end specimens were utilized in the experimental program. In one test specimen, no corrosion damage was considered and referred as healthy specimen. To investigate the effect of various bearing stiffener damage levels on the ultimate bearing

capacity, two different damage heights of 20mm and 60mm were chosen from the weld seams just above the top face of the bottom flange, on each of the remaining two test specimens pairs. However, in order to study the behaviour of different corrosion forms, the thickness of bearing stiffener was reduced to half (50% of the original thickness) uniformly and non-uniformly from one of the both pair of the specimens with 20mm and 60mm damage height respectively, as shown in the Figure 4.2. The local damage was produced by grinding the surface of the bearing stiffener in the lab. Table 4.1 shows the description of all specimens used in the experimental tests. The pictures of uniform and non-uniform damage of test specimens with 20mm and 60mm damage height are shown in Figure 4.3 and 4.4 respectively.

Table 4.1: Description of various experimental test specimens

Sr. #	Specimen Name	Damage Height		Residual Thickness, t		Damage Cases
		D_h (mm)	D_h/d (%)	(mm)	(%)	
1	Healthy	Zero	-	12	(100%)	No damage
2	S20U50	20	1.8	6	(50%)	Uniform
3	S20N50	20	1.8	6	(50%)	Non-uniform
4	S60U50	60	3.6	6	(50%)	Uniform
5	S60N50	60	3.6	6	(50%)	Non-uniform

Terminologies used in Table 4.1 are defined as following.

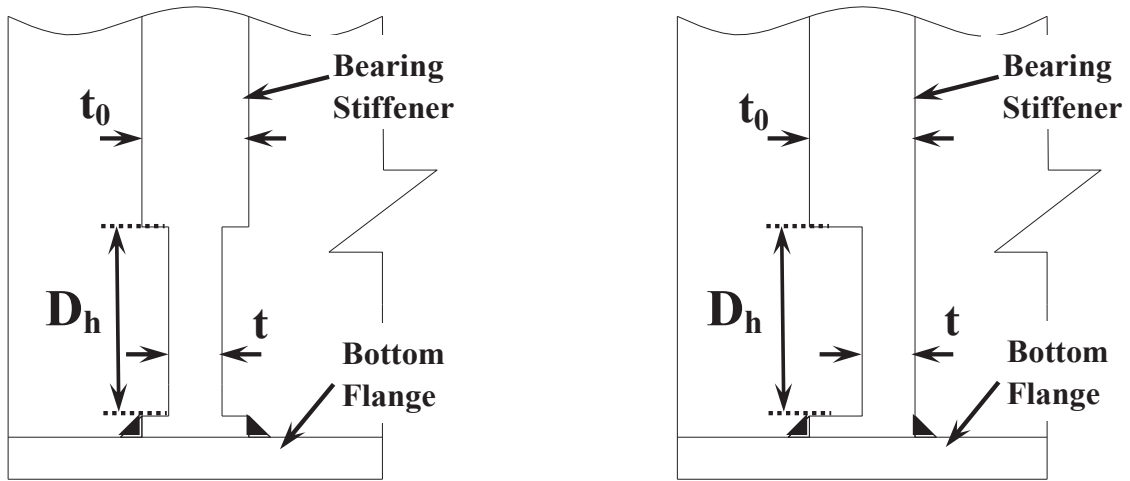
S = Bearing stiffener

d = Total depth of the bearing stiffener

20 = Damage height (D_h) of bearing stiffener in mm

U or N = Types of the damage, U for uniform damage and N for Non Uniform damage

Thus, a typical damage S20U50 is described as uniform (U) stiffener damage (S) with a damage height (D_h) 20 mm having residual thickness 50 %.



(a) Uniform Damage

(b) Non-uniform Damage

Figure 4.2: Sketch of bearing stiffener damage type in test specimens

Here, in Figure 4.2

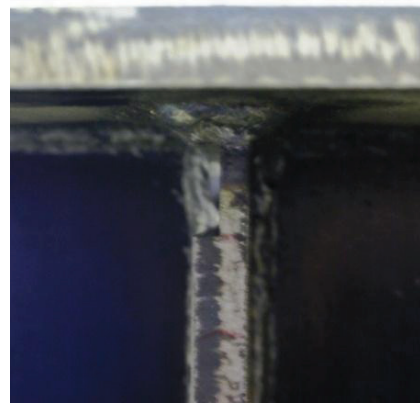
D_h = Damage height of the bearing stiffener in mm

t_0 = Original thickness of the bearing stiffener (12mm)

t = Residual thickness of the bearing stiffener in the damage zone



(a) Uniform damage



(b) non-uniform Damage

Figure 4.3: Pictures of uniform and non-uniform damage with 20mm damage height



(a) Uniform damage



(b) non-uniform Damage

Figure 4.4: Pictures of uniform and non-uniform damage with 60mm damage height

4.3 MATERIAL PROPERTIES

Due to the possibility of large deformations and strain particularly after buckling, true stress-strain relationships of a mild steel JIS-SS400 were determined to use the mechanical properties of steel in the analytical study. The material properties of SS400 steel used in the test specimens were determined by performing tensile tests in the lab. For the tensile test, coupons were cut from the used plate girder test specimens. The complete material plasticity data of JIS-SS400 steel used in different plates of test specimens is shown in Figure 4.5 and Table 4.2.

Table 4.2: Material properties of SS400 steel used in the test specimens

Sr. #	Description	Plate Thickness t (mm)	Young's Modulus E (Mpa)	Yield Stress σ_y (Mpa)
1	Web	6	185,000	240
2	Intermediate Stiffener	6	185,000	240
3	Bearing Stiffener	12	185,000	250
4	Flange	12	210,000	280

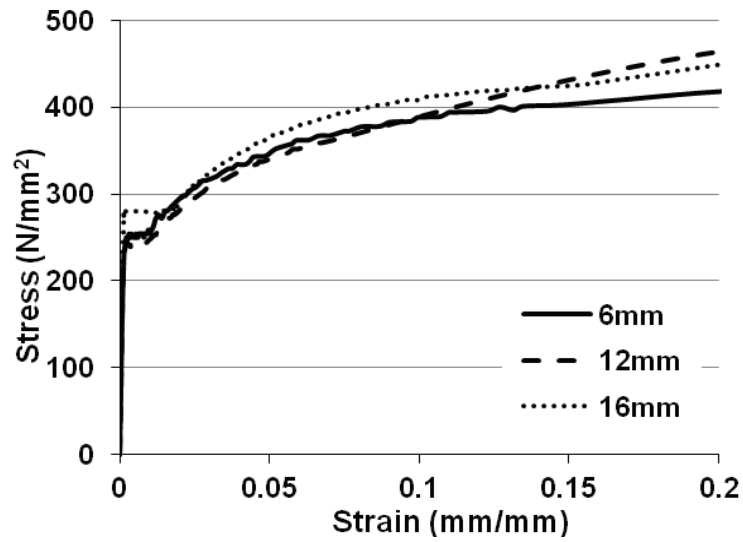


Figure 4.5: True Stress-strain data of SS400 steel used in test specimens

4.4 TESTING ARRANGEMENT

The test specimens were laid on the ground with their top flanges facing downward and bottom flanges in upward direction. The layout of the experimental setup shown in Figure 4.6 demonstrates the arrangement of the test specimen with load application and displacement measurement points.

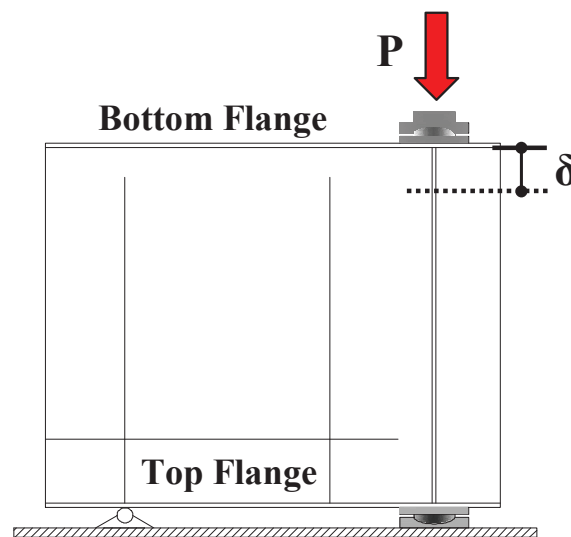


Figure 4.6: Sketch of test set-up

In order to determine the bearing strength of plate girder ends, an axial compressive load was applied by Universal Testing Machine (UTM) on the bearing stiffeners and shortening of the girder is recorded by the displacement transducer and test was conducted as a displacement control procedure. Figure 4.7 shows the picture of the experimental set-up used in the lab.



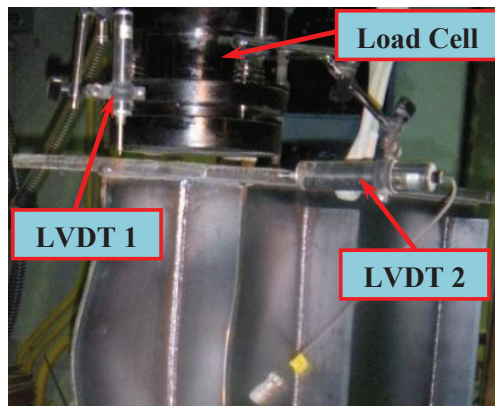
Figure 4.7: Experimental Set-up

4.4.1 Load and Displacement Measurement

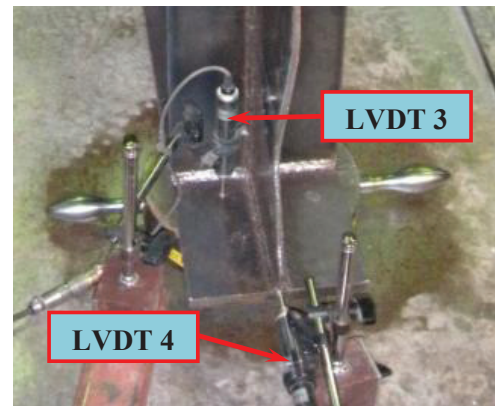
The load and displacements were recorded by a load cell and Linear Variable Displacement Transducers (LVDTs), using a data acquisition system. Besides the vertical deformation, the lateral displacement at loading point and longitudinal (slippage) displacements at boundary points were also measured to check the suitability of boundary conditions to use in the Finite Element program for the extension of the numerical study. The detail of the instrumentation used in the experimental test is shown in the Figure 4.8 and Table 4.3.

Table 4.3: Detail of the instruments used in the experimental program

Sr. #	Instrument	Description
1	Load Cell	Load Cell to measure the load in kN
2	LVDT 1	LVDT to measure vertical displacement at loading point
3	LVDT 2	LVDT to measure lateral displacement at loading
4	LVDT 3	LVDT to measure vertical displacement at loading point
5	LVDT 4	LVDT to measure longitudinal displacement (slippage) at front support
6	LVDT 5	LVDT to measure longitudinal displacement (slippage) at rear support



(a) Load and deformation measurement at loading points



(b) Displacements measurement at the front support



(c) Displacements measurement at the rear support

Figure 4.8: Detail of instruments used in the experimental program

4.5 EXPERIMENTAL RESULTS

4.5.1 Load and Displacement Curves of Test Specimens

All results obtained from the experimental program are plotted in term of load-displacement curves on a same plot for the comparison purpose as shown in Figure 4.9. All specimens depict the same initial stiffness but different ultimate loads. The healthy specimen has the highest ultimate load value. The results also revealed that a small local damage of 20mm with residual thickness of 50% does not reduce the ultimate load remarkably. It reduced the load by 1% and 2.5% for the cases of S20U50 and S20N50 respectively as presented in Table 4.4. Basically, this small reduction of ultimate load is governed by the local plastic constraints phenomena. However, in uniform type of the damage (S20U50) plastic constraint effect is more dominant as case S20U50 shows a little higher load and inclination of load displacement curve than that of non-uniform of the damage (S20N50) just before the peak load. This indicates that uniform type of the damage provides a little higher constraint against the local deformation of material in a relatively smaller damage than non-uniform types of damage. The 60mm damage height illustrates the reduction of 14.4 % and 15.8 % in ultimate capacity for the cases of S60U50 and S6050N respectively. Both uniform and non-uniform damage within damage height of 60mm provides the similar trend in the post-buckling strength but uniform types of the damage gives a little higher load after buckling due to the plastics constraint effect however, this effect is much less than the case of 20mm damage height.

Table 4.4: Ultimate capacity of experimental test specimens

Sr. #	Specimen	Ultimate Load (kN)	Load Reduction Ratio
1	Healthy	1004.97	1.00
2	S20U50	995.42	0.990
3	S20N50	979.51	0.975
4	S60U50	860.75	0.856
5	S60N50	845.69	0.842

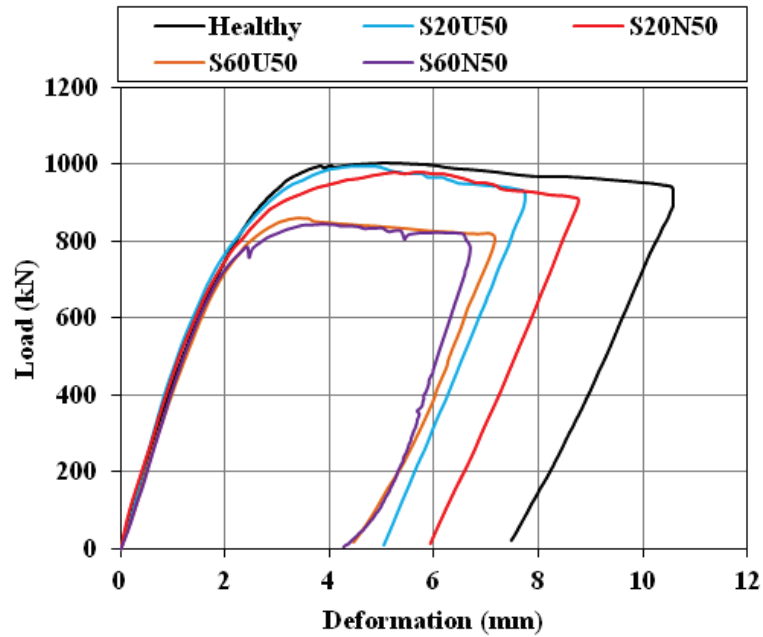


Figure 4.9: Detail of instruments used in the experimental program

4.5.2 Deformed Buckling Shapes of Test Specimens

The healthy specimen deforms as whole with buckling dominant near the loading points and maximum buckling was found at $0.7d$ distance of both web and stiffener, which indicates the partial fixed types of boundary condition that is a key factor to calculate the radius of gyration for the design of the buckling stiffener. Figure 4.10 shows the buckling of web and bearing stiffener in healthy specimen.



Buckling in Stiffener

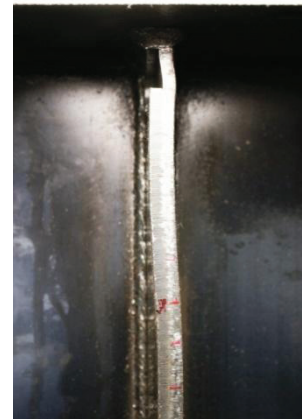
Figure 4.10: Failure mode of Healthy specimen

The compression test revealed that 20mm damage height does not change the failure mode of web and stiffener in both uniform and non-uniform type of damage. Nevertheless, some plastic deformation also occurred in the damage zone, the buckling position in web and stiffener is the same as of the healthy specimen and can be seen in the Figure 4.11 and 4.12 for S20U50 and S20N50 cases respectively.



Buckling in Stiffener

Figure 4.11: Failure mode of specimen S20U50



Buckling in Stiffener

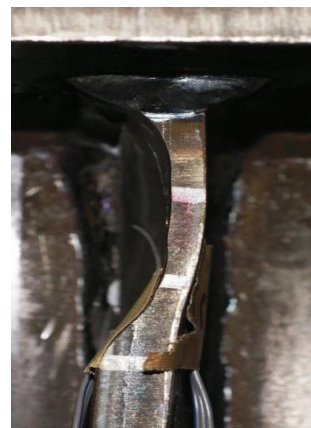
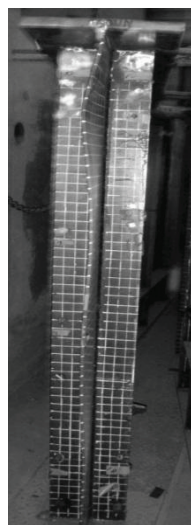
Figure 4.12: Failure mode of specimen S20N50

The experimental test of specimens with 60mm damage height, only revealed the local buckling of bearing stiffener within the damage zone with most of the buckling in the web however, maximum buckling point in the web shifted near the end towards the damage portion. Figure 4.13 and 4.14 exhibit the failure mode in specimen S60U50 and S60N50 respectively, where local buckling in the bearing stiffener is quite evident with web buckling concentrated towards the end.



Buckling in Stiffener

Figure 4.13: Failure mode of specimen S60U50



Buckling in Stiffener

Figure 4.14: Failure mode of specimen S60N50

4.6 CONCLUSIONS

On the base of the experimental study the following conclusions can be established.

1. For the case of very small local corrosion damage, local plastic constraint effect provides some extra resistance against the deformation of the material which contributes a little increase in the ultimate capacity after the buckling.
2. Local plastic constraint effect is more dominant in the uniform types of the damage and for small damage heights and this effect is much lesser in non-uniform types of the damage and even vanishes for the large damage heights.
3. A damage of 20mm does not change the buckling mode neither decrease the capacity considerably.
4. A relatively large bearing stiffener damage of 60mm shift the local buckling within the damage region and also reduce the capacity significantly.

ANALYTICAL EVALUATION OF CORRODED PLATE GIRDER ENDS UNDER COMPRESSIVE LOADING

5.1 GENERAL

Field inspections and reviewed literature depict that usually the rate of corrosion is non-uniform and increases near girder ends as compared with the other portions of the girder, due to the water leakage from construction joints and accumulation of rain water on the top surface of the bottom flange (Tamakoshi, 2006a). This corrosion is more concentrated at the bearing stiffener and adjacent web region near the bearings. On many occasion complete loss of material from the bearing stiffener was also observed. Figure 5.1 shows a typical case of complete loss of bearing stiffener thickness. Ok *et al.* (2007) stated that besides the uniform corrosion steel bridges also suffer from the pitting that may lead to increase in stress intensity factor for fatigue to occur, when observed around weld seams which are sensitive to crack initiation. In some cases local corrosion may also takes place due to bacteria attacks. The previous studies and literature like Tamakoshi (2006a) also highlighted the fatigue cracks nearby the bearing region. But in some aggressive environment, only corrosion damages may also occur without fatigue cracks.

Kayser and Nowak (1989) pointed out that the performance reliability of steel plate girder bridges highly depends upon the presence of bearing stiffeners as it governs the controlling failure mode in the bridges. For the new bridges provided with the bearing stiffeners, the controlling parameter is the bending. But any considerable loss of the material from the stiffener may shift the controlling mode from bending to bearing failure. Figure 5.2 shows buckling of the bearing stiffener at the support due to the excessive section lost by corrosion.

Thus, there is need to find the extent of the damage level in bearing stiffener region including both adjacent web and stiffener damage nearby the support that may reduce the bearing

capacity of plate girder bridge remarkably, so that suitable decision can be taken regarding the retrofitting or replacement of the structural member. The present study only focuses the investigation of the extent of the corrosion damage of bearing stiffeners and web corrosion adjacent to the bearing stiffener at the support, against the compressive loading, ignoring fatigue cracks to assess the need for retrofitting or replacement of bridges.



Figure 5.1: Bearing stiffener damage due to corrosion



Figure 5.2: Buckling of bearing stiffener caused by section loss (Murakoshi, 2006)

5.2 OBJECTIVES OF THE STUDY

The analytical study has the following objectives

1. To check the suitability and validity of the shell and solid element in the finite element modeling.

2. To clarify the governing thickness parameter *i.e.* minimum or average thickness, while modeling the local damage in plate girder end to test under compression.
3. To study the effect of various corrosion levels on the bearing capacity of the plate girder end.
4. To study the effect of local corrosion on free web end and interior web adjacent to bearing stiffener, separately and in combination with the bearing stiffener.

5.3 FINITE ELEMENT MODELLING STRATEGY

The general purpose finite element program ABAQUS was used to model and analyze the steel plate girder ends for the determination of the bearing capacity. ABAQUS is well suited software to calculate the ultimate capacity for the type of the problem which includes the both geometric and material nonlinearity considering the global and local instability, including buckling phenomenon. Moreover, this software has a wide range of element library and several multi-point-constraints (MPC) options that can be used to avoid the displacement compatibility problem between the elements and also useful in developing the shell-solid coupling model for the cost effective solution.

5.3.1 Shell Element Model

The shell model comprises of 3997 S4R elements with six degrees of freedom at each of 4084 nodes. The S4R element is a powerful four nodes standard element that allows both the changes in the thickness and finite element strain. After performing the convergence analysis a mesh size of 5mm was kept near the corrosion affected region while, a coarser mesh was used in other regions to capture the buckling.

5.3.2 Shell-Solid Coupling Model

The shell model is less flexible and results obtained by the shell modeling are regarded as less accurate due to not considering the shear force and strain in transversal direction. For any non-linear problem, containing a small local damage undergoing a large strain, the Poisson ratio effect in lateral direction may cause local constraint to deformation which may decrease

the stiffness and increase the strength after the yielding of material in the local damage. To verify the effect of local plastic constraint in the small local damage a shell-solid coupled model was developed instead of modeling a full solid model for the cost effective solution. The coupling of shell and solid element is usually achieved by using the Multi Point Constraint (MPC) equations in the ABAQUS and can also be applied for the geometrically non-linear analysis and structures with anisotropic, elastic and composite material.

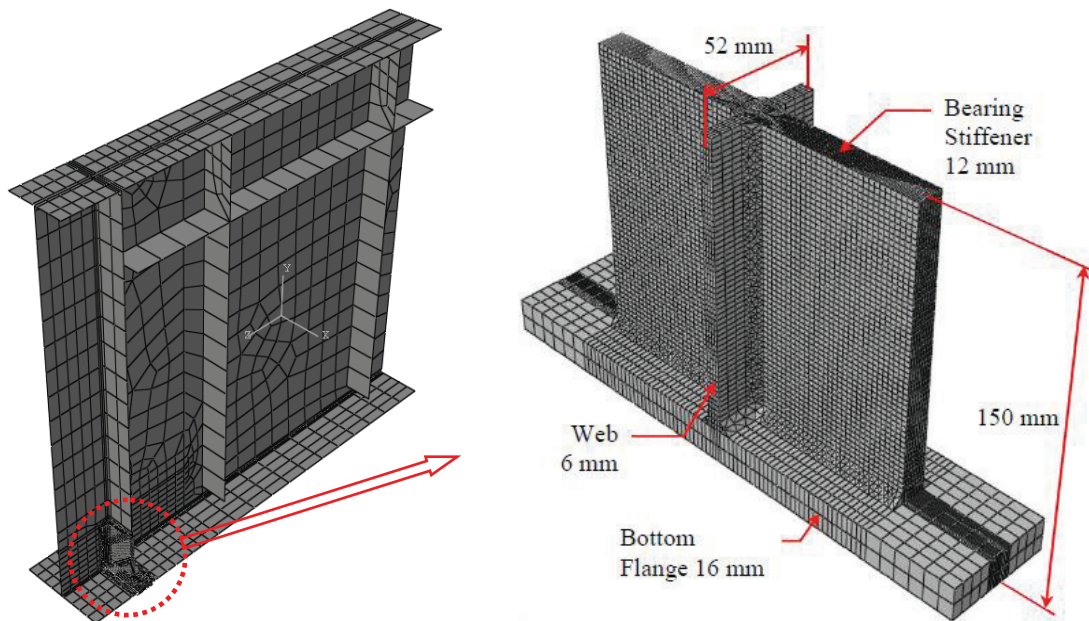


Figure 5.3: Meshing details of the Shell-Solid coupling model

Since one of the objectives of study is to examine the effect of local damage of bearing stiffener near weld seams, on its bearing capacity and maximum local damage and maximum damage to investigate in the analytical program is 100 mm. Thus, only a small portion of the bearing region with a total height of 150 mm including the bearing stiffener and flange thickness was modeled using the solid element. Normally, for the simulation of very small local damage or pitting corrosions a relatively fine mesh is used. Therefore, in the present study for the meshing of the solid part, bearing stiffener and web are divided into 16 and 4 divisions in thickness direction respectively, while a mesh size of 2.5x2.5 mm and 5x2.5 mm was mapped on the stiffener and web area. In the shell part fine mesh is only used near the

connecting region whereas, rest of the shell portion a relatively coarse mesh was used. The complete dimensions of the solid part and meshing detail are illustrated in Figure 5.3.

5.4 BOUNDARY CONDITIONS AND MATERIAL PROPERTIES

A mild steel JIS-SS400 with true stress-strain relationships, isotropic hardening effect and von Mises yield criteria was used in the analytical study due to the possibility of large deformations and strain, particularly after buckling. The material properties of SS400 steel used in the test specimens were determined by performing tensile tests in the laboratory. For the tensile test, coupons were cut from the used plate girder test specimens. The complete material plasticity data of JIS-SS400 steel used in different plates of test specimens is given in Figure 4.5 and Table 4.2 (Chapter 4).

5.5 INITIAL IMPERFECTIONS

Structural (residual stresses) and geometric imperfections are the two important parameters that play a vital role on the buckling strength of welded structures, especially when they are tested against compression.

5.5.1 Initial Deflections

The plated element and welded structures are always subjected to initial deflections due to manufacturing process and uneven heating and cooling effect in the welding process. Under in-plane loading the ideal plates without initial deflections demonstrate the bilinear behaviour and provide the sharp critical point and create bifurcation problem as illustrated in Figure 5.4(a). But in the real plates as shown in Figure 5.4(b) the initial out-of plane deviation will start growing in depth from the beginning of loading. There will not any sudden change occur in the rate of in-plane or out-of-plane deformation at the theoretical elastic critical buckling stress, but the rate will gradually increase until the maximum resistance or ultimate strength of the plate is reached. Subsequently as the resistance decreases, the in-plane and out-of-plane deformations continue to increase (Chatterjee, 2003).

The quantitative effects of initial out-of-plane deflections depend on the following factors.

1. The magnitude of the deflection
2. The pattern of the deflections
3. The type of the applied stresses or loading on the plate
4. The in-plane and out-of-plane edge conditions of the plate
5. The slenderness (i.e. the width-to-thickness ratio) of the plate and to a lesser extent its aspect ratio (i.e. the ratio of length to width).

Further, plates subjected to in-plane compression along one or both directions are most affected by initial deviations; plates in shear are least affected.

Plates with low slenderness, *e.g.* the width–thickness ratio (b/t) less than, say, 20 in the case of longitudinal in-plane compression or 50 in the case of in-plane bending or shear, are able to reach their squash loading, *i.e.* applied stress can be as high as the yield stress, in spite of any out-of-plane deviations. A more accurate measure of the plate slenderness is the parameter (β) which indicates that plates with identical dimensions but of higher yield stresses are effectively more slender, in the sense that the ratio of their ultimate strength to yield strength is more reduced. The slenderness parameter, β value has been described in equation (5.1).

$$\beta = b/t \cdot \sqrt{\sigma_y / E} \quad (5.1)$$

Where, b and t are the width and thickness of the plate, respectively and σ_y are the yield stress of the steel.

The Committee of Initial Deformation Measurement, IDM (1980) by *Japanese society of steel construction* categorizes initial deflections as out-of-flatness of subpanel, out-of-straightness of stiffener and stiffener camber deflection as shown in Figure 5.5. Mateus (2001) stated that initial deflections affect the buckling, and post buckling strength of stiffened plates, especially when they are loaded under uniaxial compression. These initial deformations contribute to one of the elastic buckling mode and eliminate the bifurcation

problem of structural behaviour under compression loading. Normally, all design codes like in USA, AASHTO (2007) and ANSI/AWS (2008) by American welding society and IDM (1980) by Japanese society of Steel construction specify the maximum tolerable limits of these initial imperfections.

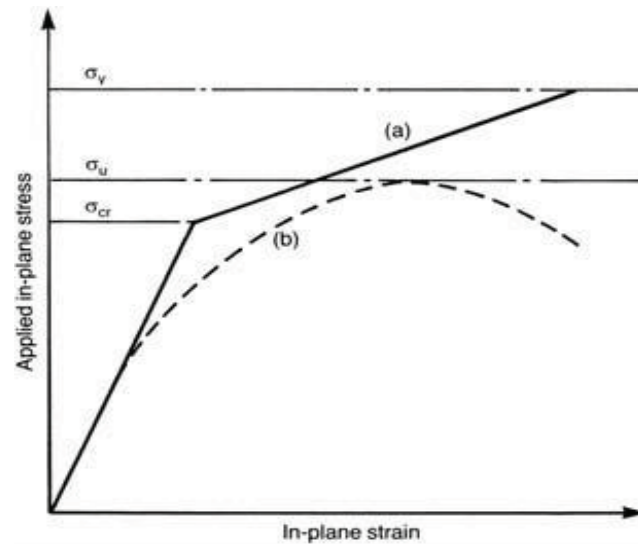


Figure 5.4: Buckling behavior of plates with initial out-of-plane deviation
(a) Ideally flat plate, (b) plate with initial out-of-plate deviation

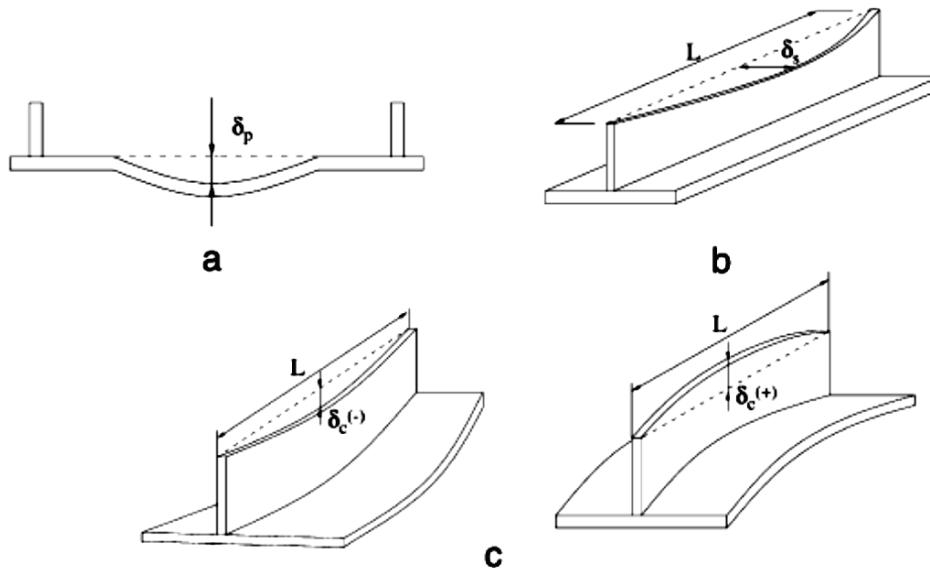


Figure 5.5: Typical initial imperfections of stiffened panels: (a) out-of-flatness of a subpanel;
(b) out-of-straightness of a stiffener; (c) stiffener camber deflection. (IDM, 1987)

For the numerical study there are many proposals regarding the inclusion of the initial deflections, but most of the researchers (Ok *et al.* 2007, Paik 2002) have used the deflection values suggested by Smith (1988) as given in the Table 5.1. As actual imperfections were not measured in this study therefore, an average initial deflection value equal to $0.1\beta^2$ was used.

Generally, initial deflections are introduced in form of the half sign wave in both orthogonal directions of the interior web panels. However, in the stiffener and free end of the web, it is provided as quarter of the sine wave in transversal direction, and half sine wave in longitudinal direction by using the expression given in equation (2) (Tamagawa 2010, Dunbar 2004).

$$w_0(x,y) = w_{0\max} \cdot \sin\left(\frac{\pi \cdot x}{L}\right) \cdot \sin\left(\frac{\pi \cdot y}{L}\right) \quad (2)$$

In this study, the initial deflections were incorporated by using the scaled deformations from the elastic buckling (eigenvalue) analysis as used by many other researchers (Choi *et al.* 2009). For this purpose an elastic buckling analysis was conducted on each model and scaled displacement values were superimposed to the actual geometry to introduce initial deflections. Figure 5.6 shows a typical buckling mode corresponding to first eigenvalue, used to induce the initial deflection in the FE model.

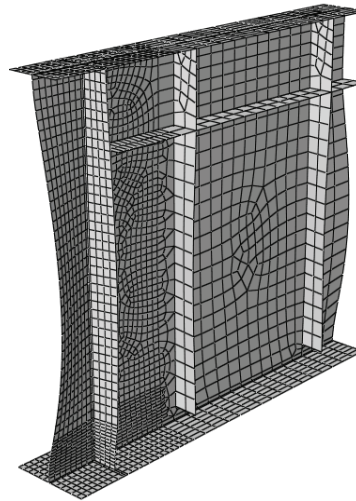


Figure 5.6: Buckling mode corresponding to first eigenvalue

Table 5.1: Imperfections and residual stresses values by Smith *et al.* 1988

Level	Imperfection (δ_p/t_p)	Residual stress ratio (σ_{RC}/σ_y)
Slight	$0.025\beta^2$	0.05
Average	$0.1\beta^2$	0.15
Severe	$0.3\beta^2$	0.3

5.5.2 Residual Stresses

Residual stresses in rolled steel sections are mainly caused by uneven cooling after rolling and in built-up sections fabricated by welding together several plates, the residual stresses are caused by the shrinkage of the material adjacent to the weld. Welding or flame-cutting induces very high temperatures in a localized strip. Shrinkage due to cooling of this strip is resisted by the remaining cold portion of the steelwork. As a result, the strip adjacent to the weld or flame cut is subjected to high tensile strains which may be several times the yield strain, and the rest of the steelwork is subjected to compression (SCC-399, 1997 and Chatterjee, 2003). A typical residual stress pattern in welded stiffened panel is shown in Figure 5.7.

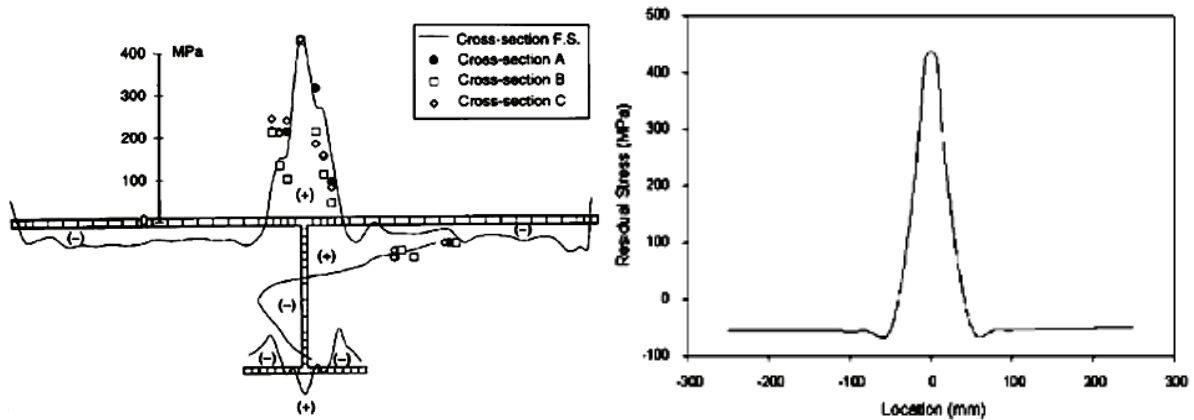


Figure 5.7: Residual stress distribution in the stiffened Panel (SCC-399, 1997).

(a) Experimental values, (b) average pattern of residual stresses

As compressive and tensile residual stresses in the cross-section are in balance condition, residual stresses do not cause any resultant axial force or bending moment on any cross-section. If it is possible for the whole of the cross-section to squash, *i.e.* yield in compression,

then the axial load or bending moment capacity of the cross-section will be unaffected by residual stresses. However, those parts of the cross-section where the residual stress is of the same nature as the applied stress will reach yield stress earlier.

For the strength of plate panels in compression the important question is whether the plate panel, in a residual-stress-free condition, behaves in a stable or unstable manner when the axial straining is continued after it reached its maximum capacity. This is described in Figure 5.8. For the case of plate (a), in the residual-stress-free condition the plate continues to sustain the peak load σ_u when further strained. The same stiffened plate cross-section with welding residual compressive stress σ_R deviates from its initial primarily linear behaviour at an applied stress $(\sigma_u - \sigma_R)$, but with further applied strains reaches an ultimate load σ'_u which is almost the same as or just below σ_u .

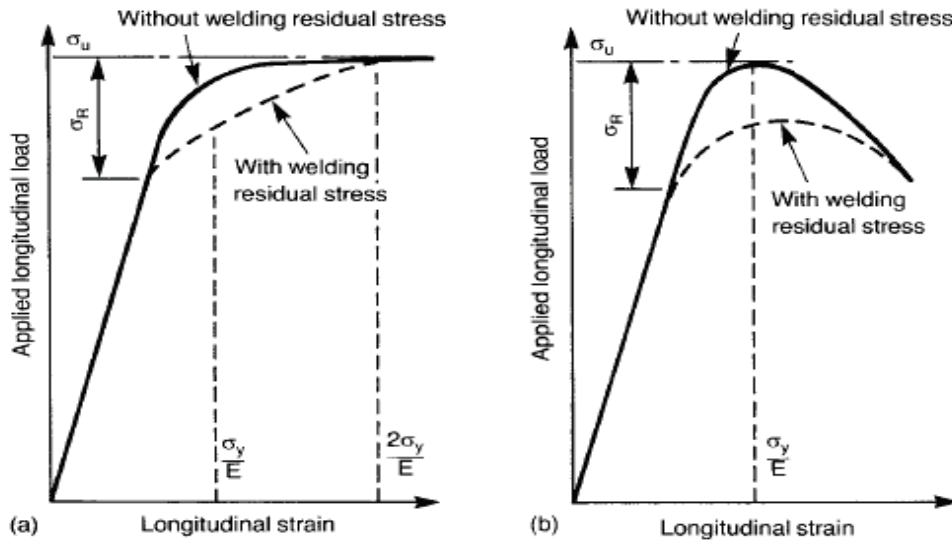


Figure 5.8: Behaviour of plates in compression, with and without welding residual stress.

Plate with (a) stable post-buckling behaviour, (b) unstable post-buckling behaviour

For the case of plate (b), in the residual-stress-free condition the plate sheds off its axial load when the straining is continued beyond the peak strength σ_u ; with residual stress the plate reaches a peak strength σ_{0u} which is substantially below σ_u . Stocky plates, i.e. with b/t ratios such that the critical buckling stress σ_{cr} is more than twice the yield stress σ_y , behave like Figure 5.8(a); so do very slender plates, i.e. those with critical buckling stress less than half

the yield stress. But plates with intermediate slenderness, i.e. with critical buckling stress between half and twice the yield stress, tend to behave as in Figure 5.8(b), and their strength is thus affected by the level of welding compressive residual stress.

The inclusion of residual stresses is very important for the welded structures, especially when they are tested against compression as they cause immature yielding and loss of stiffness (Fujikubo 1999). Usually an idealized residual stress field composed of a tensile rectangular block in the welded region and two compression stress blocks each on the both sides of the welded region is used in the numerical analysis. The Figure 5.9 shows the simplified distribution of the residual stresses in the plate girder. In this particular study, tensile residual stresses equal to the yield stress and compressive stresses equal to the 30% of the yield stress were assumed as suggested by other researchers and specification (Hung *et al.* 2002, Guidelines of the buckling design 2005). The precise distribution of desired residual stresses was generated by the thermal stress analysis. For this purpose, a combination of the negative and positive temperature field in the welded and the other plate regions was applied, respectively. After trial and error process the positive and negative temperature are fixed as $75\text{ }^{\circ}\text{C}$ and $-142\text{ }^{\circ}\text{C}$ respectively, to produce the desire residual stresses the coefficient of thermal expansion was assumed equal to the $11.0 \times 10^{-6}\text{ K}^{-1}$.

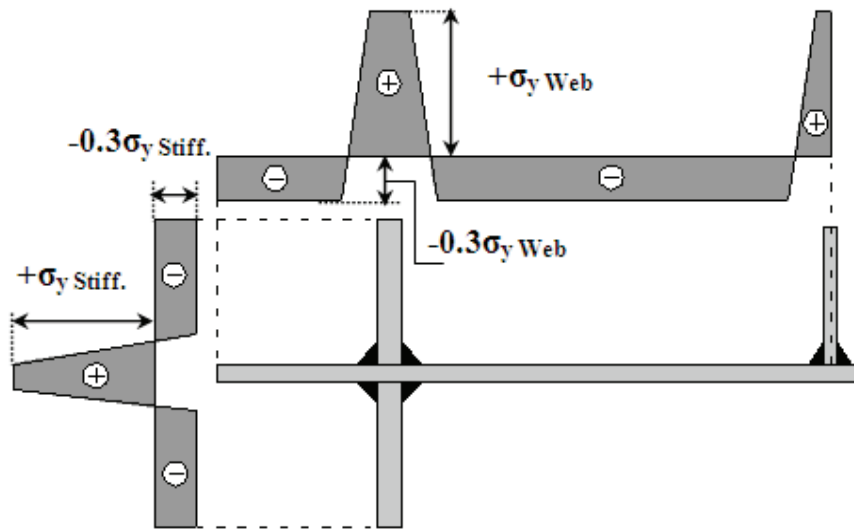


Figure 5.9: Typical welding residual stresses in the plate girder end

5.6 MODEL VERIFICATION

For the extension of the analytical study, the validity of FE model and solution is very important. For this purpose load-displacement curves and buckling modes obtained from analytical results were compared with the experimental results to verify the FE model.

5.6.1 Verification of Healthy Specimen

In the analysis, the peak load is almost the same in both healthy and damaged specimen as obtained from the experimental results. However, the initial stiffness is a little higher both in the shell-solid coupling and shell model as can be seen from the Figure 5.10. The welded structures under the axial compressive loading usually exhibit such difference in the initial stiffness due to the precise consideration of the residual stresses. The similar difference was also found in the study conducted by some other researchers like Hung *et al.* (2002). Due to less flexibility and not consideration of the stresses in out of plane direction the shell elements formulation provides a relatively higher initial stiffness than the shell-solid coupling model. As in this particular study, ultimate capacity against buckling is the main concern therefore, initial stiffness may be ignored. Figure 5.11 illustrates that both the shell and shell-solid coupling model demonstrated the identical buckling mode in web and stiffener as of the experimental specimens.

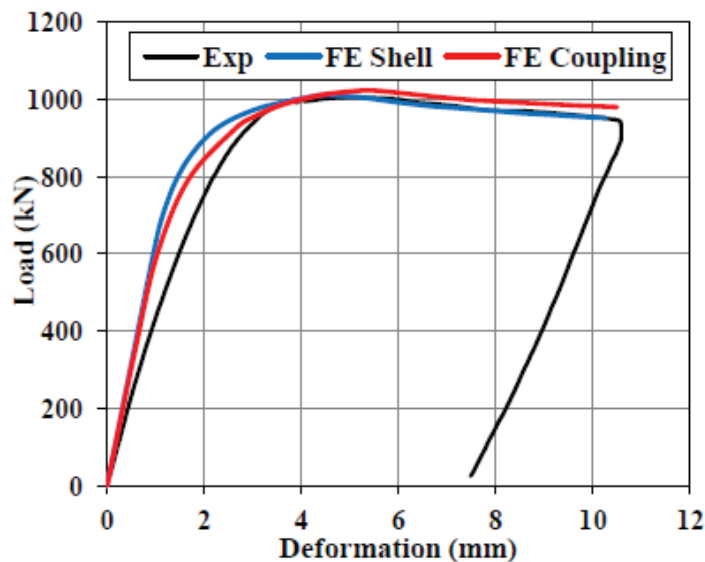


Figure 5.10: Verification of load-displacement curve of healthy specimen


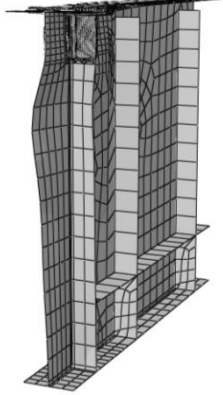
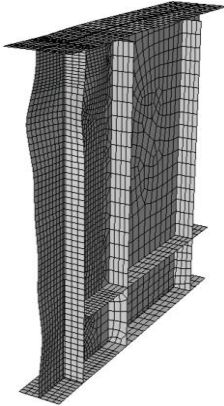


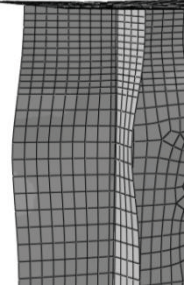
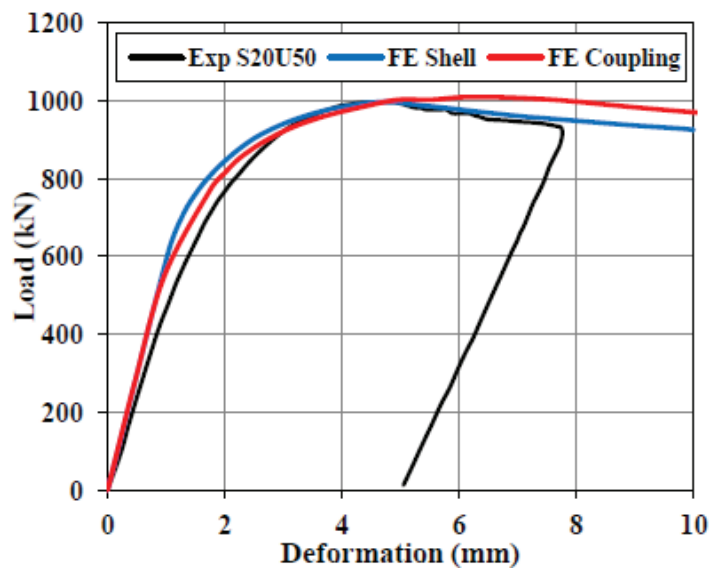
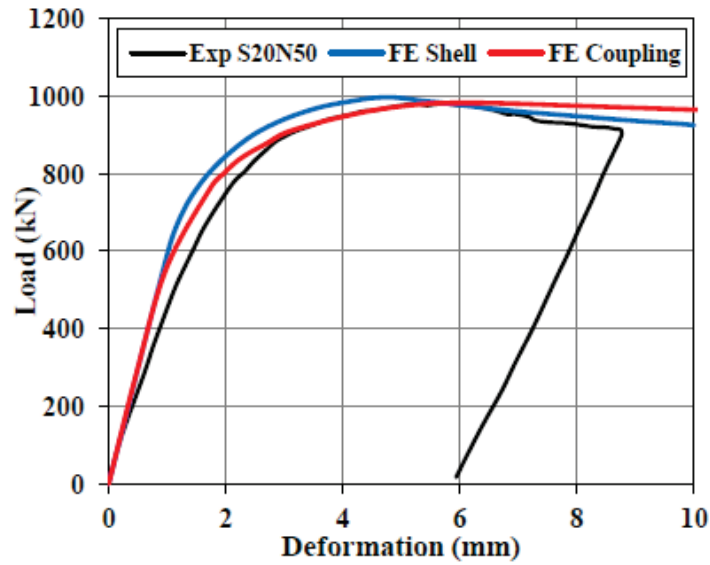
(a) Buckling in web			
(b) Buckling in Stiffener			
	Experimental	Coupling Model	Shell model

Figure 5.11: Verification of deformed shapes of healthy specimen

5.6.2 Verification of Specimens with 20mm Damage



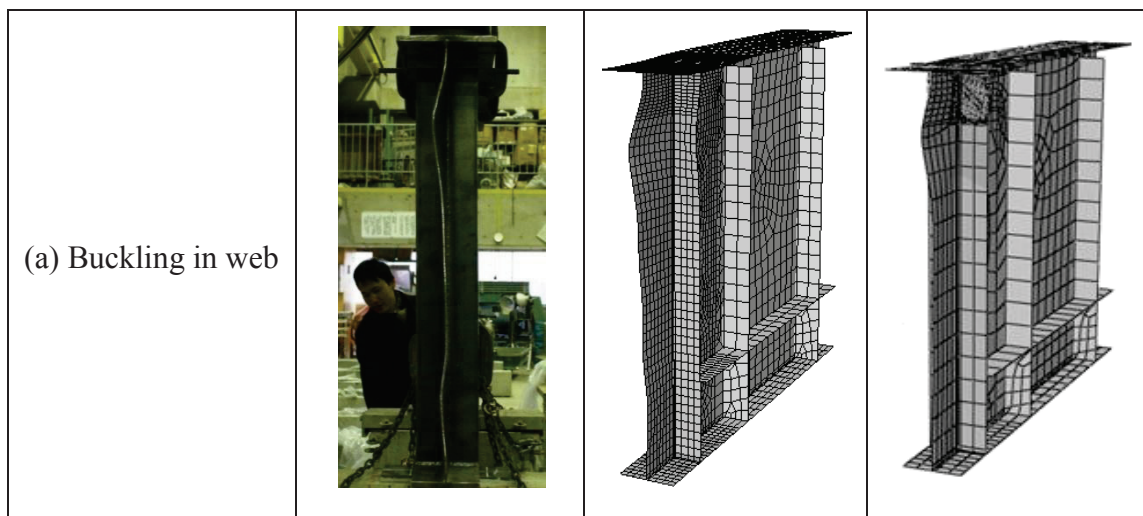
(a) Uniform damage, S20U50



(b) Non-uniform damage, S20N50

Figure 5.12: Verification of load-displacement curves of specimens with $D_h = 20\text{mm}$

The verification of load-displacement curves of both uniform and non-uniform damage with 20mm height is presented in Figure 5.12 where analytical results show the good agreement with the experimental results. Moreover, failure modes obtained from shell and shell-solid coupling formulation are also consistent with tested specimens as shown in Figure 5.13 and Figure 5.14.




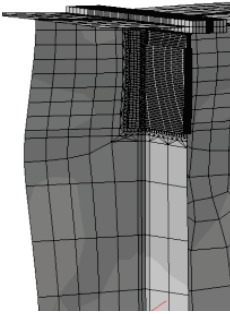
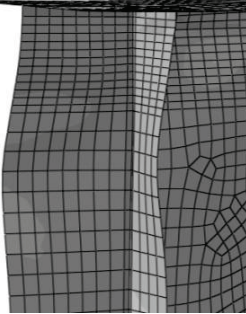
(b) Buckling in Stiffener			
	Experimental	Coupling Model	Shell model

Figure 5.13: Verification of uniformly damaged (S20U50) specimens with $D_h = 20\text{mm}$


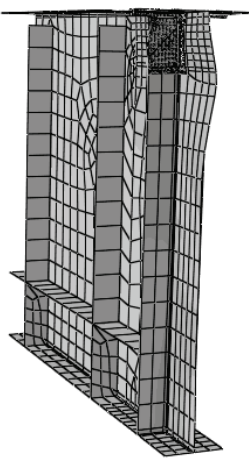
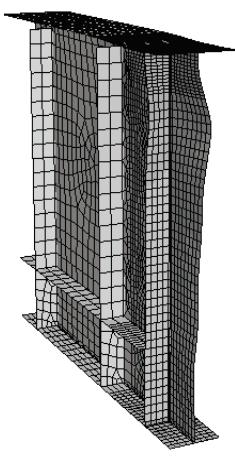

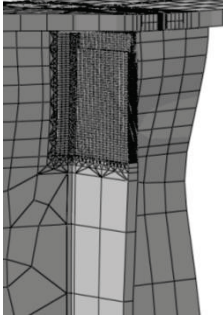
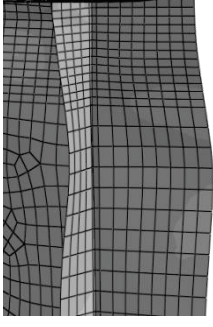
(a) Buckling in web			
(b) Buckling in Stiffener			
	Experimental	Coupling Model	Shell model

Figure 5.14: Verification of non-uniformly damaged (S20N50) specimens with $D_h = 20\text{mm}$

5.6.3 Verification of Specimens with 60mm Damage

Figure 5.17 (a) & (b) show the verification of load-displacement curves for both uniform (U) and non-uniform (N) types of the damage with 60mm damage height respectively. The analytical results confirm the validity of the FE model as they demonstrate the approximately, same ultimate load and deformed shapes *i.e.* Local buckling in bearing stiffener damage zone along with buckling in the web as can see from the Figure 5.15 and 5.16.


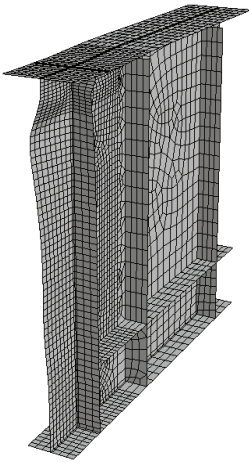
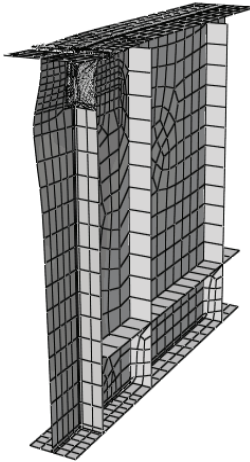
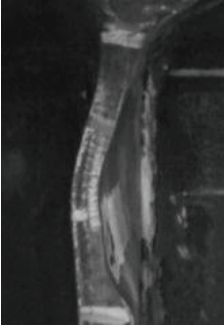
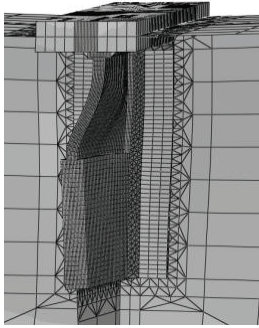
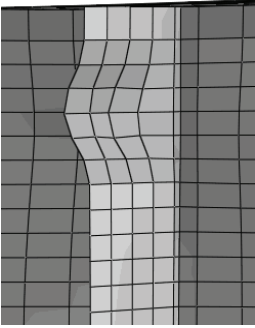
(a) Buckling in web			
(b) Buckling in Stiffener			
	Experimental	Coupling Model	Shell model

Figure 5.15: Verification of uniformly damaged (S60U50) specimens with $D_h = 60\text{mm}$


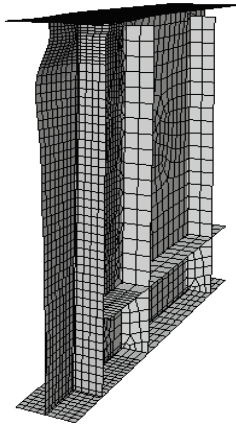
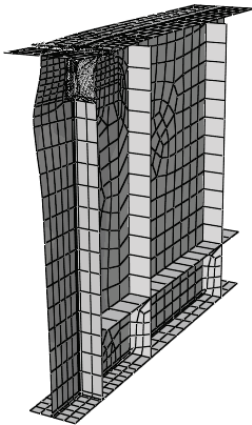

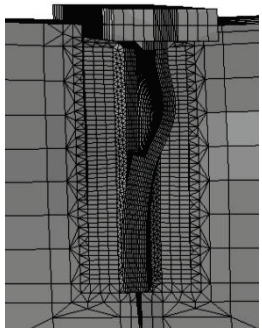
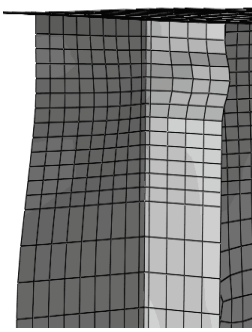
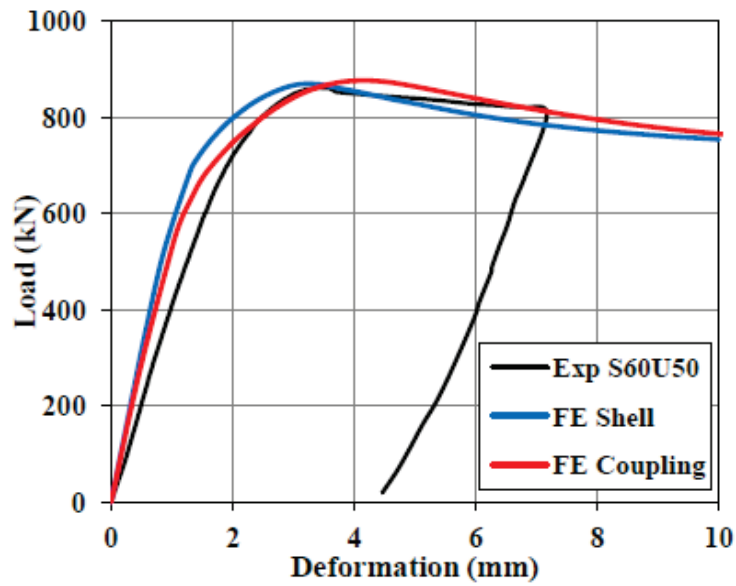
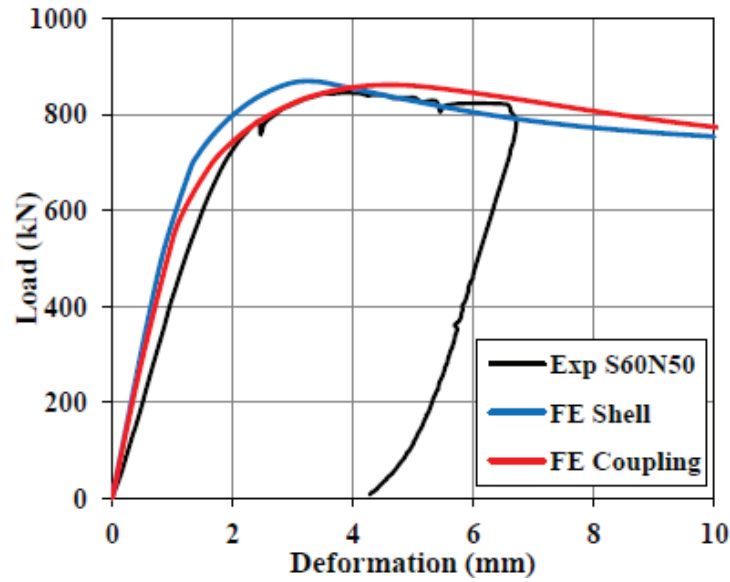
(a) Buckling in web			
(b) Buckling in Stiffener			
	Experimental	Coupling Model	Shell model

Figure 5.16: Verification of non-uniformly damaged (S60N50) specimens with $D_h = 60\text{mm}$



(a) Uniform damage, S60U50



(b) Non-uniform damage, S60N50

Figure 5.17: Verification of load-displacement curves of specimens with $D_h = 60\text{mm}$

5.7 EXTENSION OF ANALYTICAL STUDY

5.7.1 Number of Analytical Cases

In order to study the effect of local damage the analytical study was extended to various damage thicknesses of bearing stiffeners corresponding to different damage height zones. All damage cases studied are listed in Table 3.

Table 5.2: Analytical cases used in the study

Damage Height		Residual Thickness			
		75% ($t=9\text{mm}$)	50% ($t=6\text{mm}$)	25% ($t=3\text{mm}$)	Zero ($t=0\text{mm}$)
D_h (mm)	D_h/d (%)				
20	1.8	S20t75	S20t50	S20t25	S20t0
40	3.6	S40t75	S40t50	S40t25	S40t0
60	5.4	S60t75	S60t50	S60t25	S60t0
80	7.2	S80t75	S80t50	S80t25	S80t0
100	9	S100t75	S100t50	S100t25	S100t0

A typical damage in Table 5.2 is described as following *i.e.* S20-t75, where S20 represents a stiffener damage (S) of 20mm height, and t75 as 75% residual thickness (9mm) within the damaged stiffener zone whereas, the original thickness of the bearing stiffener is 12mm. Usually, corrosion damages a very shallow region of bearing stiffener and adjacent web, as also clear from the Figure 5.1 and 5.2. Therefore, a maximum damage height of 100mm was used in the analytical program.

5.7.2 Idealization of Damage Shape

In real cases corrosion yields irregular damages on the steel structure however, for the simplicity a regular and uniform type of the damage is usually incorporated in the FE simulation. Ok *et al.* (2007) used a rectangular shaped corrosion damages in his study for the concentrated pit corrosion. He used this effective cross-section by believing that ultimate strength of corroded plate under uniaxial compression is influenced by the smallest cross section. However, for the further clarification of simple damage shape, three different damage cases as described in Figure 5.18 were used with 50% section loss for all the damage heights considered in the study. In the damage case Trans.1 the damage height is considered from center to center of the transition zones whereas, in Trans.2 the damage height was considered from the edge of the transition zones at thicker part as marked in Figure 5.18.

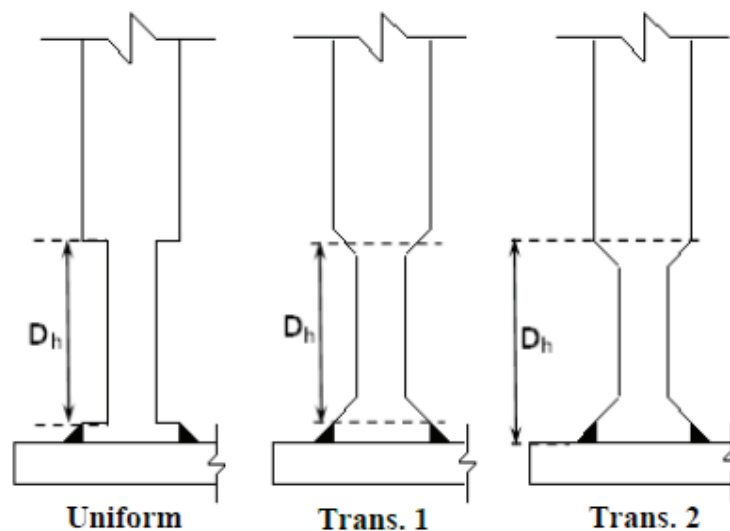


Figure 5.18: Different trail damage shapes

Figure 5.19 shows the simulated shape of the triangular type of the trial damage. The section was reduced gradually by using 1:1 slope. For the small damage height like 20mm, uniform rectangular type of damage demonstrated the ultimate capacity a little less than that of other cases as clear from the Figure 5.20 but in all the other cases where damage height is greater than 40mm all the trial cases revealed almost the same ultimate strength. As this study focus only on the corrosion damages ignoring the fatigue problem, a simple uniform rectangular type of the damage was considered in the entire analytical study.

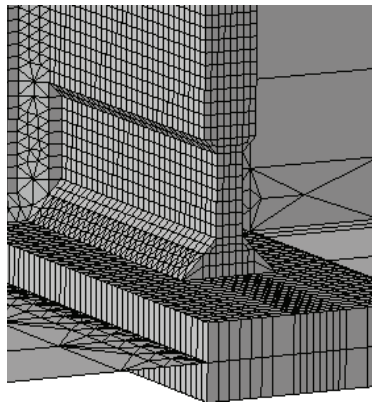


Figure 5.19: Mesh of triangular type of damage

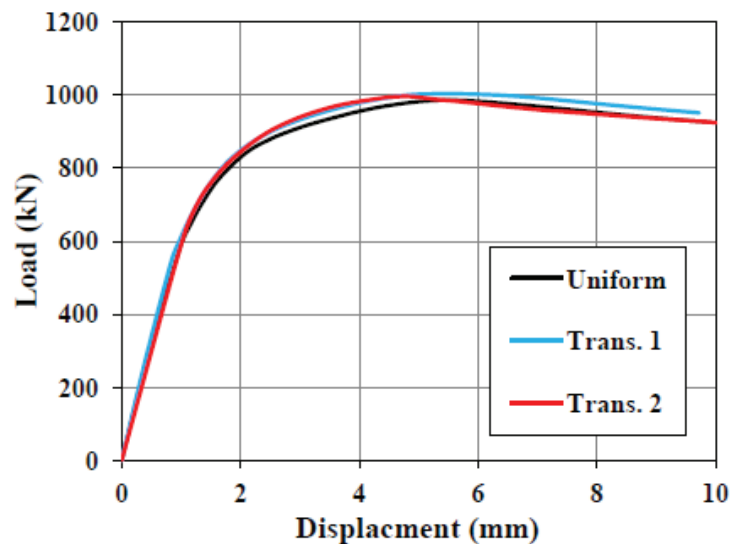


Figure 5.20: Load-displacement curves of different damage shapes for $D_h = 20\text{mm}$ with 50% section loss

5.7.3 Effect of Corrosion Damage Form

As corrosion highly depends on the exposure conditions and it may proliferate into thickness, either from one or both side of the section. Thus, the residual thickness within any corrosive damage may be uniform, non-uniform or straggle in nature as highlighted in Figure 5.21. These different damages forms, possessing the same damage height may exhibit the different behaviour of load-displacement relationships. To clarify the effect of various damage conditions, there different damage forms as mentioned in Figure 5.21 are studied for the all the analytical cases mentioned in Table 5.2.

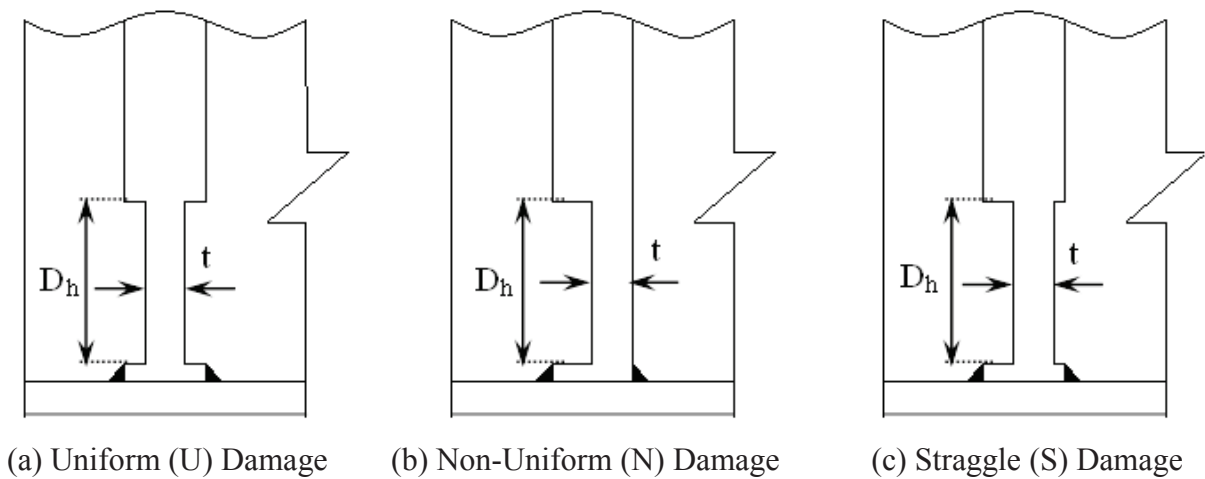
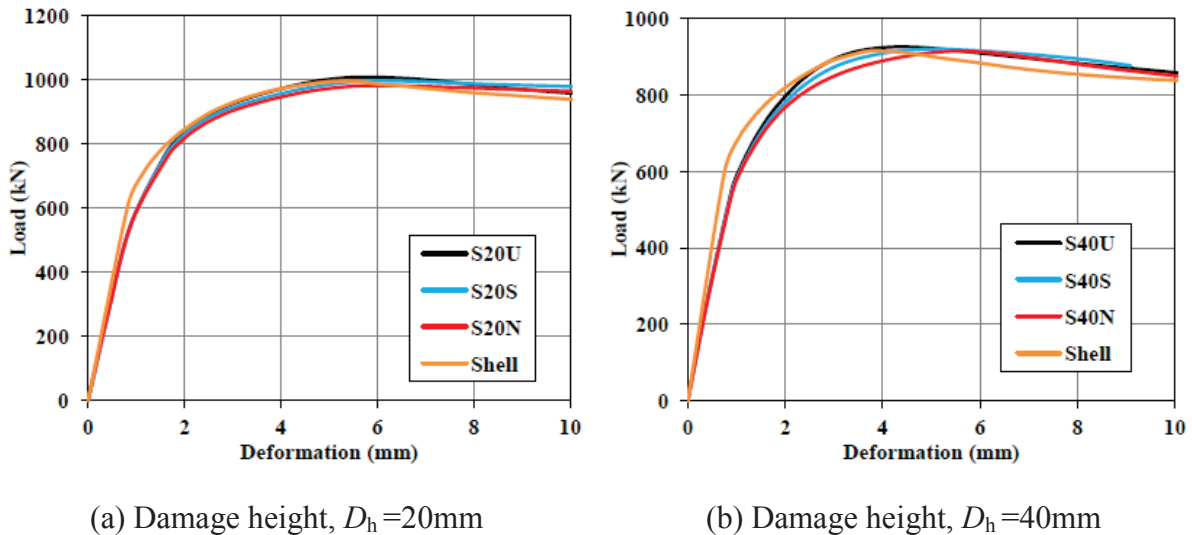


Figure 5.21: Various damage forms considered in the study



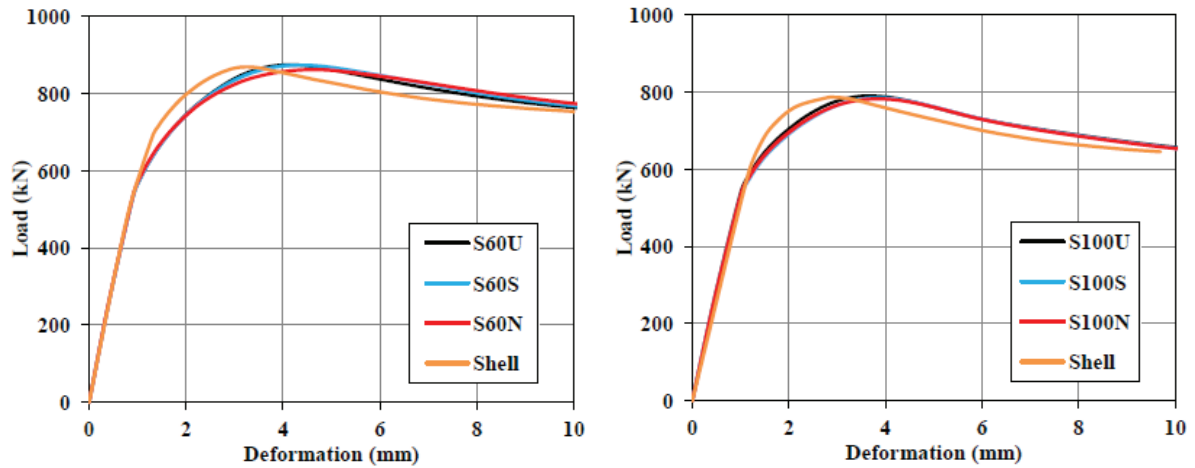
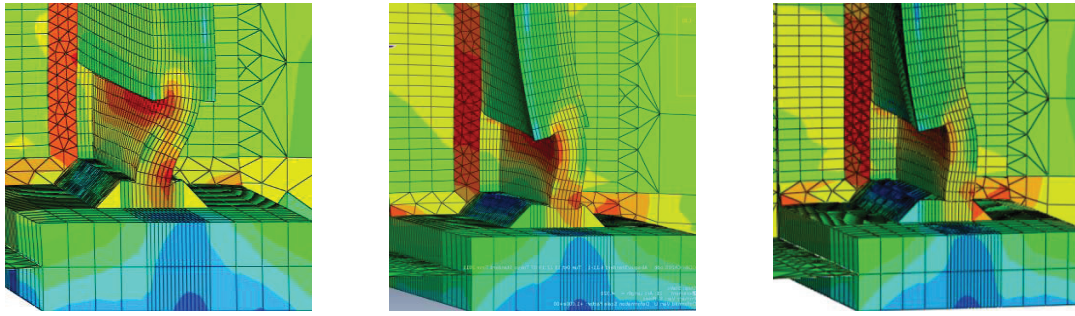
(a) Damage height, $D_h = 60\text{mm}$ (b) Damage height, $D_h = 100\text{mm}$

Figure 5.22: Effect of various corrosion forms for different damage heights with 50% residual thickness

For the comparison purpose, load-displacement curves of all damage forms are compared with each other and with the results obtained from the shell formulations. However, in Figure 5.22 results of various damage shapes only with 50% residual thickness for different damage heights are illustrated. The small damage height like 20mm and 40mm exhibited a little higher strength for the case of uniform (U) damage as compared with other forms of the damage as clear from the Figure 5.22 (a) & (b).

It is due to the reason of local yielding and plastic constraint against the deformation within the damage zone (Figure 5.23(a)) and due to lesser confinement and constraint from one side only, the non-uniform type of the damage depicts a relatively less ultimate load as can be judged from the Figure 5.23(c). However, the plastic constraint effect decreases with the increase of the damage height, which is quite evident in the Figure 5.24 where similar buckling modes of different damage forms for the 100mm damage height can be seen. Thus, all the damage forms almost provide the same ultimate load and load-displacement trends as can be seen in the Figure 5.22 (b) & (c). Being relatively less flexible in nature and not considering the strain in the out of plane direction shell element demonstrates the initial stiffness a little higher than the solid elements but Figure 5.21 shows that shell elements model depicts the ultimate load in a quite good agreement with the shell-solid element.

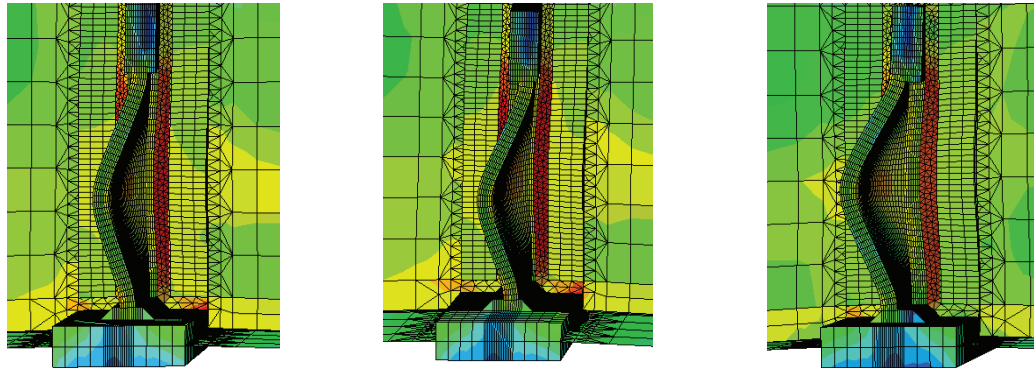


(a) Uniform, U

(b) Straggle, S

(c) Non-uniform, N

Figure 5.23: Buckling of different stiffener damage forms for 20mm damage height



(a) Uniform, U

(b) Straggle, S

(c) Non-uniform, N

Figure 5.24: Buckling of different stiffener damage forms for 100mm damage height

5.8 ANALYTICAL RESULTS

5.8.1 Load-Displacement Curves

The comparison of capacity curves are made by plotting the load versus vertical displacement corresponding to different damage heights " D_h " for the same residual thickness " t " of bearing stiffener in the damage height zones. It can easily be seen in Figure 5.25 that reduction of bearing stiffener thickness decreases the bearing capacity for the all damage heights. However, this reduction is very less for the cases with smaller damage height. The Figure 5.25(a) clearly shows that 25% reduction of bearing stiffener thickness does not reduce the capacity remarkably for any damaged height and all curves are almost identical. But on the other hand, the complete loss of the bearing stiffener (Figure 5.25(d)) causes the significant

loss in the bearing capacity and decreases the stiffness of plate girder. The Figure 5.25(b) demonstrates the decrease in the peak load displacement values for the damage height greater than the 20mm, which are due to the local buckling of the stiffener. In the Figure 5.25(c) the reduction of the peak load and displacement is a function of both the local buckling of stiffener and large damaged height.

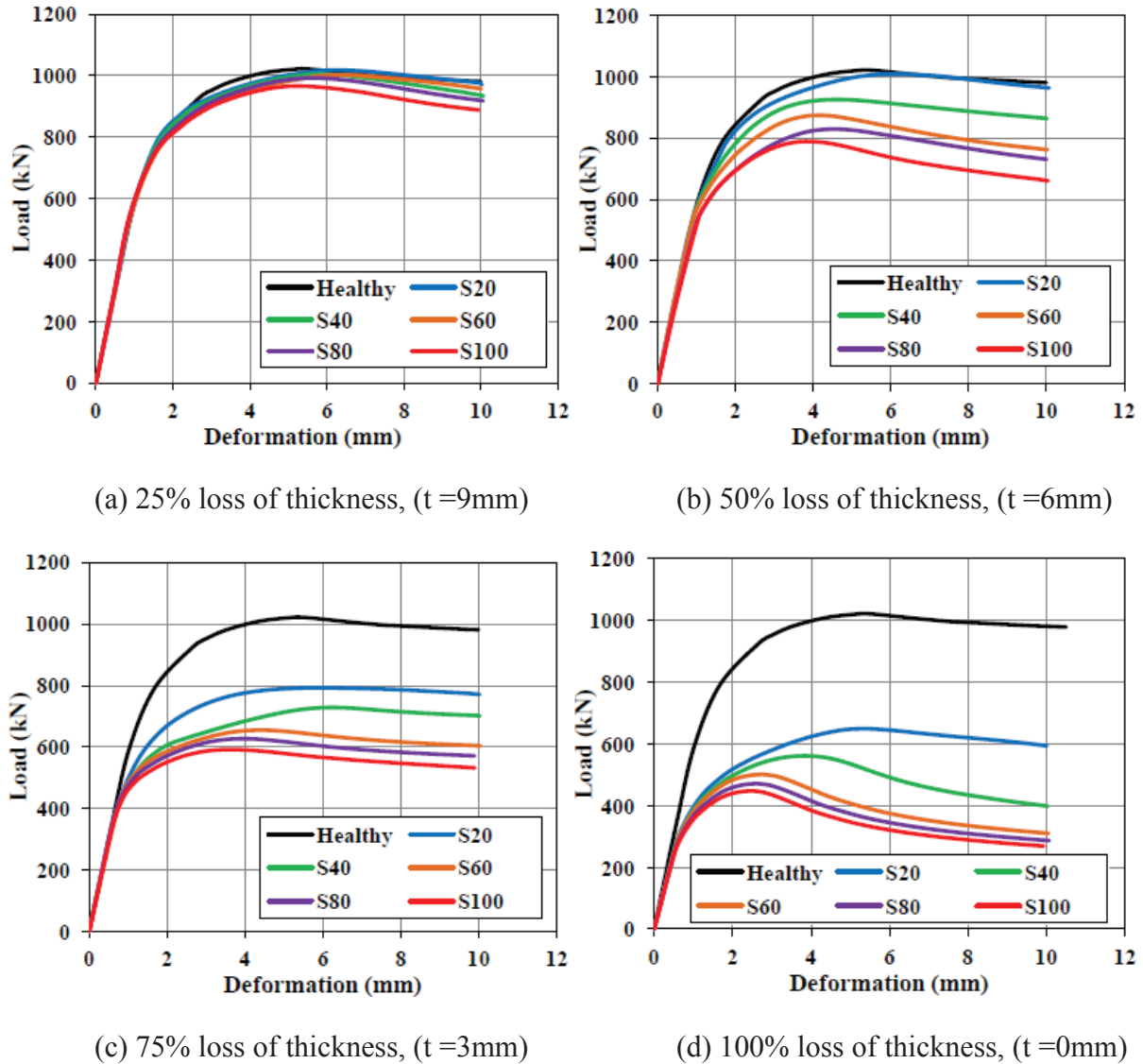


Figure 5.25: Load capacity curves for different damage heights

5.8.2 Buckling Failure Modes

The effect of the corrosion on bearing capacity can also be judged by failure (buckling) modes from the numerical models. Failure modes obtained from FE analysis are categorized into three different types, *i.e.* Normal Buckling, Crippling and Local Buckling. The out-of-plane deformation over most of the depth of the web is defined as the Normal Buckling whereas, crippling is localized buckling of both web and stiffener in the presence of plasticity within the damaged region and Local Buckling is defined as local deformation only within the damaged bearing stiffener zone with normal buckling trend in the web.

It is quite clear from failure modes of the healthy specimen and case S100t75, as shown in Figure 5.26, that 25% of the reduction of the stiffener thickness does not change the buckling shape of the web and stiffener. It means that there is no remarkable stress concentration in the damage zone that results a slight reduction in the ultimate capacity. The 50% reduction of the bearing stiffener for all damage heights shifted the buckling only within the stiffener damage zone as shown in the case S100t50, where local buckling in stiffener is quite clear with the normal buckling trend in web. Thus reduction of strength is due to the stress concentration in the damaged stiffener zone. While a 75% loss of bearing stiffener thickness causes local buckling only in the cases where damage height is very small like 20mm as case S20t25 depicts. But for all the other cases it cause the local deformation both in bearing stiffener and web at the damage zone, which lead to the crippling of web and stiffener. The study also revealed that the complete loss of bearing stiffener material diminishes the role of the bearing stiffener and bearing strength is only incorporated by the web. The failure mode S40t0 in the Figure 5.25 shows the web crippling/crushing due to complete loss of the stiffener material.

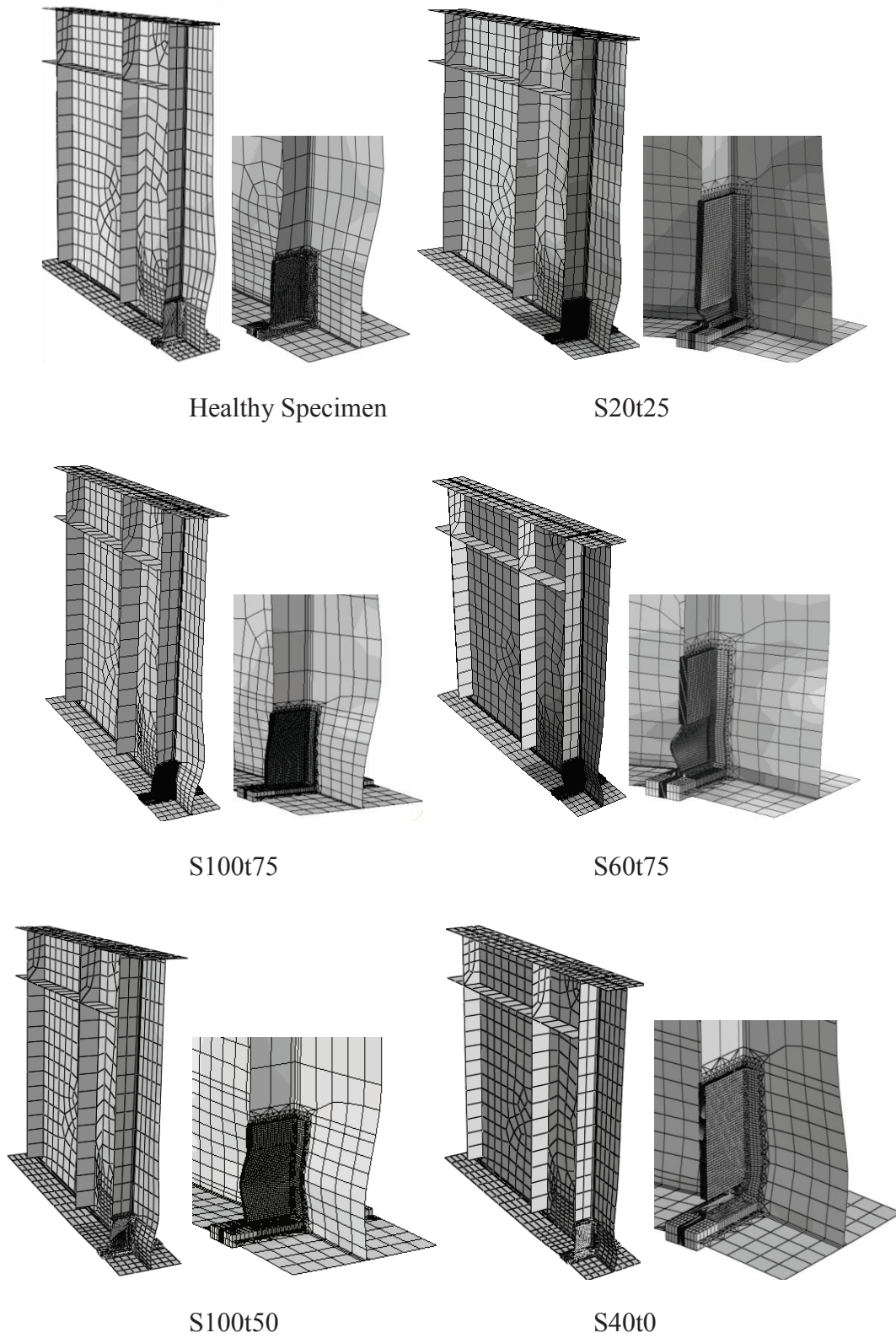


Figure 5.26: Deformed Buckling Modes

5.8.3 Comparison of Shell and Shell-Solid Coupling Results

The comparison of the analytical results of the shell-solid coupling and shell elements formulations are made to check the validity of both method as given in the Table 5.3.

Table 5.3: Comparison of ultimate capacity of shell and shell-solid models

Damage Height D_h (mm)	Analytical Case	Shell-Solid Coupling $P_{Coup.}$ (kN)	Shell P_{Shell} (kN)	$P_{Coup.}/P_{Shell}$
0	Healthy	1022.36	1011.84	1.0104
20	S20t75	1017.84	1007.47	1.0103
	S20t50	1008.84	996.51	1.0123
	S20t25	792.34	818.10	0.9685
	S20t0	649.35	698.96	0.929
40	S40t75	1004.37	994.73	1.010
	S40t50	925.93	915.97	1.011
	S40t25	728.91	732.75	0.9947
	S40t0	561.70	589.19	0.9533
60	S60t75	1002.34	986.04	1.0165
	S60t50	874.32	868.34	1.0069
	S60t25	654.39	660.08	0.9914
	S60t0	500.96	507.60	0.9869
80	S80t75	992.01	972.07	1.02051
	S80t50	829.68	818.86	1.0132
	S80t25	626.49	624.73	1.0028
	S80t0	470.90	478.09	0.9850
100	S100t75	966.38	952.44	1.01463
	S100t50	789.96	786.82	1.0039
	S100t25	591.41	612.64	0.9653
	S100t0	447.35	451.82	0.9901

As already expressed in Figure 5.25, the ultimate capacity does not change significantly for different damage shapes therefore, in the Table 5.3 for the shell-solid coupling analysis ultimate capacities of only uniform type of the damage are mentioned.

Table 5.3 shows that shell-solid coupling analysis depicts the ultimate capacity slightly higher than the shell element analysis except for the cases where residual thickness is less than the 50% that is primarily due to high stress concentration in the damage zone. Through this investigation it can be concluded that if initial stiffness is not important than simple uniform type of the damage with minimum thickness criteria can be used in FE simulation to calculate the ultimate bearing capacity of steel plate girder locally corroded at bearings.

5.9 SERIES OF FE ANALYSIS

Since, the objective of study is to relate the extent of plate girder end damage with the ultimate capacity and failure modes thus, for this purpose the analytical study was extended to a series of the finite element analyses considering various damages cases as described in the Table 5.4 and Figure. 5.27. A typical uniform rectangular type of the damage in the stiffener and web region as already described in Figure 5.21(a) was considered in all damage cases. In Table 5.4 four different damage groups has been shown corresponding to damage heights in millimetre and also as percentage of the girder heights (D_h/d). In damage case S20t75, 20 shows the damage height in mm and t represents the residual thickness of the bearing stiffener and/or web in percentage of original thickness, *i.e.* t75 shows the thickness of stiffener and/or web as 75%. The original thickness of stiffener (t_s) and web (t_w) are 12mm and 6mm respectively. Field survey depicts that normally corrosion damages the very small portion nearby the bearing region (Figure 1.2 & 1.3). Therefore, maximum height of damage is considered as 100mm and length of the damage in the interior web region is considered equal to the free end length, which is 160mm for cases of test specimens used in the present study.

Table 5.4: Various analytical cases for bearing capacity analysis

D_h (mm)	D_h/d (%)	t (%)	Damage type	Analysis Case	t_s (mm)	t_w (mm)	Damage type	Analysis Case	t_s (mm)	t_w (mm)	Damage type	Analysis Case	t_s (mm)	t_w (mm)	Damage type	Analysis Case	t_s (mm)	t_w (mm)
20	1.8	75	Stiffener Damage only (S)	S20t75	9	6	Stiffener Plus Web Free End Damage (WES)	WES20t75	9	4.5	Stiffener Plus Inner Web Damage (IWS)	IWS20t75	9	4.5	Stiffener Plus Web Damage from both Sides (BWS)	BWS20t75	9	4.5
		50		S20t50	6	6		WES20t50	6	3		IWS20t50	6	3		BWS20t50	6	3
		25		S20t25	3	6		WES20t25	3	1.5		IWS20t25	3	1.5		BWS20t25	3	1.5
		0		S20t0	0	6		WES20t0	0	0		IWS20t0	0	0		BWS20t0	0	0
40	3.6	75		S40t75	9	6		WES40t75	9	4.5		IWS40t75	9	4.5		BWS40t75	9	4.5
		50		S40t50	6	6		WES40t50	6	3		IWS40t50	6	3		BWS40t50	6	3
		25		S40t25	3	6		WES40t25	3	1.5		IWS40t25	3	1.5		BWS40t25	3	1.5
		0		S40t0	0	6		WES40t0	0	0		IWS40t0	0	0		BWS40t0	0	0
60	5.4	75		S60t75	9	6		WES60t75	9	4.5		IWS60t75	9	4.5		BWS60t75	9	4.5
		50		S60t50	6	6		WES60t50	6	3		IWS60t50	6	3		BWS60t50	6	3
		25		S60t25	3	6		WES60t25	3	1.5		IWS60t25	3	1.5		BWS60t25	3	1.5
		0		S60t0	0	6		WES60t0	0	0		IWS60t0	0	0		BWS60t0	0	0
80	7.2	75		S80t75	9	6		WES80t75	9	4.5		IWS80t75	9	4.5		BWS80t75	9	4.5
		50		S80t50	6	6		WES80t50	6	3		IWS80t50	6	3		BWS80t50	6	3
		25		S80t25	3	6		WES80t25	3	1.5		IWS80t25	3	1.5		BWS80t25	3	1.5
		0		S80t0	0	6		WES80t0	0	0		IWS80t0	0	0		BWS80t0	0	0
100	9	75		S100t75	9	6		WES100t75	9	4.5		IWS100t75	9	4.5		BWS100t75	9	4.5
		50		S100t50	6	6		WES100t50	6	3		IWS100t50	6	3		BWS100t50	6	3
		25		S100t25	3	6		WES100t25	3	1.5		IWS100t25	3	1.5		BWS100t25	3	1.5
		0		S100t0	0	6		WES100t0	0	0		IWS100t0	0	0		BWS100t0	0	0

In the Table 5.4 the analytical cases are defined as following.

Analytical case WES20t75, represent the damage group type WES and remaining thickness (t) of stiffener and web as 75% of original thickness.

S: represents the damage group with the corrosion damage on bearing stiffener only

WES: represents the damage group with corrosion damage on the stiffener and web free end

BWS: represents the damage group with corrosion damage on the stiffener and web on both sides of the stiffener.

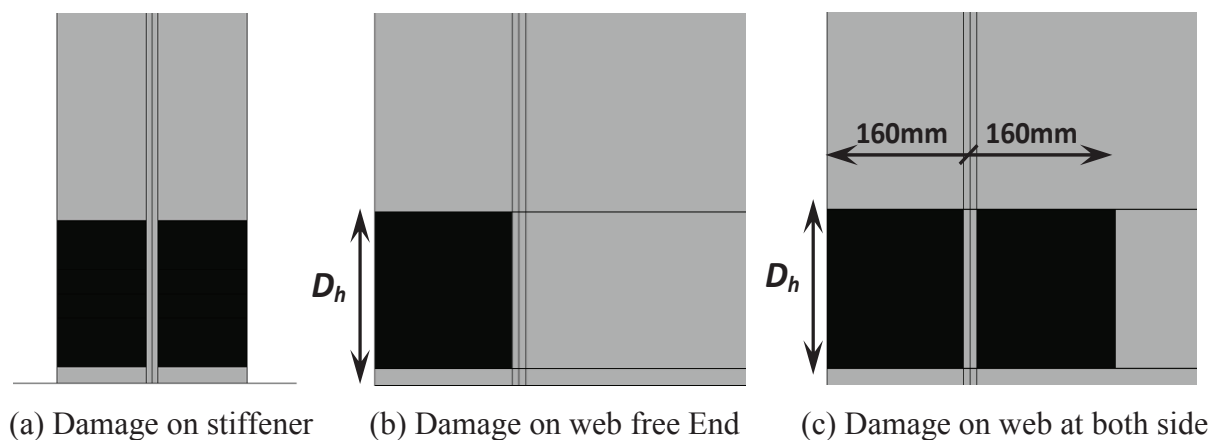


Figure 5.27: Various damage cases considered in the study

5.10 EFFECT OF WEB CORROSION ON LOAD CARRYING CAPACITY

Before analysing the web damage cases in combined with the stiffener damage, many trial analysis on the plate girder end were performed by considering the web damage only, without any stiffener damage to check the sensitivity of the web damages on the bearing capacity of plate girder.

5.10.1 Effect of Exterior Web Corrosion

Figure 5.28 illustrates that the only exterior web damage does not change critical load and initial stiffness of the plate girder end for any residual thickness with the maximum damage

height of 100mm considered in the study. It only reduced the ultimate strength fractionally. However, the post buckling strength remains almost the same.

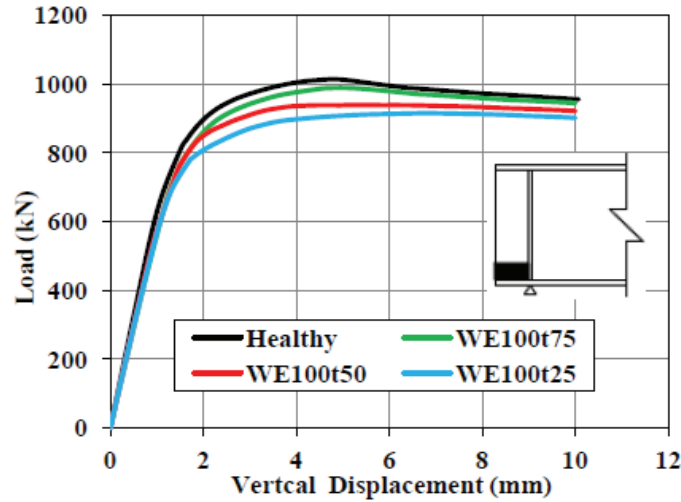


Figure 5.28: Effect of exterior web damage on bearing capacity

5.10.2 Effect of Interior Web Corrosion

The interior web damage also exhibits the identical trend of load-displacement curve as of the load displacement curve with the exterior web damage which is quite evident in Figure 5.29, where only small reduction in the ultimate capacity can be seen without any significant effect on the elastic critical load and post buckling strength.

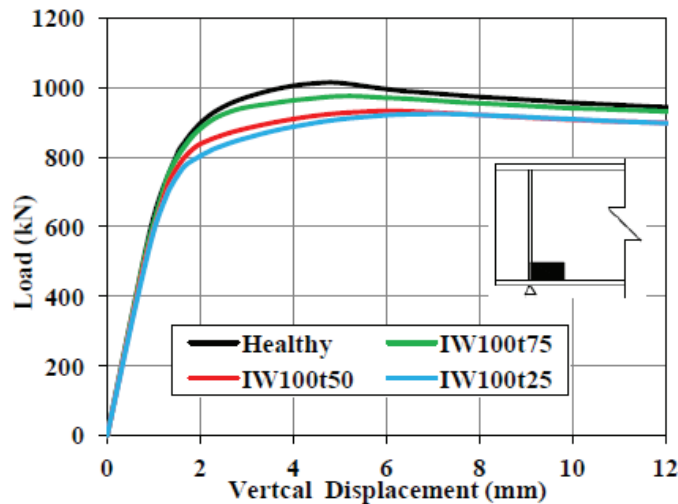


Figure 5.29: Effect of interior web damage on bearing capacity

5.10.3 Effect of Web Corrosion at Both Side of the Stiffener

It was also observed in the study that web damage from both side of the bearing stiffener does not reduce the strength significantly for the small damage height however, for the relatively large damage *i.e.* 100mm ($D_b/d = 9\%$) considered in the study it reduces the ultimate strength and post buckling strength only for the residual thickness less than the 0.5 as shown in Figure 5.30. Thus, web damages are not considered separately in the study and are combined with stiffener damage.

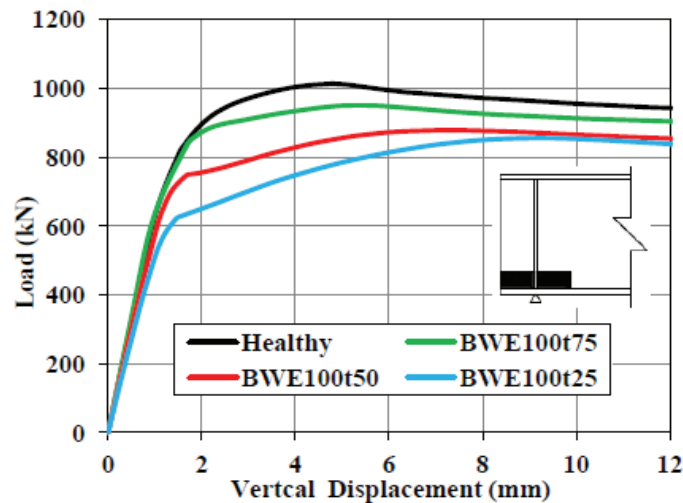


Figure 5.30: Effect of web damage at both side of stiffener on bearing capacity

5.11 BUCKLING FAILURE MODE

Generally, three different types of the failure modes, normal buckling, Crippling and crushing were observed from the FE analysis. Buckling of the web occurs with out-of-plane deformation over most of the depth of the web whereas, crippling is localised buckling of the web in the presence of plasticity and crushing is local yielding of the web without any buckling. Besides these failure modes, in some analysis case where reduction of the bearing stiffener is more than 50% and damage height is small, local buckling was found in stiffener accompanied with the over all buckling of the web. The typical deformed shapes obtained through analytical study have been shown in the Figure 5.31. The deformed shapes of all the analysis cases along with ultimate capacities P_{ult} and as the ratio with $P_{H,ult}$ are reported in the

Table 5.5. The study revealed that 25% reduction of the material in all the cases do not change the failure mode and a normal buckling mode as depicted by the healthy specimen was obtained with the exception of BWS100t25 where, failure mode is the local buckling in the damage zone along with overall buckling of the web. For the very small damage height with reduction of the stiffener and/or web plate more than 75 %, *i-e.* Cases of S20t75 and BWS20t0 the crushing type of the failure was found without any buckling of the web. In some cases where the bearing stiffener thickness is less than 50% and damage height is less than 40mm (3.6% of girder height) with/without web damage, a local buckling within the stiffener damage zone was observed. However, in the most of the cases where damage of stiffener and web is more than 50 % the crippling failure was obtained.

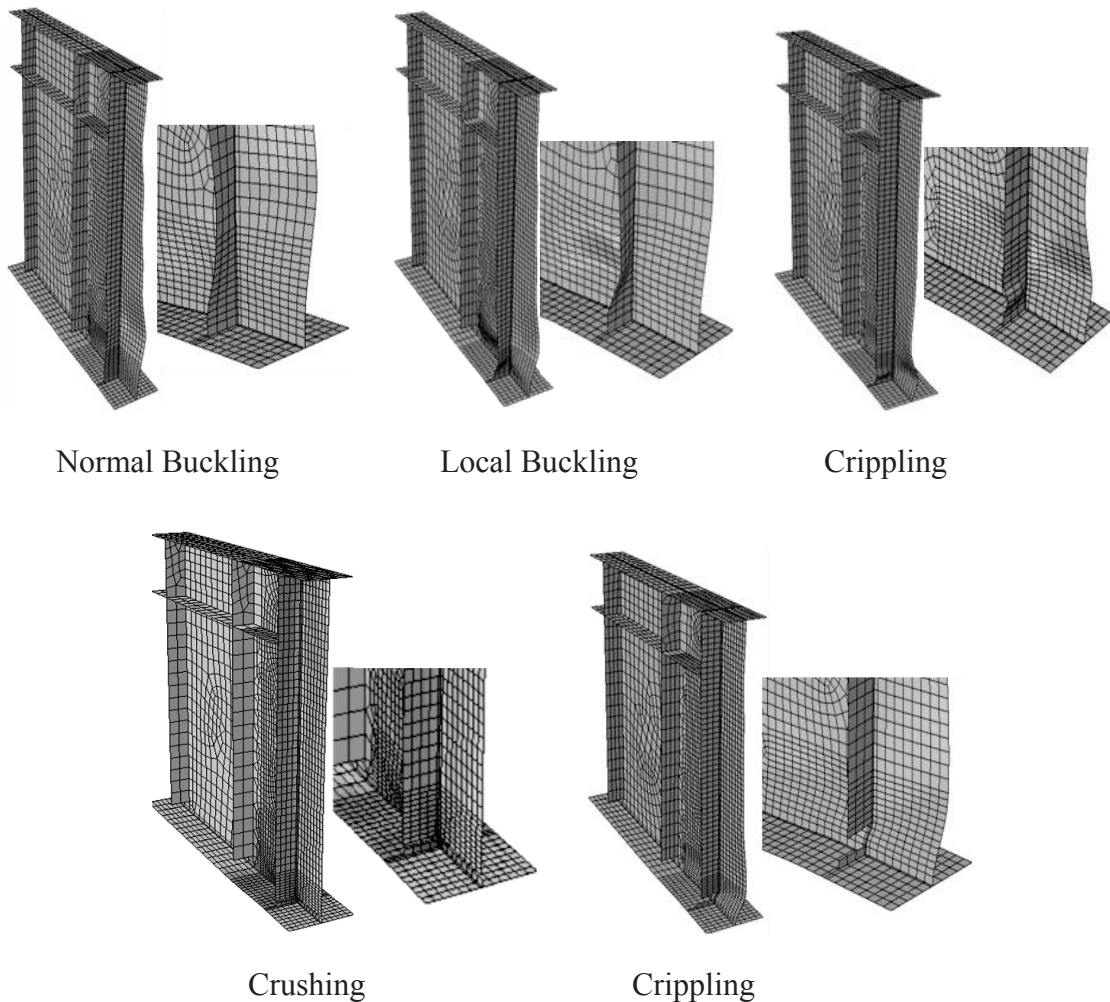


Figure 5.31: Various deformed shapes

Table 5.5: Ultimate bearing capacity and deformed shape for various analytical cases

Damage type	Analysis Case	P_{ult} (kN)	$P_{ult} / P_{H,ult}$	Failure mode	Damage type	Analysis Case	P_{ult} (kN)	$P_{ult} / P_{H,ult}$	Failure mode	Damage type	Analysis Case	P_{ult} (kN)	$P_{ult} / P_{H,ult}$	Failure mode
Stiffener Damage only (S)	S20t75	1007	0.996	Normal	Stiffener Plus Web Free End Damage (WES)	WES20t75	1005.2	0.993	Normal	Stiffener Plus Web Damage from both Sides (BWS)	BWS20t75	1000.6	0.989	Normal
	S20t50	996.5	0.985	Normal		WES20t50	977.69	0.966	Normal		BWS20t50	927.19	0.916	Normal
	S20t25	818.1	0.809	Local		WES20t25	666.36	0.659	Local		BWS20t25	560.01	0.553	Local
	S20t0	699	0.691	Crushing		WES20t0	439.57	0.434	Crushing		BWS20t0	91.253	0.090	Crushing
	S40t75	994.7	0.983	Normal		WES40t75	988.44	0.977	Normal		BWS40t75	960.38	0.949	Normal
	S40t50	916	0.905	Local		WES40t50	849.43	0.839	Local		BWS40t50	740.02	0.731	Crippling
	S40t25	732.8	0.724	Local		WES40t25	553.77	0.547	Crippling		BWS40t25	339.86	0.336	Crippling
	S40t0	589.2	0.582	Crippling		WES40t0	345.36	0.341	Crushing		BWS40t0	91.253	0.090	Crushing
	S60t75	986.9	0.975	Normal		WES60t75	961.31	0.950	Normal		BWS60t75	925.21	0.914	Normal
	S60t50	868.3	0.858	Local		WES60t50	756.61	0.748	Crippling		BWS60t50	637.13	0.630	Crippling
	S60t25	660.8	0.653	Crippling		WES60t25	481.62	0.476	Crippling		BWS60t25	293.91	0.290	Crippling
	S60t0	507.6	0.502	Crippling		WES60t0	306.32	0.303	Crippling		BWS60t0	91.253	0.090	Crippling
	S80t75	972.1	0.961	Normal		WES80t75	930.98	0.920	Normal		BWS80t75	884.8	0.874	Normal
	S80t50	818.9	0.809	Local		WES80t50	711.44	0.703	Crippling		BWS80t50	573.6	0.567	Crippling
	S80t25	624.7	0.617	Crippling		WES80t25	453.04	0.448	Crippling		BWS80t25	264.57	0.261	Crippling
	S80t0	478.09	0.472	Crippling		WES80t0	309.00	0.305	Crippling		BWS80t0	91.25	0.090	Crippling
S100t75	949.9	0.939	Normal	WES100t75	903.45	0.893	Normal	BWS100t75	848.19	0.838	Local			
S100t50	786.5	0.777	Local	WES100t50	675.94	0.668	Crippling	BWS100t50	528.82	0.523	Crippling			
S100t25	612.4	0.605	Crippling	WES100t25	439.66	0.435	Crippling	BWS100t25	253.95	0.251	Crippling			
S100t0	451.6	0.446	Crippling	WES100t0	313.79	0.310	Crippling	BWS100t0	91.253	0.090	Crippling			

5.12 ANALYSIS OF THE RESULTS

Since the primary objective of the study is to evaluate the effect of corrosion damage level at plate girder ends, on the reduction in bearing capacity. Therefore, all the results were plotted in form of the residual capacity ($P_{ult}/P_{H,ult}$) with respect residual thickness (t/t_0) corresponding to different damage heights. Three separate graphs were plotted for three different damage groups considered in the study as shown in the Figure 5.33. Although, the thickness reduction rate 25%, 50%, 75% and 100% were considered for all damage group as mentioned in the Table 5.4 however, to check the trend of curve the ultimate strength of intermediate points corresponding to 12.5%, 37.5%, 62.5% and 87.5% reduction in thickness were also calculated and plotted in Figure 5.33. As already shown in Figure 5.1 the complete loss of bearing stiffener has been observed by the author, it may be considered in this parametric study only for stiffener damage group (S) but on the other hand, 100% reduction of material may be ignored in the damage groups of WES and BWS for realistic point of view.

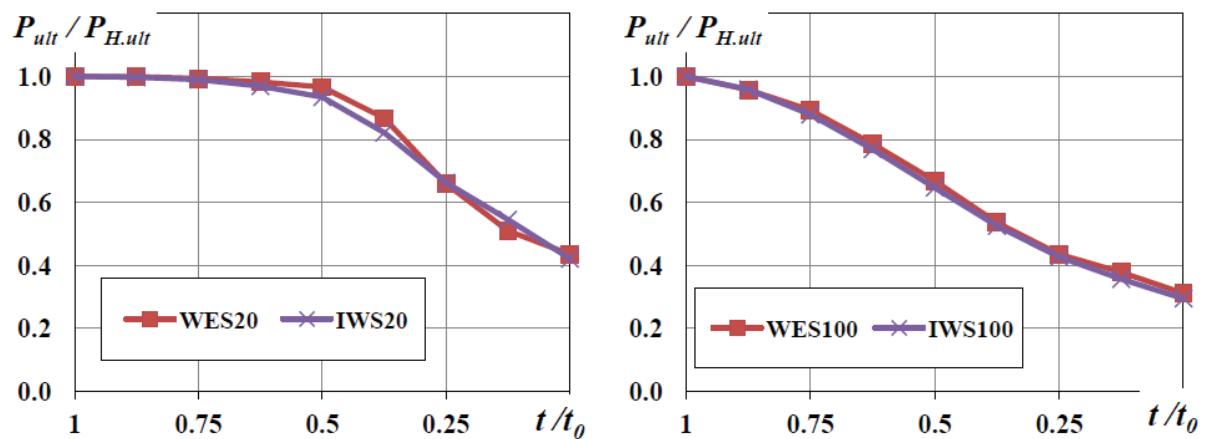
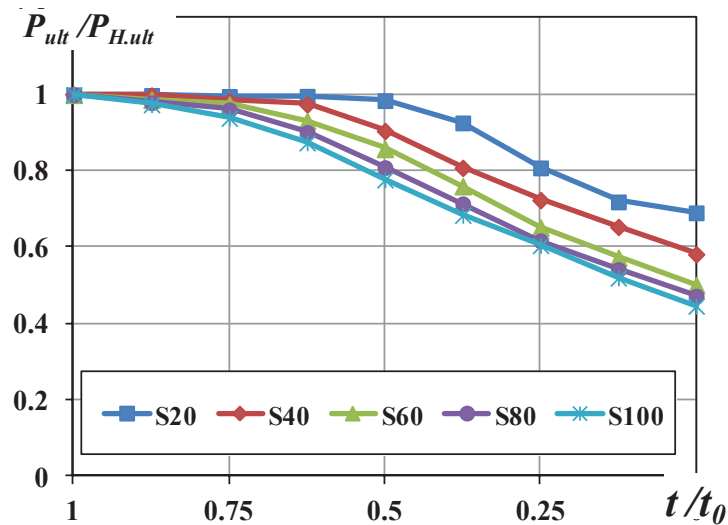


Figure 5.32: Ultimate load comparison of damage groups WES and IWS

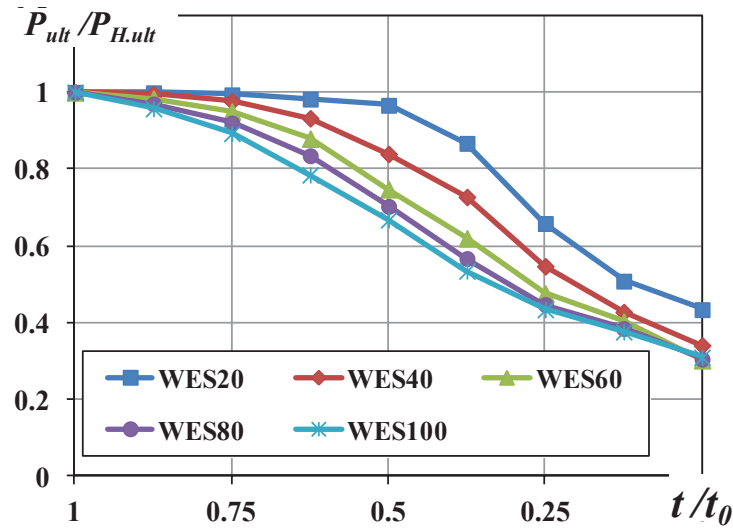
Besides the analytical cases mention in the Table 5.4, an analysis damage group IWS (Stiffener damage plus interior web damage) was also consider. However, analytical results of both damage groups WES (Stiffer plus exterior web damage) and IWS (Stiffener damage plus interior web damage) revealed the similar strength reduction trend in their ultimate capacity which can be observed from the Figure 5.32, where identical trends in ultimate loads is quite evident for the damage height of 20mm and 100mm. Therefore, the analytical results

for the damage group of IWS are omitted from the Table 5.4 and results for the BWS group can be considered for the IWS damage group as well.

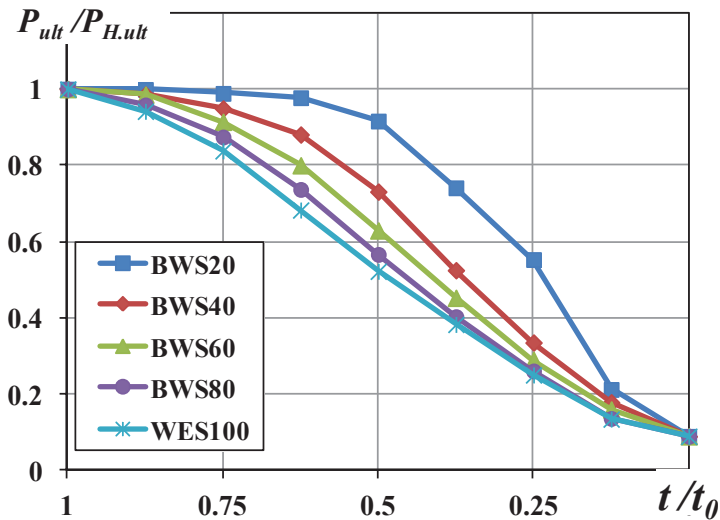
The analytical results as shown in Figure 5.33 depict that 25% corrosion damage for the maximum damage height of 100mm considered in the study does not reduce the strength remarkably. Thus a reduction of bearing capacity around 6.1%, 10.7% and 17.2% was found in the cases of S100t5, WES100t75 and BWS100t75 respectively. It was also observed in the study that for the small damage height cases while considering the damage only on bearing stiffener, ultimate strength does not reduce remarkably even for the 75% loss of stiffener thickness which is due to the local plastic concentrate phenomenon. This local concentrating phenomenon also control the failure mode of the plate girder as can be seen in the Table 5.5 for the case of S40t25, where the failure mode was found as local buckling instead of crippling or crushing that were found in higher damage cases or when damages are combined with web. In local buckling the material goes in plastic range in damage zone that causes the local buckling within the damage zone along with overall buckling of the web. This phenomenon also slightly increases the strength and it can be seen that analytical case S40t25 illustrates the ultimate load around 10% and 24% more as compared with S60t25 and WES40t25 respectively.



(a) Damage group S



(b) Damage group WES



(c) Damage group BWS

Figure 5.33: Relationships between residual strength and residual thickness

The complete loss of the thickness diminishes the role of the bearing stiffener and all the compressive load is taken by the web alone. It reduces the ultimate strength around 50% and gives rise to the failure mode crippling as can be seen for the case of S60t0 in Table 5.5. However, in cases of 75% section loss for the damage group WES and BWS with damage height 40mm and more, the ultimate strength decreases remarkably and cause the crippling failure mode as shown in Figure 5.2, obtained from the field investigation.

5.13 CONCLUSIONS

It can be observed from the Table 5.5 that normal buckling mode appear at the bearing capacity loss less than 10% and most of the local buckling failures cause a loss of ultimate capacity up to 30%. Similarly all the cases which show the remaining capacity less than 70% yield the crippling or crushing type of the failure.

On the bases of analytical results the following general conclusion can be established.

1. The local damage on web does not affect the elastic critical load it just slightly reduces the ultimate and post buckling strength.
2. Bearing stiffener plays an important role in resisting the compressive load even for the complete loss of the web in a locally small damage.
3. The ultimate strength reduces drastically if web damage is combined with the stiffener damage and it also shifts the failure mode from buckling to the crippling.
4. For the small damage height cases ($D_h/d < 4\%$) where residual thickness is around 50% the local plastic concentrate phenomenon slightly contribute the ultimate capacity and control the failure mode as well.

ANALYTICAL EVALUATION OF CORRODED PLATE GIRDER END UNDER SHEAR LOADING

6.1 GENERAL

As already discussed in chapter 2 (literature review), many field inspection and surveys indicate the excessive loss of material near the bearing region. The loss of girder material due to corrosion has more influence on the web and bearing stiffener than the flanges and this causes a huge reduction in shear and bearing reliability than bending and further, thinning of thickness due to corrosion may change class of section *i.e.* compact, semi compact, and slender (Kayser 1989). Figure 6.1 & 6.2 illustrate the some typical corrosion damages nearby plate girder ends, where severe corrosion is quite evident and in one case full loss of bearing stiffener material can also be seen.

Since bearing stiffener are designed for both to resist the bearing load and to provide the anchorage to develop tension field action to increase the post buckling strength of the plate girder (Hoglund 1997). Normally, the post buckling strength is 3 to 4 time more than the critical shear strength and any severe corrosion damage at bearing stiffener may reduce the anchorage to resist and balance the horizontal component of the force developed by tension field action which further may cause the crippling/crushing near the bearing without developing the shear failure collapse mechanism as shown in Figure 6.3. Therefore, for the maintenance and retrofitting purpose the steel bridges damaged by end panel corrosion require the proper evaluation to examine the corrosion effect on the bearing and shear capacity.

In the recent study Khurram et al. (2012) analyzed the effect of local bearing stiffener damage in his study to evaluate its effect on bearing capacity. He states that more than 50% loss of the bearing stiffener for a damage height more than 40mm may reduce the bearing

capacity and can also cause the crippling or crushing failure. Nakayama (2006) considered the complete loss of the web in rectangular form along lower flange and bearing stiffener. The study depicted that local corrosion adjacent to the bearing stiffener and flange at bearings decreases the ultimate shear strength fractionally however, the delectionation of the girder corresponding to the peak load increases prominently as compared to the undamaged girder. Liu et al. (2011) investigated the shear capacity of the corroded plate girder by considering the different damage cases only in the interior web. Rahgozar (2009) analyzed the effect of uniform surface corrosion on bending stresses, shear failure, lateral torsion buckling and bearing for the steel beam and developed the minimum capacity curves for the ultimate corresponding to various thickness losses. But his study is based on the hot rolled steel beam without the bearing and intermediate stiffeners and for the built-up member like plate girder these relationships may not be valid due to the welding and other design criterion difference. The presence of stiffener increases the critical shear buckling stress (Maquoi 2000). Thus, any corrosions damage in stiffener along with the web damage may reduce the critical shear load and post buckling shear capacity significantly and may shift/change the failure mode as well. Currently, no significant study is available that describe/explain the effect of bearing stiffener damage on the shear behavior of the steel plate girder. Also, effect of the web corrosion at free end on its load carrying characteristics is not investigated yet. Therefore, this study presents the effect of the local corrosion damage at the bearing stiffener along with the adjacent free end and interior web on the shear capacity of plate girder.



Figure 6.1: Typical corrosion damages at plate girder end by Tamakoshi (2006b)



Figure 6.2: Complete loss of bearing stiffener by Khurram (2012)

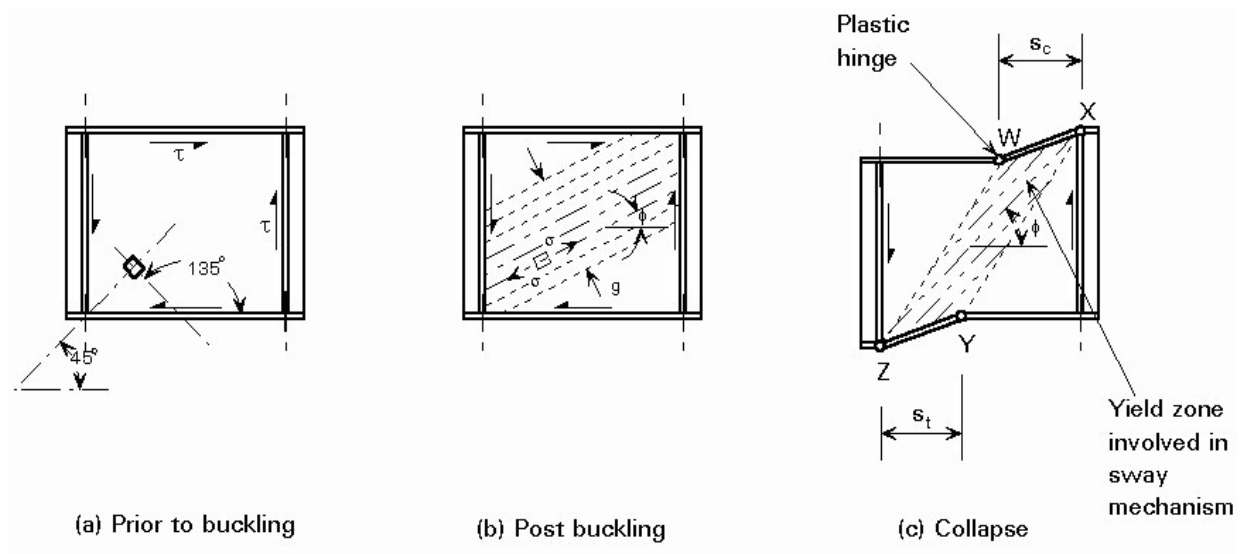


Figure 6.3: Phases in behaviour up to collapse of a typical panel in shear

6.2 FE MODEL CHARACTERISTICS

6.2.1 Model Geometry and Boundary Conditions

Alinia (2009) states that a detached web panel simulation model, a simply supported web plate in shear, or even single-panel experimental tests cannot truly represent the behavior of plate girder web plates, since:

- A web plate is bound to have some bending moments due to lateral loadings.
- The torsional rigidity of girder flanges must be accounted for in the rotational stiffness of panel boundary conditions. The true behavior of flange–web junction is neither simply supported nor clamped.
- In reality, flanges are allowed to move towards or apart from each other, and their weak axis second moment of area becomes an important factor in this regard. A free or restrained in-plane movement of panel edges cannot represent the real behavior of web plates.
- The number of sub-plates created by intermediate transverse stiffeners and conditions of end-posts (end stiffeners) have considerable effects on the behavior of plate girders.

Alinia (2009) performed some sensitivity analysis on different panel girder to check the shear response of the 2, 4 and 6 panel girder. The out-of-plane deformation versus midpoint applied shown in Figure 6.5 illustrates that all plate girder model possess a good agreement. In the Figure 6.5 out-of-plane deformation was measured at the midpoint of central panel.

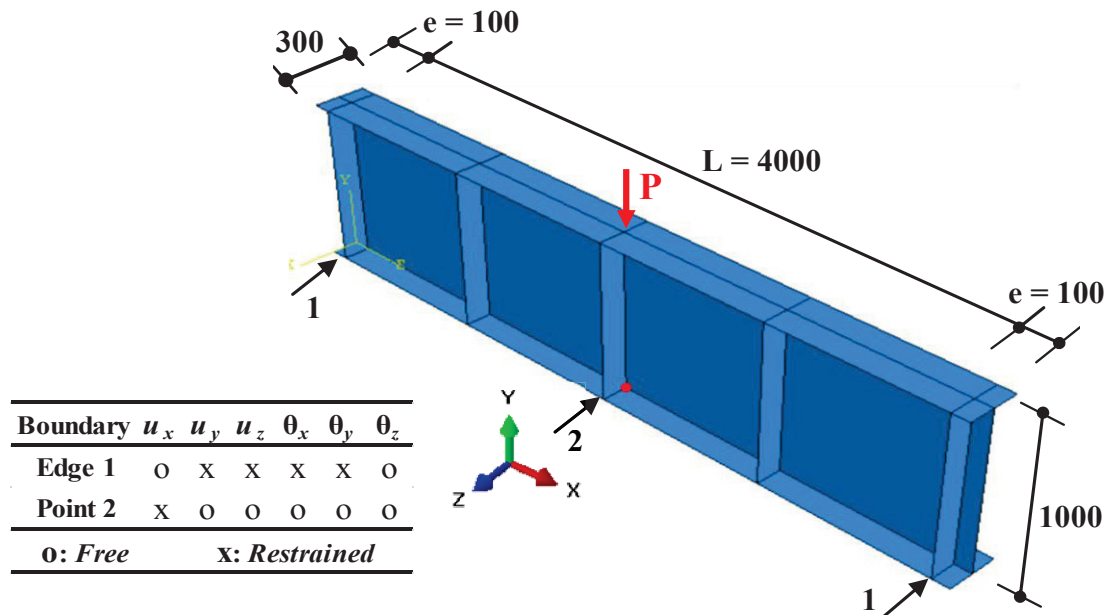


Figure 6.4: Detail dimensions of the girder model (Dimensions are in mm)

Therefore, in the present analytical study a four panel plate girder model as used by Alinia (2009) was selected to make sure the constant shear and small flexure in the end panel. The plate girder was modeled using powerful software package ABAQUS. Figure 6.4 shows the detail dimensions and boundary conditions of the four panel rectangular plate used in the analytical study, possessing each panel length and height equal to 1000mm. The thickness of flange, all stiffeners and web is fixed as 12mm, 8mm and 4mm respectively as per the AASHTO guidelines for the moderate flange thickness as given in the Table 6.1. The simply supported boundary conditions are applied to make sure the constant shear in the web panels. As shown in Figure 6.4, the right and left supports are released to translate in direction 3 and to rotate about axis 1 and all other translations and rotations are restricted. At the center point only the translation in direction 3 is restrained.

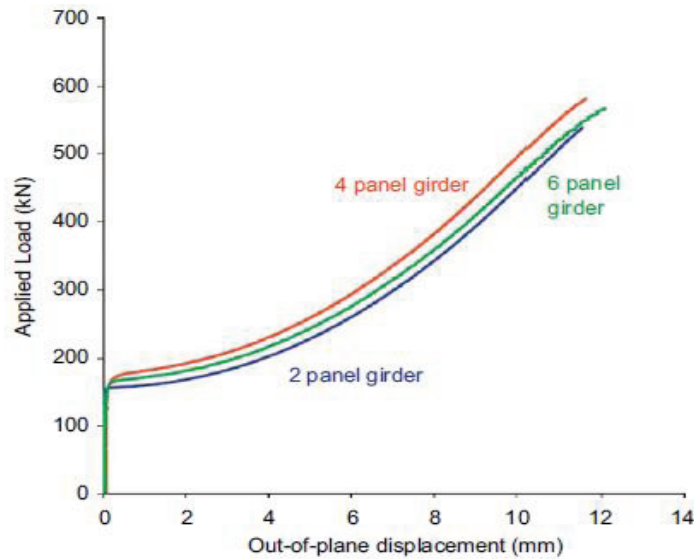


Figure 6.5: Correlation between plate girders with different panels

Table 6.1: ASSHTO classification for flange types

Flange Type	t_f/t_w	b_f/h_w
Light	1.0	0.25
Moderate	3.0	0.30
Heavy	5.0	0.35

6.2.2 FE Mesh and Material Properties

After the convergence study, the geometry was divided into sufficient mesh numbers to trap the shear buckling with good accuracy of result. However, a very fine mesh of size 2.5x2.5mm was adopted in the stiffener and web damage zone as shown in Figure 6.6. A mild steel with yield stress = 345Mpa, Poisson's ration $\nu = 0.3$ and elastic modulus $E=210\text{Gpa}$ are used. The material is considered elastic perfectly plastics (EPP) with no strain hardening and plasticity.

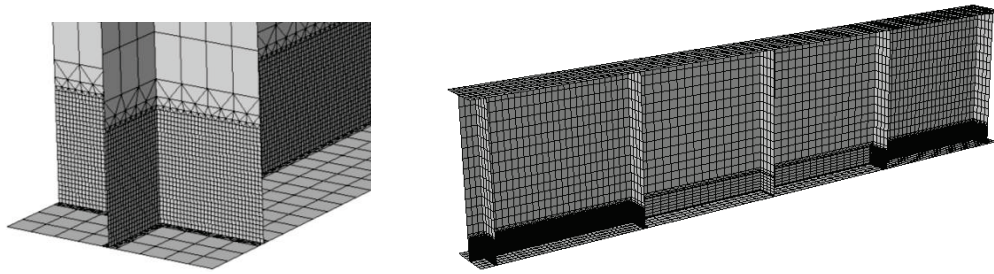


Figure 6.6: Meshing detail of FE model

6.2.3 Initial Imperfections

An imperfection value equal to $hw/250$ was superimposed to the model geometry based on the first eignvalue buckling mode shape to incorporate the out of plane deflection. Figure 6.7 shows the first buckling eignvalue mode used for the initial deflection. The residual stress has no effect on the shear and bending stress capacity of plate girders and welded plates, this is because the applied stresses and welding residual stresses are likely to be of different nature. Therefore, welding residual stresses are not considered in the study.

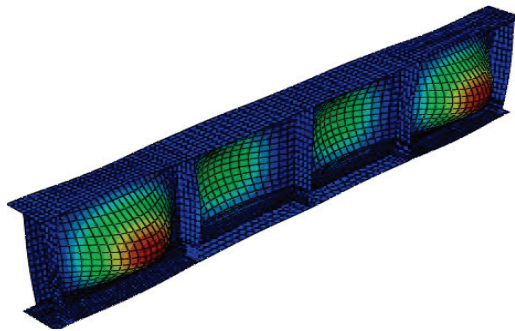


Figure 6.7: First buckling eignvalue mode shape of plate girder

6.3 VALIDATION OF FINITE ELEMENT MODEL

A mid span load was applied by using an elasto-plastic nonlinear modified ricks analysis procedure. The material plasticity data is incorporated under the kinematics hardening rule and Mises yield criterion. Vertical displacement was measured at the center point 2 of the girder as shown in Figure 6.4. The FE model was verified firstly, with the study conducted by Real (2007) using the identical model and boundary condition with the stainless steel and secondly, with the analytical results of Alinia (2009) as shown in Figure 6.8 and 6.9 respectively. Figure 6.10 depicts the deformed buckling mode of the plate girder.

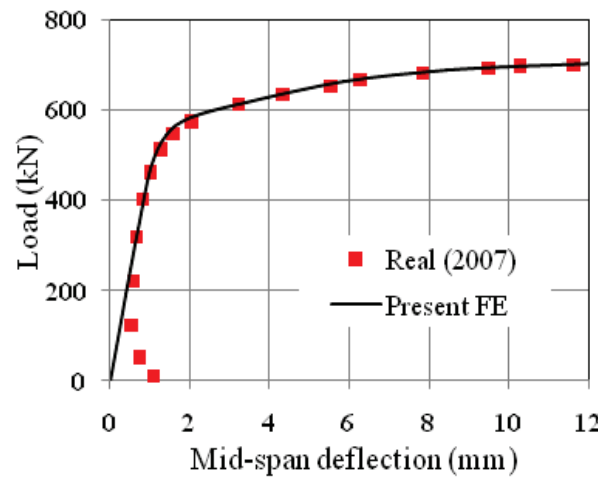


Figure 6.8: Verification of load-displacement curves with results of Real (2007)

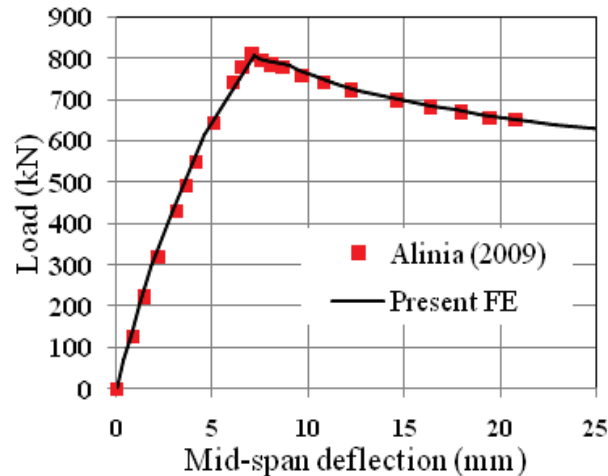


Figure 6.9: Verification of load-displacement curves with results of Alinia (2009)

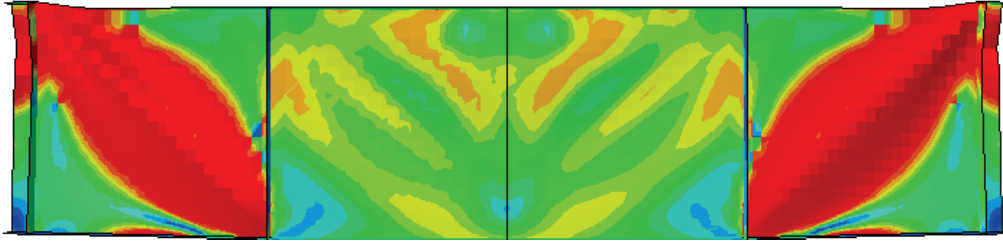


Figure 6.10: Deformed buckling shape

6.3.1 Method of Study

After the verification of the FE model the different damage thickness levels (residual thicknesses) are considered within the various damage heights *i.e.* 20, 40, 60, 80 and 100mm. Four different damage categories as shown in the Figure 6.11 are considered in the analytical program. Some descriptive analytical cases are shown in Table 6.2. The damage zones as shown in Figure 6.11 are considered from the top face of the bottom flange near the weld seam. As the study is targeted to evaluate the effect of a small local damage on its shear capacity therefore, height and width of damage adjacent to bearing stiffener maximum are assumed equal to 100mm as highlighted in Figure 6.11.

In the Table 6.2 similar analytical cases are defined as for the compression analysis cases and described as following.

Analytical case WES20t75, represent the damage group type WES and remaining thickness (t) of stiffener and web as 75% of original thickness.

S: represents the damage group with the corrosion damage on bearing stiffener only

WES: represents the damage group with corrosion damage on the stiffener and web free end

IWS: represents the damage group with corrosion damage on the stiffener and interior web damage

BWS: represents the damage group with corrosion damage on the stiffener and web on both sides of the stiffener.

Table 6.2: Analytical cases for shear capacity evaluation

D_h (mm)	D_h/d (%)	t (%)	Damage type	Analysis Case	t_s (mm)	t_w (mm)	Damage type	Analysis Case	Damage type	Analysis Case	Damage type	Analysis Case	t_s (mm)	t_w (mm)
20	2	75	Stiffener Damage only (S)	S20t75	6	4	Stiffener Plus Web Free End Damage (WES)	WES20t75	Stiffener Plus Interior Web Damage (IWS)	IWS20t75	Stiffener Plus Web Damage from both Sides (BWS)	BWS20t75	6	3
		50		S20t50	4	4		WES20t50		IWS20t50		BWS20t50	4	2
		25		S20t25	2	4		WES20t25		IWS20t25		BWS20t25	2	1
		10		S20t10	0	4		WES20t0		IWS20t0		BWS20t0	0	0
40	4	75		S40t75	6	4		WES40t75		IWS40t75		BWS40t75	6	3
		50		S40t50	4	4		WES40t50		IWS40t50		BWS40t50	4	2
		25		S40t25	2	4		WES40t25		IWS40t25		BWS40t25	2	1
		10		S40t10	0	4		WES40t0		IWS40t0		BWS40t0	0	0
60	6	75		S60t75	6	4		WES60t75		IWS60t75		BWS60t75	6	3
		50		S60t50	4	4		WES60t50		IWS60t50		BWS60t50	4	2
		25		S60t25	2	4		WES60t25		IWS60t25		BWS60t25	2	1
		10		S60t10	0	4		WES60t0		IWS60t0		BWS60t0	0	0
80	8	75		S80t75	6	4		WES80t75		IWS80t75		BWS80t75	6	3
		50		S80t50	4	4		WES80t50		IWS80t50		BWS80t50	4	2
		25		S80t25	2	4		WES80t25		IWS80t25		BWS80t25	2	1
		10		S80t10	0	4		WES80t0		IWS80t0		BWS80t0	0	0
100	10	75	S100t75	6	4	WES100t75	IWS100t75	BWS100t75	6	3				
		50	S100t50	4	4	WES100t50	IWS100t50	BWS100t50	4	2				
		25	S100t25	2	4	WES100t25	IWS100t25	BWS100t25	2	1				
		10	S100t0	0	4	WES100t0	IWS100t0	BWS100t0	0	0				

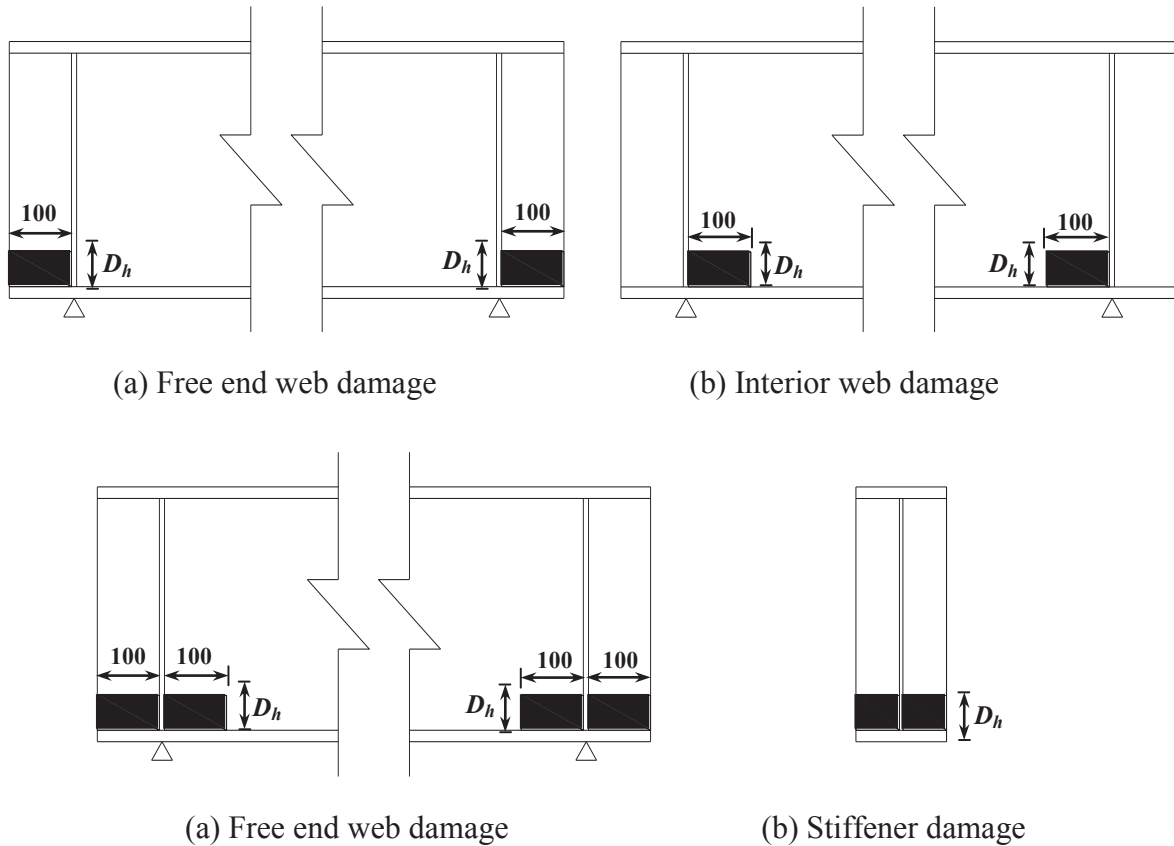


Figure 6.11: Different damage cases for shear capacity analysis

6.4 RESULTS AND DISCUSSION

For the analysis purpose, all the results obtained from finite element simulation are plotted in term of the vertical load verses and deflection measured at the midpoint of the bottom flange as already explained in Figure 6.4. Further, deformed shapes obtained from each analysis group mentioned in Figure 6.11 and Table 6.2 were also compared to assess the local corrosion effect. Analytical results show that only the local web damage from either/both side of the bearing stiffener for any residual thickness does not change the ultimate capacity, post buckling behavior and failure mode of plate girder therefore, results with the web damaged are not discussed in the following sections.

6.4.1 Stiffener Damage only

The analytical results show that loss of bearing stiffener less than 50% for all the damage heights considered in the study has no effect on the shear capacity. A loss of 60% in the stiffener thickness does not reduce the capacity for a small damage of 20mm ($D_h/d = 2\%$). Figure 6.12(a) illustrates that a relatively large damage of 40mm ($(D_h/d > 4\%)$) with residual thickness (t/t_s) equal to 0.4, reduces the ultimate capacity fractionally but it cause an abrupt loss in the post buckling capacity. On the other hand, loss of thickness more than 40 reduces the both the ultimate load and post buckling strength of the plate girder for all the damage heights as can be seen in the Figure 6.12(b). Figure 6.13 shows the deformed modes for the various stiffener damage cases which clearly depicts that with the increase of the bearing stiffener damage, plate girder does not achieve its full strength (Figure 6.13(b & c)) and cause a crippling failure as shown in Figure 6.13(d).

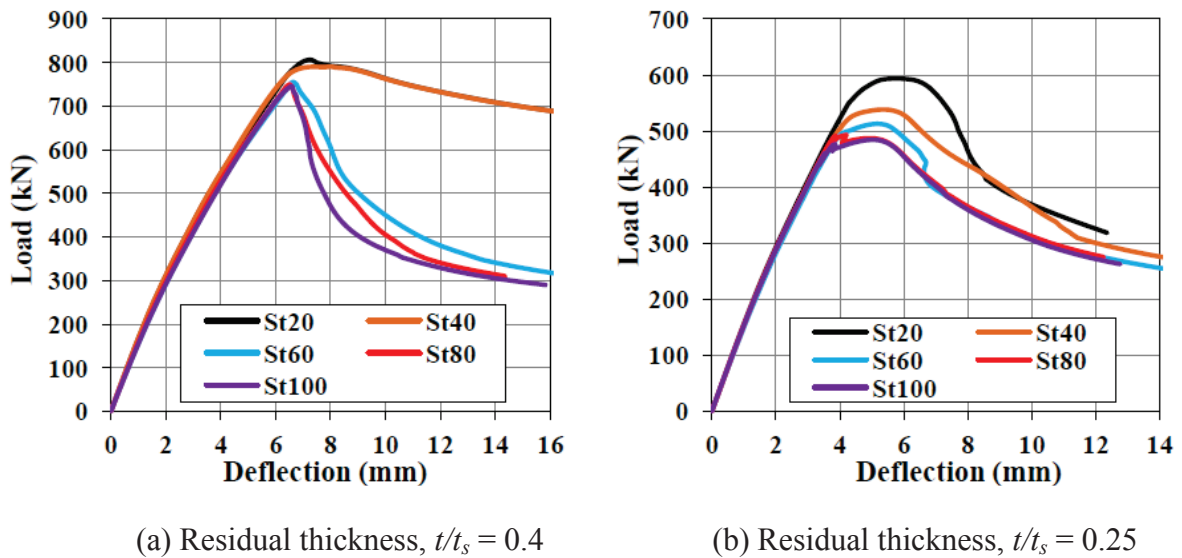
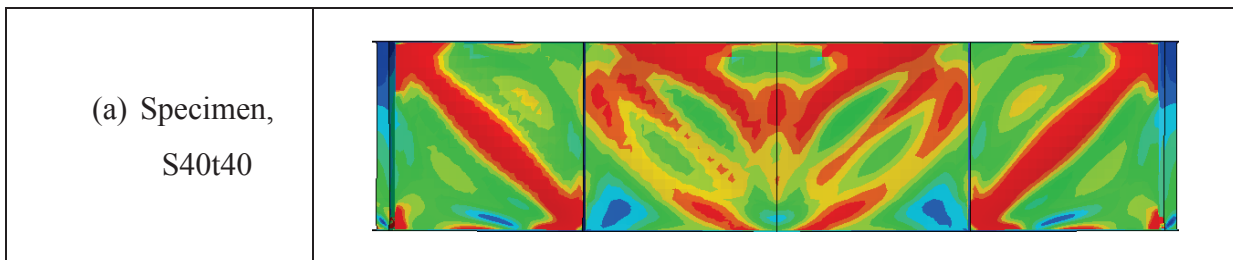


Figure 6.12: Load-displacement curves for the cases with stiffener damage only



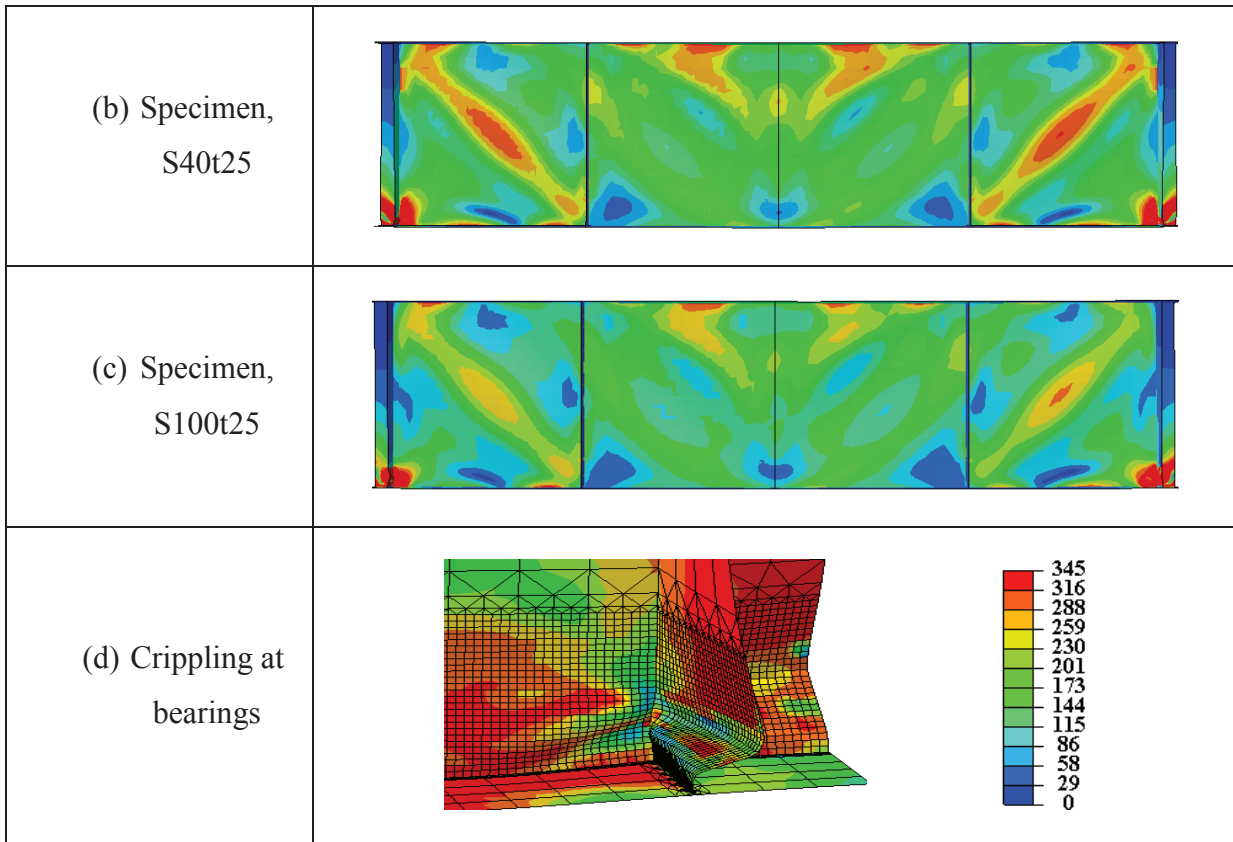
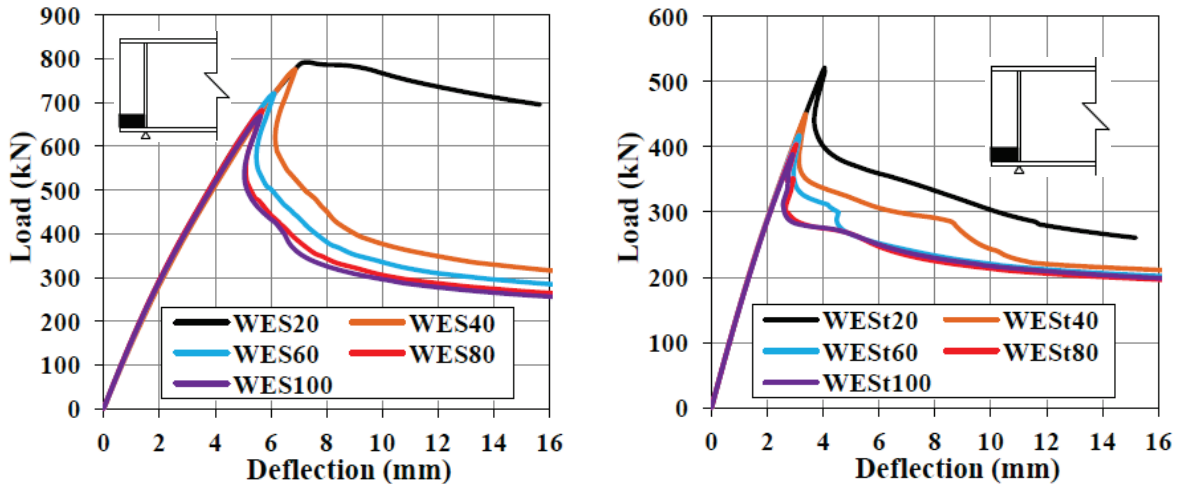


Figure 6.13: Deformed modes for the cases with stiffener damage only

6.4.2 Stiffener Damage plus Free Web End

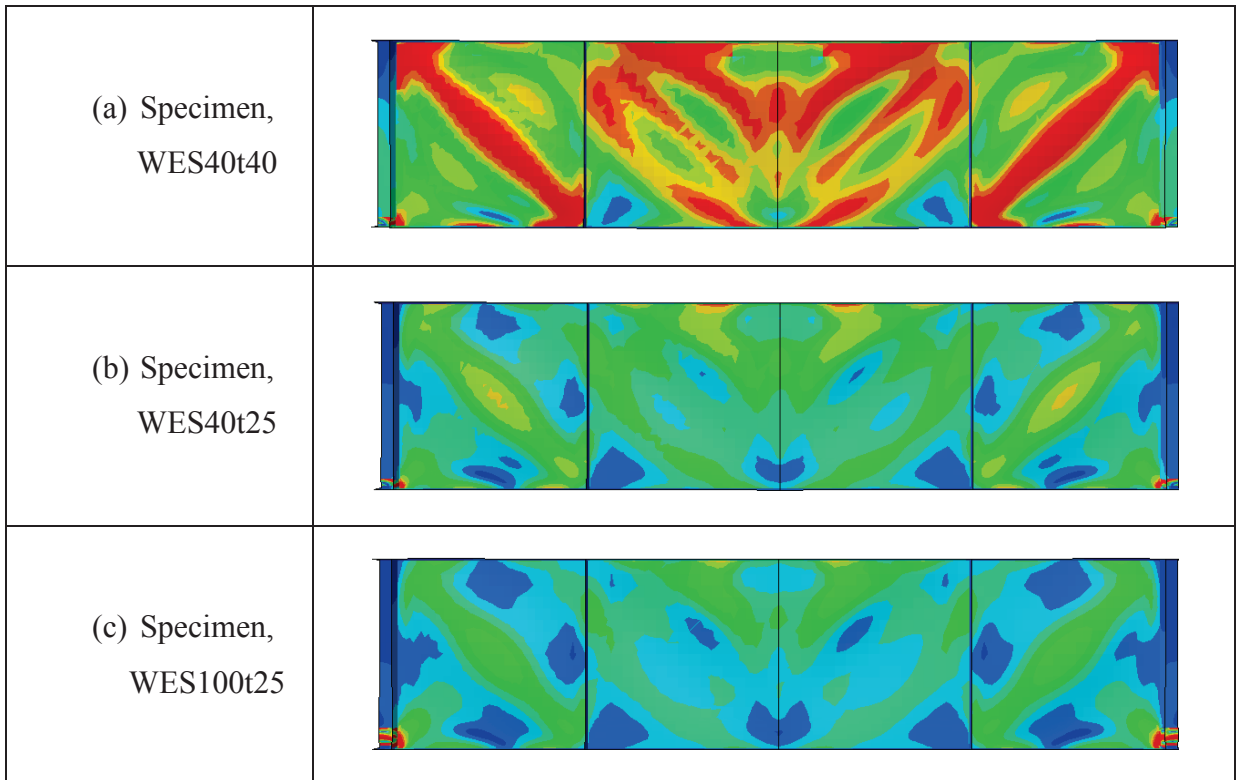
Addition of the exterior web damage along with the stiffener damage does not change the ultimate capacity and post buckling strength significantly for the residual thickness of 0.4 as Figure 6.14(a) depicts. However, loss of thickness more than 60% in the exterior web and stiffener reduces the ultimate capacity and post buckling capacity more drastically as compared with the cases with the stiffener damage only as can be seen in the Figure 6.14(b). The deformed shapes with stress contour given in Figure 6.15(a, b & c) shows the ultimate stress level corresponding the various damage, which also indicates the stress concentration in the damage zone before developing the tension band in the web and causes the buckling within the damage region as shown in Figure 6.15(d).



(a) Residual thickness, $t/t_s = 0.4$

(b) Residual thickness, $t/t_s = 0.25$

Figure 6.14: Load-displacement for the cases with stiffener plus exterior web damage



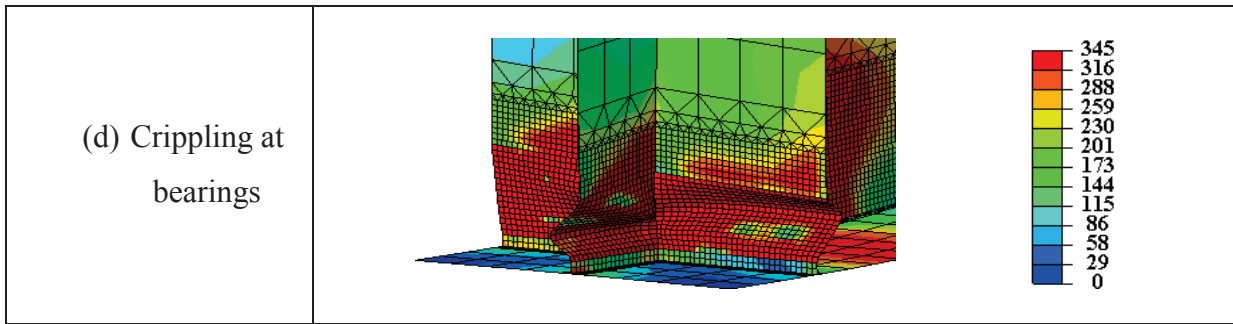
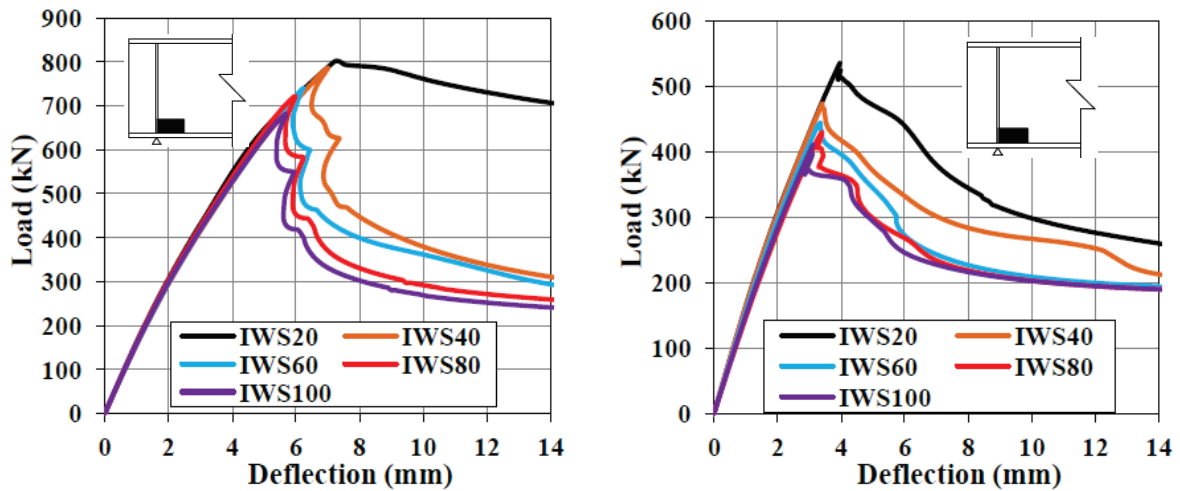


Figure 6.15: Deformed modes for the cases with stiffener plus exterior web damage

6.4.3 Stiffener Damage plus Inner Web

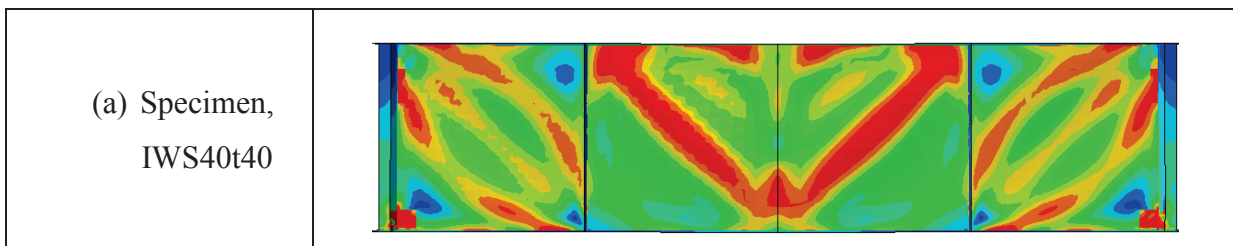
Figure 6.16 (a & b) reflects the inner web damage along with stiffener also shows the similar trend in the strength reduction in the ultimate capacity and post buckling strength as the exterior web damage with the stiffener damage cases. The failure mode, stresses at peak load are also the similar to the damage group of WES as can be seen in the Figure 6.17.



(a) Residual thickness, $t/t_s = 0.4$

(b) Residual thickness, $t/t_s = 0.25$

Figure 6.16: Load-displacement for the cases with stiffener plus interior web damage



(a) Specimen, IWS40t40

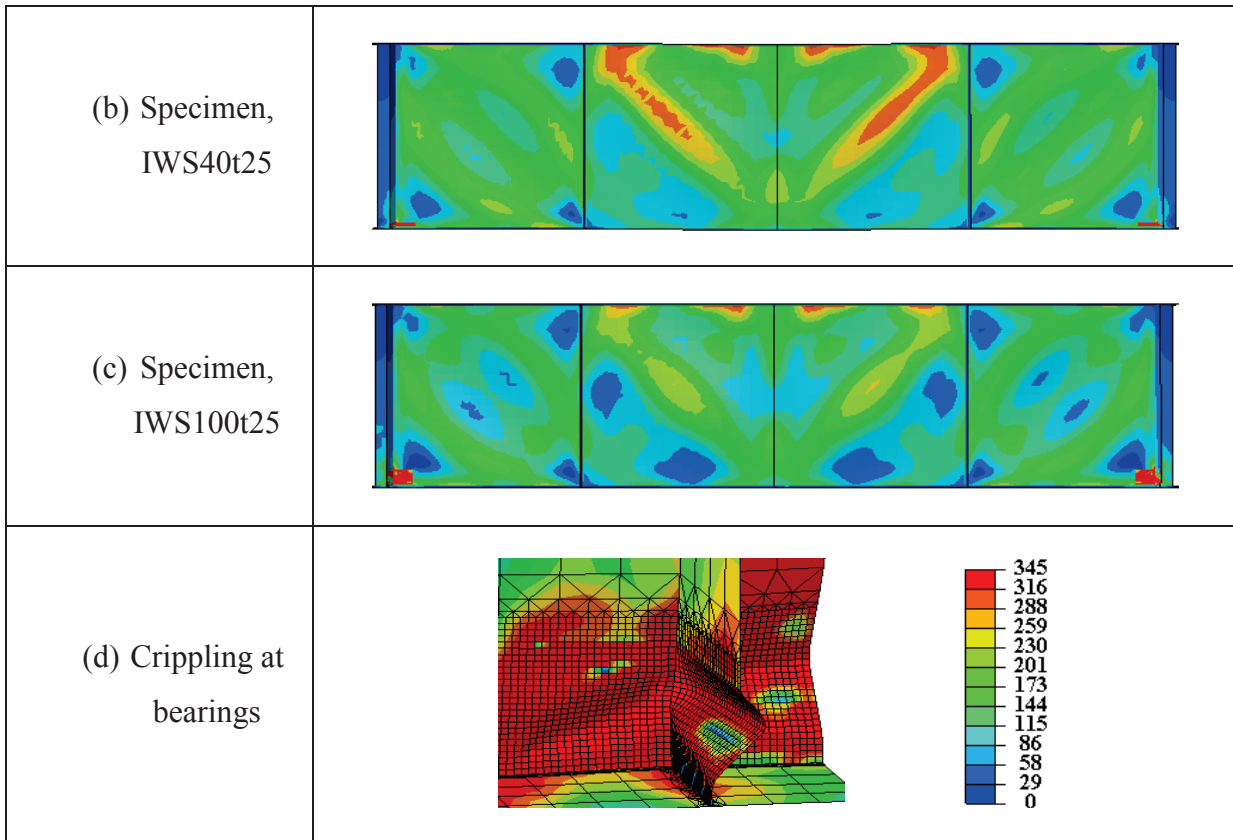
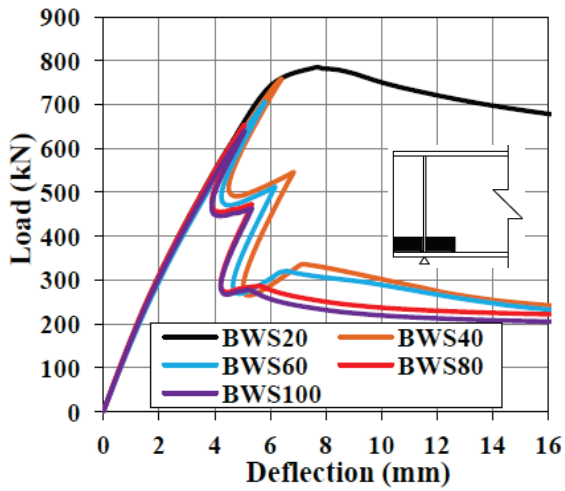


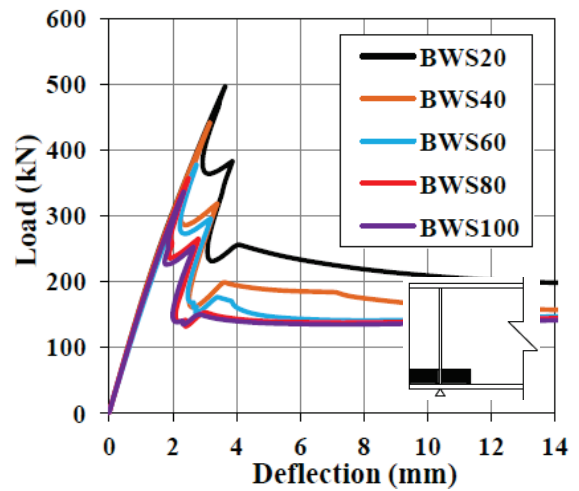
Figure 6.17: Deformed modes for the cases with stiffener plus interior web damage

6.4.4 Stiffener Damage plus Web on Both Sides

The stiffener damage along with the web damage from the both side of the stiffener is more critical for the shear capacity of the plate girder even if the damage height is very small and causes the crushing type of the failure as presented in Figure 6.19(d). Any damage with reduce thickness less than 0.4 reduces the ultimate and post buckling strength more drastically than the stiffener damage with the web damage from either side as can be noticed from Figure 6.18(a & b). It also diminishes the anchorage ability of the stiffener to support and balance the horizontal component of shear force developed in the web and thus web does not achieve it full strength and fail locally near the bearing as Figure 6.19 depicts.



(a) Residual thickness, $t/t_s = 0.4$



(b) Residual thickness, $t/t_s = 0.25$

Figure 6.18: Load-displacement for the case with stiffener plus both sides web damage

<p>(a) Specimen, BWS40t40</p>	
<p>(b) Specimen, BWS40t25</p>	
<p>(c) Specimen, BWS100t25</p>	

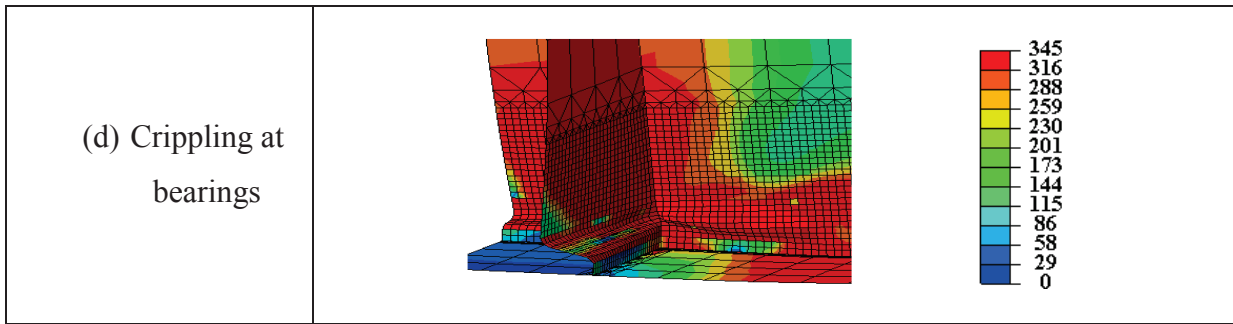


Figure 6.19: Deformed modes for the case with stiffener plus both sides web damage

6.5 DISCUSSION ON RESULTS

For the analytical comparison the results are plotted in term of the remaining ultimate shear capacity ($P_{ult}/P_{H,ult}$) versus residual thickness (t/t_0) corresponding to the various damage heights for the damage cases considered in the study as shown in the Figure 6.20, 6.21, 6.22 and 6.23. These plots indicate clearly that 50% loss of material in all the damage cases has no effect on the ultimate shear capacity and further loss of the thickness reduces the ultimate shear capacity linearly. The remaining ultimate shear capacities presented in Table 6.3 illustrate that stiffener has the main contribution in providing the anchorage for the shear stress and only local web damage from either side of bearing stiffener along with bearing stiffener damage has a less role in strength reduction. Also, it can be observed from the Table 6.3 that solely a small damage like 40mm with residual thickness less than 0.25 may be very fatal for the shear capacity of plate girder and gives rise to the crushing/crippling failure. Moreover, local damage of stiffener along with the web adjacent to both side of bearing stiffener is more susceptible to the shear capacity of plate girders.

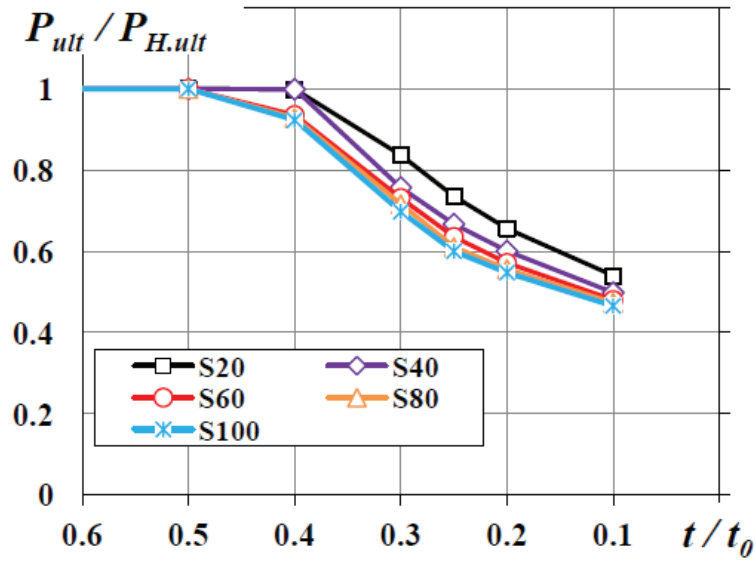


Figure 6.20: Remaining capacity of specimen with stiffener damage

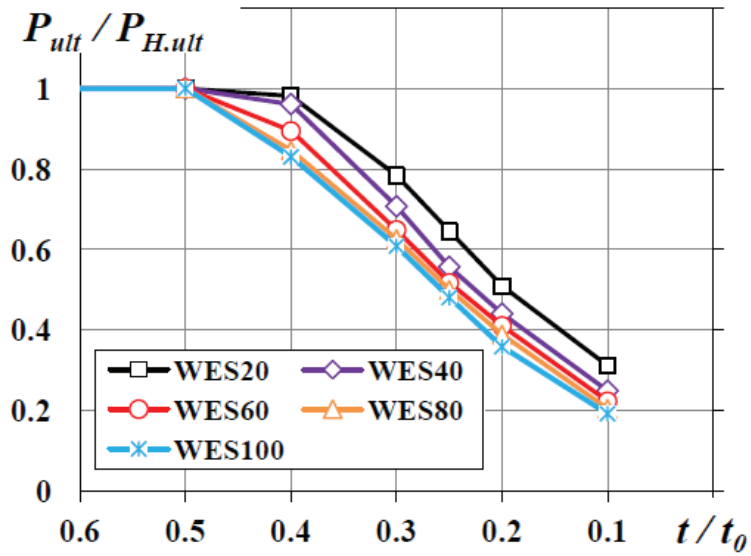


Figure 6.21: Remaining capacity of specimen with stiffener plus exterior web damage

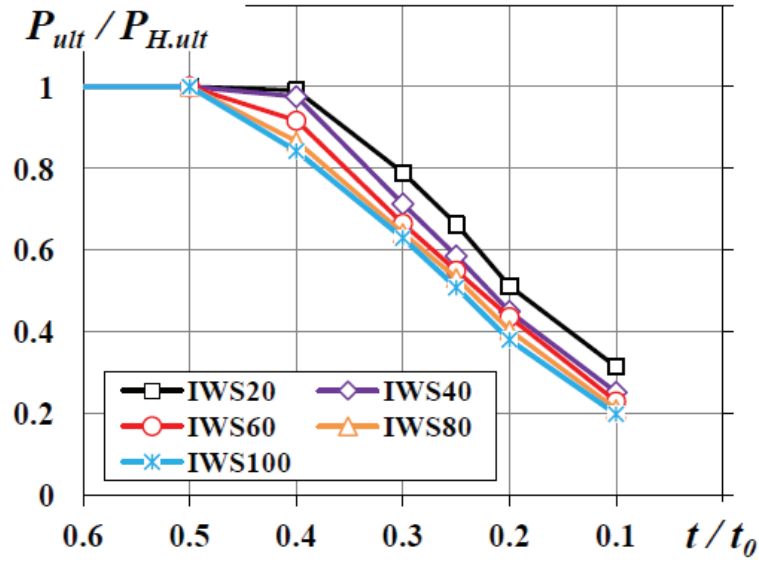


Figure 6.22: Remaining capacity of specimen with stiffener plus interior web damage

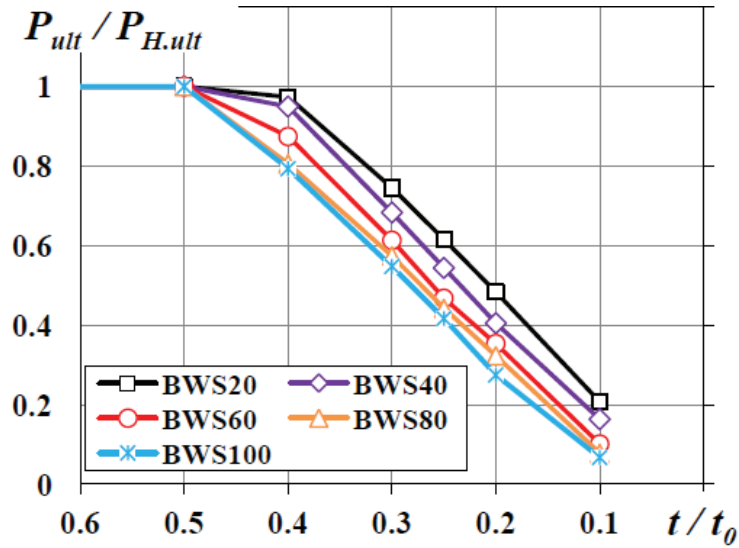


Figure 6.23: Remaining capacity of specimen with stiffener plus both sides web damage

Table 6.3: Remaining shear capacity for different damage cases

Damage Height		Damage Case	Thickness Reduction (t/t_0)						
D_h	D_h/d		1	0.5	0.4	0.3	0.25	0.2	0.1
(mm)	(%)								
20	2	St	1	1	0.999	0.837	0.736	0.657	0.540
		WES	1	1	0.981	0.784	0.646	0.509	0.311
		IWS	1	1	0.991	0.790	0.663	0.512	0.314
		BWS	1	1	0.973	0.745	0.615	0.484	0.207
40	4	St	1	1	0.999	0.757	0.667	0.601	0.498
		WES	1	1	0.961	0.707	0.557	0.441	0.249
		IWS	1	1	0.976	0.713	0.586	0.449	0.252
		BWS	1	1	0.950	0.683	0.544	0.405	0.163
60	6	St	1	1	0.936	0.731	0.635	0.572	0.480
		WES	1	1	0.894	0.649	0.517	0.410	0.222
		IWS	1	1	0.917	0.665	0.550	0.436	0.228
		BWS	1	1	0.874	0.613	0.467	0.354	0.101
80	8	St	1	1	0.928	0.716	0.611	0.557	0.474
		WES	1	1	0.846	0.627	0.500	0.389	0.206
		IWS	1	1	0.867	0.642	0.532	0.404	0.214
		BWS	1	1	0.806	0.574	0.442	0.323	0.078
100	10	St	1	1	0.923	0.698	0.600	0.548	0.466
		WES	1	1	0.830	0.609	0.481	0.359	0.191
		IWS	1	1	0.843	0.630	0.508	0.380	0.200
		BWS	1	1	0.793	0.548	0.417	0.274	0.067

6.6 CONCLUSIONS

From the study following conclusions are be made.

1. Local damage on web only, near the bearing region neither changes the failure mode nor affects the ultimate and post buckling strength.
2. More than 50% loss of the Bearing Stiffener can shift the failure mode from Shear to crippling
3. Complete loss of bearing stiffener thickness reduce the anchorage to resist the horizontal component of the shear stresses in the web and thus reduce ultimate strength and Tension Filed Action to develop, which reduce the safety factor to fail in shear substantially.

EMPERICAL RELATIONSHIPS

7.1 GENERAL

For the maintenance of the steel bridges, it is very important to assess the residual capacity of corrosion damaged steel bridge structures to take the decision regarding the repair or retrofiting of the bridges. This chapter discusses the some empirical relationships between the residual capacity and damage parameters to assess the remaining ultimate bearing and shear capacity of the steel plate girder bridges and also the failure modes.

7.2 PREDICTION OF BUCKLING MODE

For the parametric analysis, the ultimate capacity has been plotted with respect to a non-dimensional damage parameter “ R ” named as the *Reduced Thickness Ratio* (t/t_s) for different damage heights as shown in Figure 7.1. As the buckling sensitivity is proportional to the slenderness ratio (b/t) of the plate element, reduced thickness ratio t/t_s was derived by taking the ratio between the *breath/thickness* value of the healthy part and damage part of the bearing stiffener regions as illustrated in equation (7.1). Miki *et al.* (1998) showed that buckling modes of circular piers with two different sections are controlled by the ratio between the diameter-thickness ratios of thicker section and thinner section connected by the thickness changing section. In this study, R defined by equation (7.1) was proposed based on their idea.

$$R = \frac{\left(\frac{b}{t_s}\right)_{\text{healthy}}}{\left(\frac{b}{t}\right)_{\text{damaged}}} = \frac{t}{t_s} \quad (7.1)$$

Here, reduced thickness ratio is defined as the ratio between the residual thickness of the bearing stiffener “ t ” in the damage zone and original thickness of the stiffener “ t_s ”. The

height of damage zone “ D_h ” is also one of the parameter that affects the ultimate capacity and buckling behaviour of the plate girder end. However, in this particular study R value is used to establish the main conclusions as various damage heights “ D_h ” provided the similar trends of the remaining capacity curves corresponding to different R values as illustrated in Figure 7.1. Furthermore, R value can also be used to assess the failure mode of the girder end (*i.e.* Normal buckling, local buckling and crippling). To elaborate the trend of curves and failure modes, results of supplementary analysis corresponding to 87.5%, 62.5%, 37.5% and 12.5% of the residual thickness of the bearing stiffener were also added in the Figure 7.1 and also in Table 7.1 and Table 7.2 as well. It can easily be concluded from Table 7.1 and Figure 7.1 that a reduced thickness ratio value greater than or equal to 0.75 for any damage height does not change the buckling mode or reduce the strength significantly. The ultimate capacity reduces non-linearly when R value starts decreasing from 0.75 to 0.5 and failure modes also shift to the local buckling in the damaged stiffener due to the stress concentration in damage zone. The ultimate capacity tends to reduce linearly for the reduced thickness ratio less than 0.5, where the buckling modes change into crippling and buckling can be found in both bearing stiffeners and web plates (crippling in S60-t3) in the damage zone. The local plastic constraint assists the strength of the steel girder ends, especially in the cases where damage height is small. All the failure mode obtained from the analytical results were found to be consistent with the R value except for the smaller damage heights *i.e.* S20-t3 and S40-t3 (Figure 7.1 & Table 7.2) where failure modes are local buckling instead of the crippling due to the reason of local plastic constraint as mentioned earlier.

Table 7.1 Comparison of ultimate bearing capacities

Damage height		Reduced Thickness Ratio (R), t/t_s								
		1	0.875	0.75	0.675	0.5	0.375	0.25	0.125	0
D_h (mm)	D_h/d (%)									
20	1.8	100	99.84	99.57	99.63	98.48	92.64	80.85	71.94	69.08
40	3.6	100	99.82	98.31	97.47	90.52	80.85	72.42	65.38	58.23
60	5.4	100	98.69	97.45	93.15	85.82	76.06	65.24	57.31	50.17
80	7.2	100	97.92	96.07	90.13	80.93	71.45	61.74	54.21	47.25
100	9.6	100	97.49	94.13	87.48	77.76	68.46	60.55	52.03	44.65

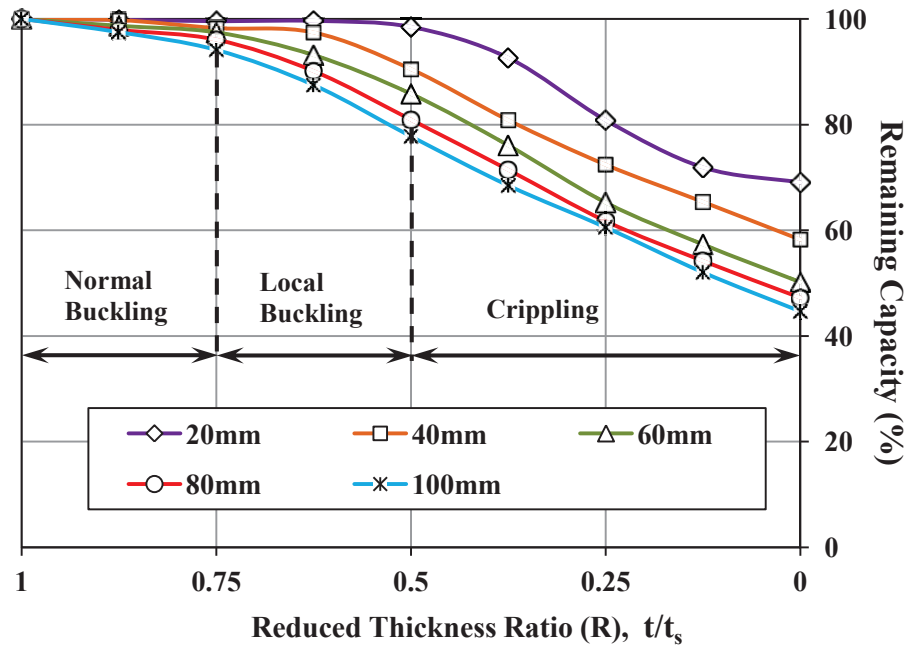


Figure 7.1: Remaining capacity versus reduced thickness ratio

The study revealed that reduced thickness ratio (t/t_s) value not less than 0.75 for the stiffener of all damage height cases, does not reduce bearing capacity remarkably. Thus only a small reduction in capacity around 8% was observed for the cases of $t/t_s = 0.75$ with damage height up to the 100mm. In all the cases where reduced thickness ratio is higher than the 0.5, the stress concentration in the damage zone results the local buckling except the 20mm damage height case, where normal buckling failure mode was recorded with almost no loss in capacity that can be seen from the much flat trend of the curve in Figure 7.1 in between t/t_s value of 0.75 and 0.5. The t/t_s values between 0.5 and 0.25 with small damage height like 20mm and 40mm cause the stress concentration in damage stiffener region and increase the post buckling strength due to local plastic constraint effect that provides the local buckling only in the damaged stiffener instead of the crippling. But the larger damage heights with t/t_s less than 0.5 lead to the crippling and stress concentration near the damage zone and reduce the bearing capacity substantially, *i.e.* around 40% loss in case of S100t25. The complete loss of the material from the bearing stiffener for any damage height drop off the strength remarkably *i.e.* 50% loss in case of S60-t0, which indicate that contribution of stiffener diminishes and bearing strength is governed by the web only.

Table 7.2 Failure modes of different analytical cases

		Damage Height, D_h (mm)				
		20	40	60	80	100
t (mm)	t/t_s					
10.5	0.875	Normal Buckling	Normal Buckling	Normal Buckling	Normal Buckling	Normal Buckling
9	0.75	Normal Buckling	Normal Buckling	Normal Buckling	Normal Buckling	Normal Buckling
7.5	0.625	Normal Buckling	Local Buckling	Local Buckling	Local Buckling	Local Buckling
6	0.5	Normal Buckling	Local Buckling	Local Buckling	Local Buckling	Local Buckling
4.5	0.375	Local Buckling	Local Buckling	Crippling	Crippling	Crippling
3	0.25	Local Buckling	Local Buckling	Crippling	Crippling	Crippling
1.5	0.125	Crippling	Crippling	Crippling	Crippling	Crippling
0	0	Crippling	Crippling	Crippling	Crippling	Crippling

7.3 EMPIRICAL RELATIONSHIPS FOR BEARING CAPACITY

Two different empirical relationships are developed to determine the residual strength of the steel plate girder for the cases of stiffener damage only and the stiffener damage in combined with the web damage.

7.3.1 Relationships for Bearing Capacity with Stiffener Damage

The ultimate bearing capacity of the plate girder end with stiffener damage can be calculated by the following proposed formula given in equation (7.2)

$$\frac{P_{Ult.}}{P_{Hult.}} = \left[1 + \frac{(1-R_{t_{min}})^b}{a + (1-R_{t_{min}})^b} \right] \quad (7.2)$$

R_{min} is the residual thickness ratio and defined in the equation (7.3)

Variables “ a ” and “ b ” are proportional to the damage height of the stiffener and can be calculated from the equation (7.4) & (7.5).

$$R_{t_{\min}} = \frac{t_{\min}}{t_0} \quad (7.3)$$

$$a = 2.25 \cdot R_d^{-0.46} \quad (7.4)$$

$$b = 4.95 \cdot R_d^{-0.37} \quad (7.5)$$

In equation (3) & (4) “ R_d ” is the Damage height as a percentage of the girder height and can be calculated as following in eqn. (7.6)

$$R_d = \frac{D_h}{d} \times 100 \quad (7.6)$$

D_h = height of the damage

d = depth of the plate girder

t_{\min} = minimum thickness of the plate within the damage portion

t_0 = original thickness of the Plate or stiffener

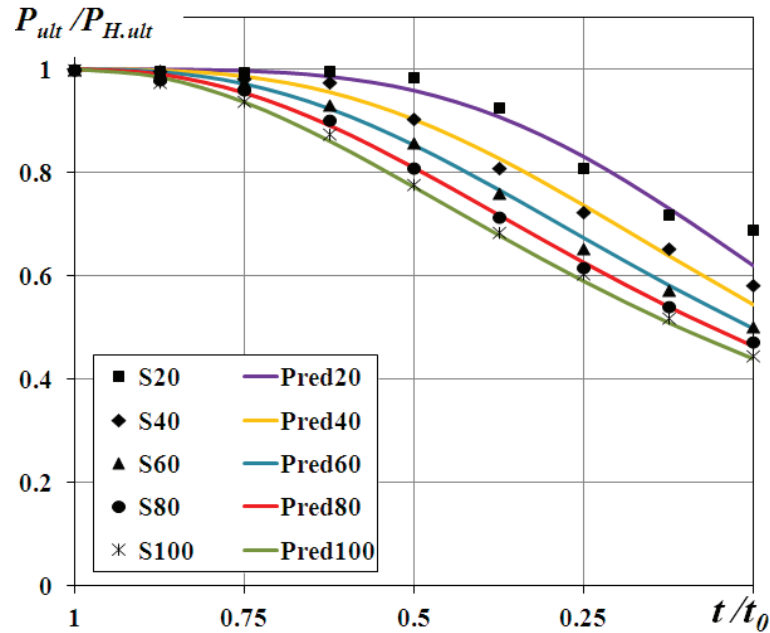
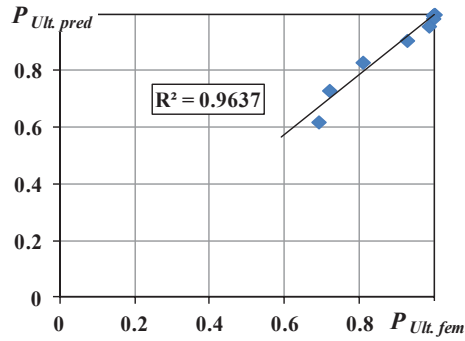
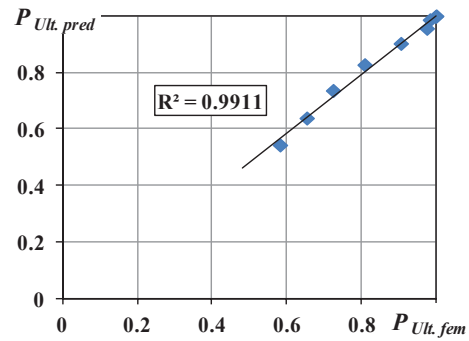


Figure 7.2: Comparison of ultimate shear capacities determined analytically and by empirical formula with stiffener damage

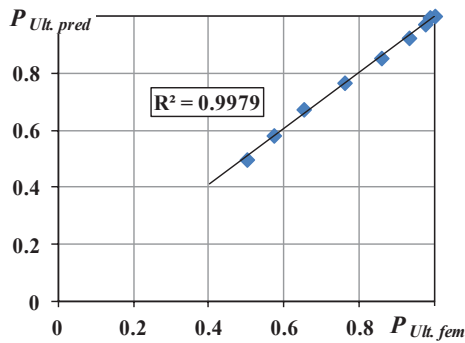
Figure 7.2 shows the comparison of the ultimate capacities determined analytically through FE procedure and calculated through the proposed empirical formula. Further, the correlation of analytical and calculated ultimate bearing capacities of the plate girder for different damage heights presented in Figure 7.3 depicts the good agreement between the analytical results and values calculated by the proposed empirical relationship.



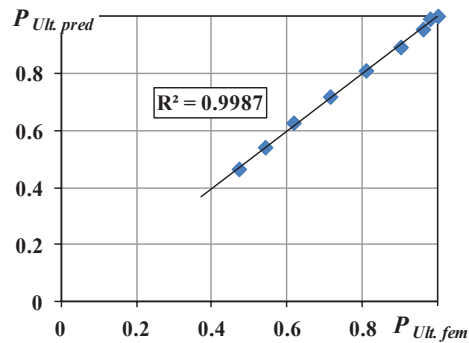
(a) Damage height = 20 mm (1.8%)



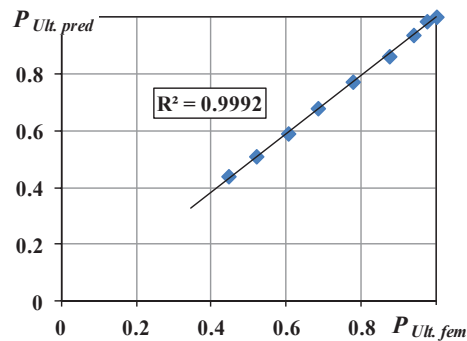
(b) Damage height = 40 mm (3.6%)



(c) Damage height = 60 mm (5.4%)



(d) Damage height = 80 mm (7.2%)



(e) Damage height = 100 mm (9%)

Figure 7.3: Correlation between evaluated and predicted capacities for different damage heights with stiffener damage

7.3.2 Relationships for Bearing Capacity with Stiffener plus Web Damage

The equation for ultimate bearing capacity of the plate girder end with stiffener plus web damage can also be calculated by same formula given in equation (7.2). However, the relationships to calculate the variable “ a ” and “ b ” are different as given in equation (7.7) & (7.8). The analytical results given in Table 5.5 indicate that stiffener damage combined with exterior web damage (damage group WES) and interior web damage (damage group WIS) demonstrate the similar trend of loss in their ultimate capacities with increase of the damage. Moreover, the analytical results of stiffener damage along with the web damage on the both side (damage group BWS) has a little difference from the damage group of WES and IWS and also rarely observed from the field therefore, coefficients “ a ” and “ b ” given in equation (7.7) and (7.8) can be used for any web damage case along with the stiffener damage.

The comparison of the ultimate capacities determined analytically through FE procedure and calculated through the proposed empirical formula is shown in Figure 7.4. Further, the correlation of analytical and calculated ultimate bearing capacities of the plate girder with stiffener damage along with the web damage for different damage heights are presented in Figure 7.5.

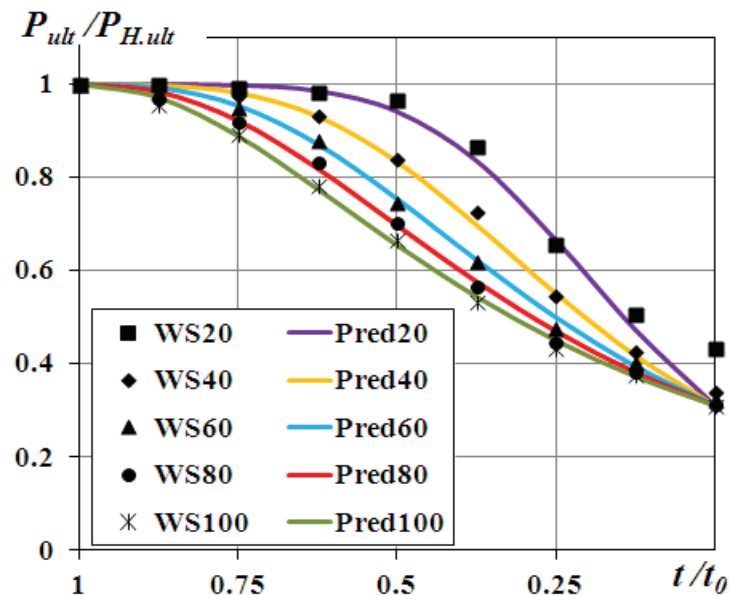
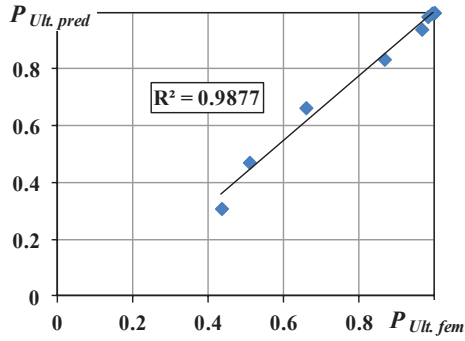


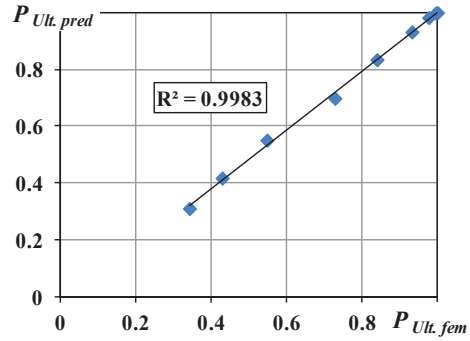
Figure 7.4: Comparison of ultimate bearing capacities determined analytically and by empirical formula with stiffener plus web damage

$$a = 0.45 \tag{7.7}$$

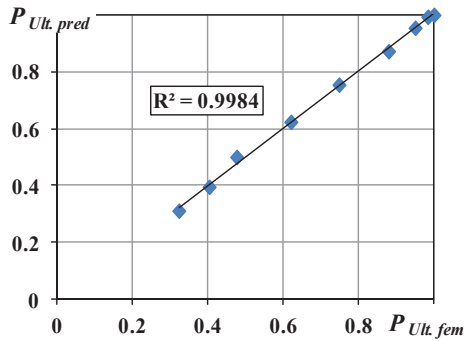
$$b = 7.65 \cdot R_d^{-0.56} \tag{7.8}$$



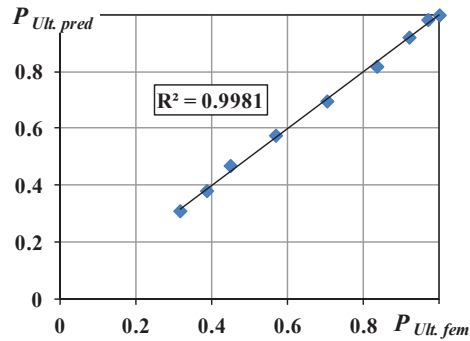
(a) Damage height = 20 mm (1.8%)



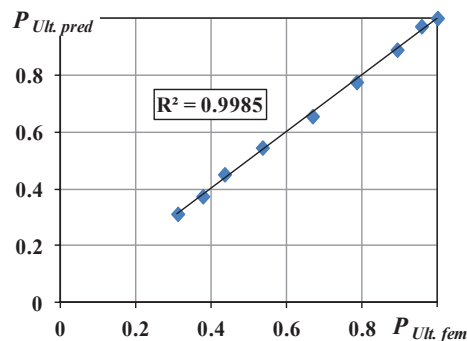
(b) Damage height = 40 mm (3.6%)



(c) Damage height = 60 mm (5.4%)



(d) Damage height = 80 mm (7.2%)



(e) Damage height = 100 mm (9%)

Figure 7.5: Correlation between analytically evaluated and predicted capacities for different damage heights with stiffener plus web damage

7.4 EMPIRICAL RELATIONSHIPS FOR SHEAR CAPACITY

The analytical results presented in Table 6.3 regarding the residual ultimate shear capacity of the steel plate girder with different corrosion damage nearby bearing revealed that the any loss of material from the stiffener and adjacent web less than the 50% has no effect on the ultimate and post buckling shear strength. And loss of the material more than 50% from the stiffener and adjacent web decreases the ultimate shear capacity linearly.

7.4.1 Relationships for Shear Capacity with Stiffener Damage

To estimate the residual shear capacity of the plate girder affected by the local stiffener damage a linear relationship as given in equation (7.9) is developed. The value of “ R_{avg} ” is mentioned in equation (7.10). The comparison of ultimate shear capacity calculated analytical through FE analysis and estimated from the empirical relationship given in (7.9) are illustrated in Figure 7.6.

$$\frac{P_{Ult.}}{P_{Hult.}} = 1.55 \cdot R_{t.avg} - \frac{R_d}{83} + 0.375 \quad (7.9)$$

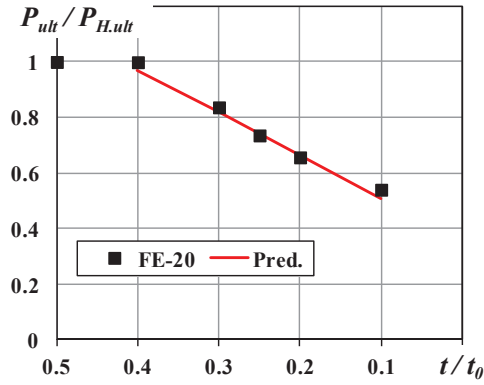
$$R_{avg} = \frac{t_{avg}}{t_0} \quad (7.10)$$

The notations used in equation (7.9) & (7.10) are defined as following and value of the R_d has already be defined equation (7.6).

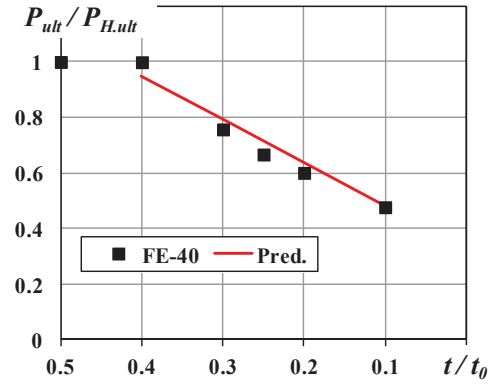
R_{avg} = Average residual thickness ratio

t_{avg} = average residual thickness within the damage region

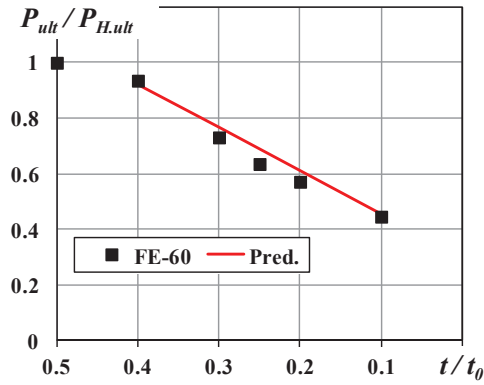
t_0 = Original plate thickness



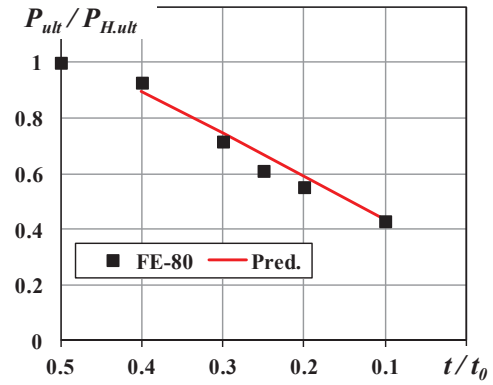
(a) Damage height = 20 mm (2%)



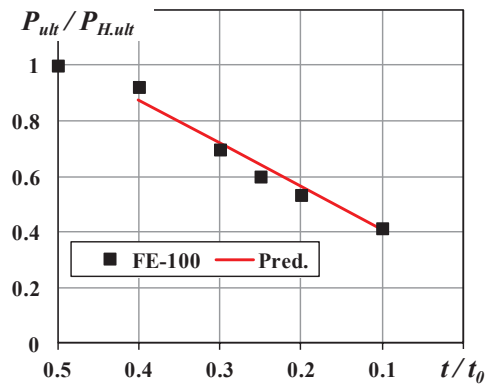
(b) Damage height = 40 mm (4%)



(c) Damage height = 60 mm (6%)



(d) Damage height = 80 mm (8%)



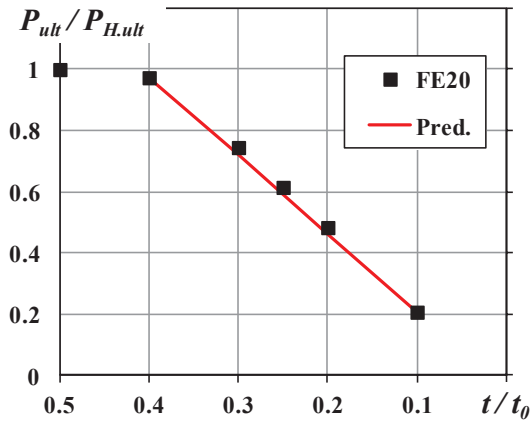
(e) Damage height = 100 mm (10%)

Figure 7.6: Comparison of ultimate shear capacities determined analytically and by empirical formula with stiffener damage

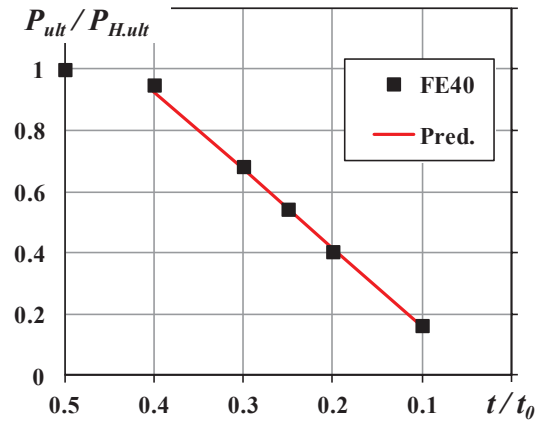
7.4.2 Relationship for Shear Capacity with Stiffener plus Web Damage

For a conservative estimation the relationship given in equation (7.11) can be utilized to calculate the shear capacity of the steel plate girder affected by the stiffener damage plus the web damage.

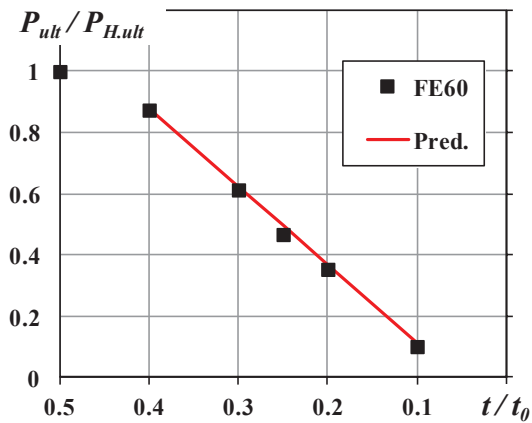
$$\frac{P_{Ult.}}{P_{H.ult.}} = 2.55 \cdot R_{avg} - \frac{R_d}{42.5} \quad (7.11)$$



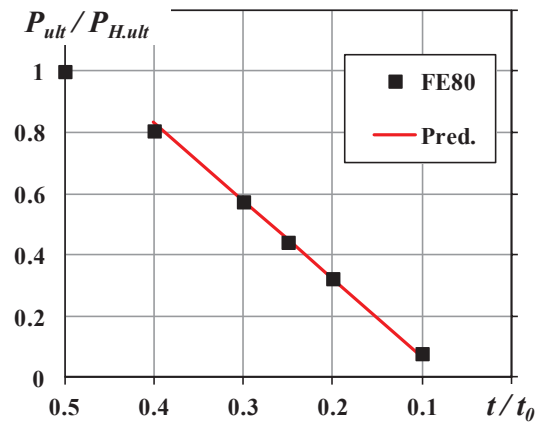
(a) Damage height = 20 mm (2%)



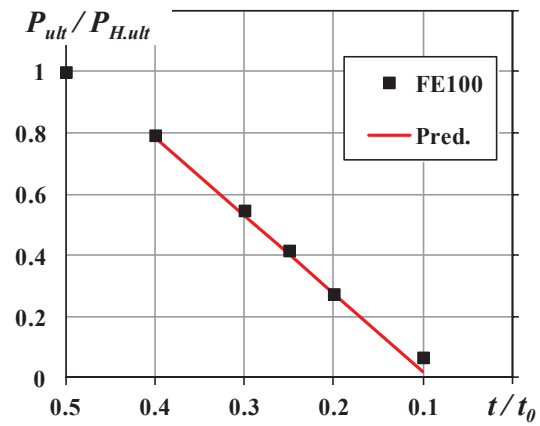
(b) Damage height = 40 mm (4%)



(c) Damage height = 60 mm (6%)



(d) Damage height = 80 mm (8%)



(e) Damage height = 100 mm (10%)

Figure 7.7: Comparison of ultimate shear capacities determined analytically and by empirical formula with stiffener plus web damage

CONCLUSIONS AND FUTURE RECOMMENDATIONS

8.1 CONCLUSIONS AND SUMMARY

On the basis of experimental and analytical study conducted on the corroded plate girder end the following conclusions are established.

1. Corrosion damages at plate girder ends nearby bearing stiffener are more frequent. Normally, the maximum damage height reported in the field inspection surveys is around 8% of the damage height and usually the critically corrosion damaged area at the inner panel adjacent to the bearing stiffener is equal to the free web end which is normally 100 to 200mm in length.
2. A simple Rectangular Shaped corrosion damage with Minimum Residual Thickness can be utilized in finite element simulation to evaluate the bearing capacity of plate girder ends
3. For the time and cost effective analysis, shell element formulation can be adopted to estimate the ultimate capacity of corroded plate girder.
4. The deformed shape of the plate girder end under bearing loading in the experimental test revealed that partially fixed nature of the bearing stiffener strut which is in consistent with the value $K = 0.7$, effective length factor value used in AASHTO. Thus, the value of effective length factor (K) 0.5 in Japanese Code of High Bridges seems to be much conservative.
5. For the case of very small local corrosion damage, local plastic constraint effect provides some extra resistance against the deformation of the material which contributes a little increase in the ultimate capacity after the buckling.

6. Any significant damage or complete loss of bearing stiffener may cause the crippling/Crushing failure which may further raise the stability problem to overall structure.
7. Web damage alone does not affect the ultimate bearing capacity significantly but it reduced the bearing capacity remarkably when combined with stiffener damage.
8. Local corrosion damage at bearing becomes more sensitive to shear loading where residual thickness $< 50\%$, as girder end subjected to the compression and in plane forces simultaneously.

8.2 FUTURE RECOMMENDATION

The present study discusses the effect of the local corrosion damage at the plate girder ends on its compression and shear behaviour. However, for the future extension of the study the following recommendations are suggested.

1. In the currents study load carrying and deformation characteristics of only a single steel plate girder affected by local corrosion damage are investigated. Thus, a detail study is required to evaluate the effect of local deformation of one girder specimen on the overall stability of bridge structures.
2. The research work can also be extended to study the various suitable retrofitting and repairing techniques to increase the service life of the bridge structure.
3. It is also recommended to study the effect of the fatigue problem in conjunction with the corrosion.

REFERENCES

- AASHTO. LRFD Bridge design specifications, 4th ed. (2007). *American Association of State Highway and Transportation Officials*. Washington (DC) USA.
- Albrecht, P., and Naemi, A. H. (1984). "Performance of weathering steel in bridges." Report 72, National Cooperative Highway Research. Program, Transp. Res. Board, Washington, D.C.
- Alinia, M. M., Shakiba, M., and Habashi, H.: Shear Failure Characteristic of Steel Plate girders, *Thin Walled Structures*, 47, 2009, pp. 1498-1506.
- ANSI/AASHTO/AWS D1.5, (2008). "Bridge welding code." *American Association of State Highway and Transportation Officials and American Welding Society*, Washington (DC), USA.
- Chatterjee, S., (2003). "The Design of Modern Steel Bridges, 2nd Edition." *Blackwell Science UK*, ISBN 0-632-05511-1.
- Choi, B.H., Hwanga, M., Yoona, T., and Yoo, C.H. (2009). "Experimental study of inelastic buckling strength and stiffness requirements for longitudinally stiffened panels." *Engineering Structures*, 31, pp. 1141_1153.
- Committee of Initial Deformation Measurement (IDM). (1980). "Statistical study on the initial deformations and the ultimate strengths of steel bridge members." *JSSC Steel Construction Engineering (Japanese Society of Steel Construction)*, 16(170), pp. 10-43.
- Committee on Marine Bridges and Steel bridges (2009) "Major damages on highway bridges: recent cases", Japan.
- Curve fitting best practice,
<http://www.excelcurvefitting.com/pdfs/Curve%20Fitting%20Best%20Practice%20Part%203.pdf>
- Dunbar, T.E., Pegg, N., Taheric, F., and Jianga, L. (2004). "A computational investigation of the effects of localized corrosion on plates and stiffened panels." *Marine Structures*, 17, pp. 385–402.
- Fukumoto., Y, (1995) "Survey Reports on Safety of Steel Structures", *Committee of Steel Structures*. JSCE, Tokyo, Japan.

-
- Ghavami, K., and Khedmati, M.R. (2006). “Numerical and experimental investigations on the compression behaviour of stiffened plates.” *Journal of constructional Steel Research*, 62, pp. 1087–1100.
- Khurram, N., Sasaki, E., Kihira, H., Katsuchi, H., and Yamada, H. (2012). “Analytical Demonstrations to Assess Residual Bearing Capacities of Steel Plate Girder Ends with Stiffeners Damaged By Corrosion.” *Structure and Infrastructure Engineering*, (ID: 697904 DOI:10.1080/15732479.2012.697904)
- Liu, C., Miyashita, T., and Nagai, M. (2011) “Analytical study on Shear Capacity of Steel I-Girder with Local Corrosions nearby Girder Ends”, *Journal of Structural Engineering*, JSCE, 57-A, pp. 715-723.
- Hibbit, Karlson, & Sorenson Inc. (HKS), (2007). ABAQUS user’s manual 6.8, Pawtucket, R.I.
- Hoglund, T. (1997). “Shear Buckling Resistance of Steel and Aluminium Plate Girders.” *Thin-Walled Structures*, Vol. 29, Nos. 1-4, pp. 13 30
- Hung, V.T., Nagaswa, H., Sasaki, E., Ichikawa, A., and Natori, T. (2002). “An experimental and analytical study on bearing capacity of supporting point in corroded steel bridges” *Journal of Structure Engineering*, JSCE No. 710/I-60, pp. 141-151.
- Kayser, J.R., and Nowak, A.S. (1989). “Reliability of corroded steel girder bridges.” *Structural Safety*, 6, pp. 53-63.
- Kayser, J.R. (1988). “The Effects of Corrosion on the Reliability of Steel Girder Bridges.” *Ph.D. Thesis*, Dept. of Civil Eng., University of Michigan, USA.
- Kitada, T. (2006). “Considerations on recent trends in, and future prospects of, steel bridge construction in Japan”, *Journal of Constructional Steel Research*, Vol.62, pp.1192-1198.
- Komp, M. E. (1987). "Atmospheric corrosion ratings of weathering steels—Calculation and significance." *Mater. Perf.* 26(7), pp. 42-44.
- Maquoi, R., and Skaloud, M. (2000). “Stability of Plates and Plated Structures General Report.” *Journal of Constructional Steel Research*, 55, pp. 45-68.
- Matteus, A.F., and Witz, J.A. (2001). “A parametric study of post-buckling behaviour of steel plates” *Engineering Structures*, 23, pp. 172-185
- Ministry of Communications (Railway wing), “Bridge Rules.” Government of the Pakistan.
- Ministry of Communications (Railway wing), “Steel bridge Code.” Government of the Pakistan, Railway Code of Practice for the Design of Steel or wrought Iron Bridges Carrying Rail, Road or Pedestrian Traffic.

-
- Murakoshi, J. (2006). "Maintenance of steel bridges." *The 15th Conference on Public work & Development in Asia*, National Institute for Land & Infrastructure Management, MLIT, Aichi, Japan
- Nakayama, T. Kimura, M, Ishikawa, T, and Matsui, S. (2006). "Shear strength of steel girders with corrosion hole", *Journal of structural engineering*, Vol.52A, pp.49-56, Japan Society of Civil Engineers, (in Japanese).
- Natori, T. Nishikawa, K. Murakoshi, J. and Ohno, T. (2001). "Study on Characteristics of Corrosion Damages in Steel Bridge Members", *Journal of Structural Mechanics and Earthquake Engineering*, Vol. 668, No. 54, pp. 299- 311(in Japanese).
- Ok, D., Pu, Y., and Incecik, A. (2007). "Computation of ultimate strength of locally corroded unstiffened plates under uniaxial compression." *Marine Structures*, 20, pp. 100–114.
- Paik, J.K., and Kim, B.J. (2002) "Ultimate strength formulation for the stiffened panels under combined axial load, in-plan bending and lateral pressure: a benchmark study." *Thin-Walled Structures*, 40, pp. 44-83.
- Rahgozar, R. (2009). "Remaining capacity assessment of corrosion damages beams using minimum curves." *Journal of Construction Steel Research*, 65, pp. 299-307.
- Real, E., Mirambell, E., and Estrada, I. (2007). "Shear Response of Stainless Steel Plate Girders", *Engineering Structure*, 29. Pp. 1626-1640.
- Rules for developing a model <http://mathbits.com/MathBits/TISection/Statistics2/Rules.htm>
- Ship Structure Committee, (1997), "Strength and Stability of Stiffened Plate Components." SSC-399.
- Smith, C.S., Davidson, P.C., and Champman, J.C.D. (1988). "Strength and stiffness of ships plating under in-plane compression and tension." *RINA Trans*, 130. pp. 277-296.
- Sommer, A.M., Nowak, A.S., and Christenson, P.T. (1993). "Probability-Based Bridge Inspection Strategy." *Journal of Structural Engineering*, ASCE, 119(12), pp. 3520-3536.
- Specifications for highway bridges, Part-II Steel bridges Steel Bridges, 2002, Japan Road Association
- Tamagawa, S., and Kim, Y.C. (2010). "Effect of welding residual stress on compressive behavior and ultimate strengths of corroded plate." *International Journal of Steel Structures*, 10(2), pp. 147-155.
- Tamakoshi, T., Yoshida, Y., Sakai, Y., and Fukunaga, S. (2006). "Analysis of damage occurring in steel plate girder bridges on national roads in Japan." *22th US-Japan Bridge Engineering Workshop*, Seattle, Washington, USA

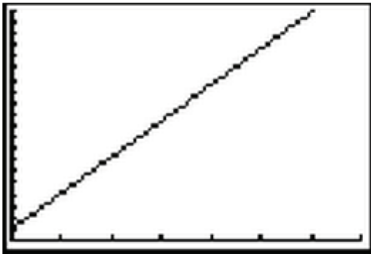
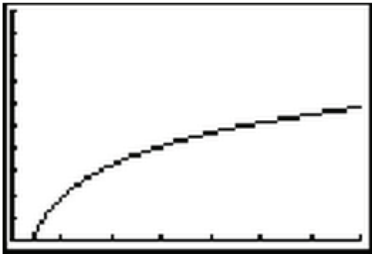
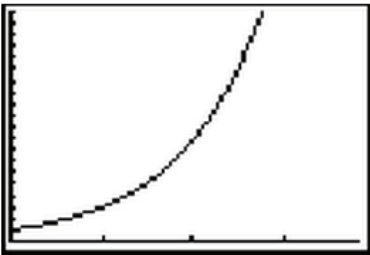
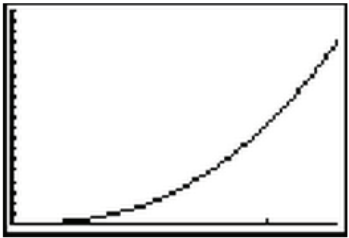
- Tamakoshi, T., Nakasu, K., Ishio, M., Takeda, T., and Suizu, N.: Research on Local Corrosion of Highway Steel Bridges. Report No. 294, National Institute of Land and Infra Structure Management, Ministry of Land, Infrastructure and Transport, JAPAN, 2006.
- Usami., T. (2005) “Buckling Design Guideline”, *Committee of Steel Structures* , JSCE, Tokyo Japan
- Van de Lindt, J.W., and Ahlborn, T.M. (2005). “Development of steel beam end deterioration guidelines.” *MDOT Research Report RC-1454*, Michigan Technology University. USA.

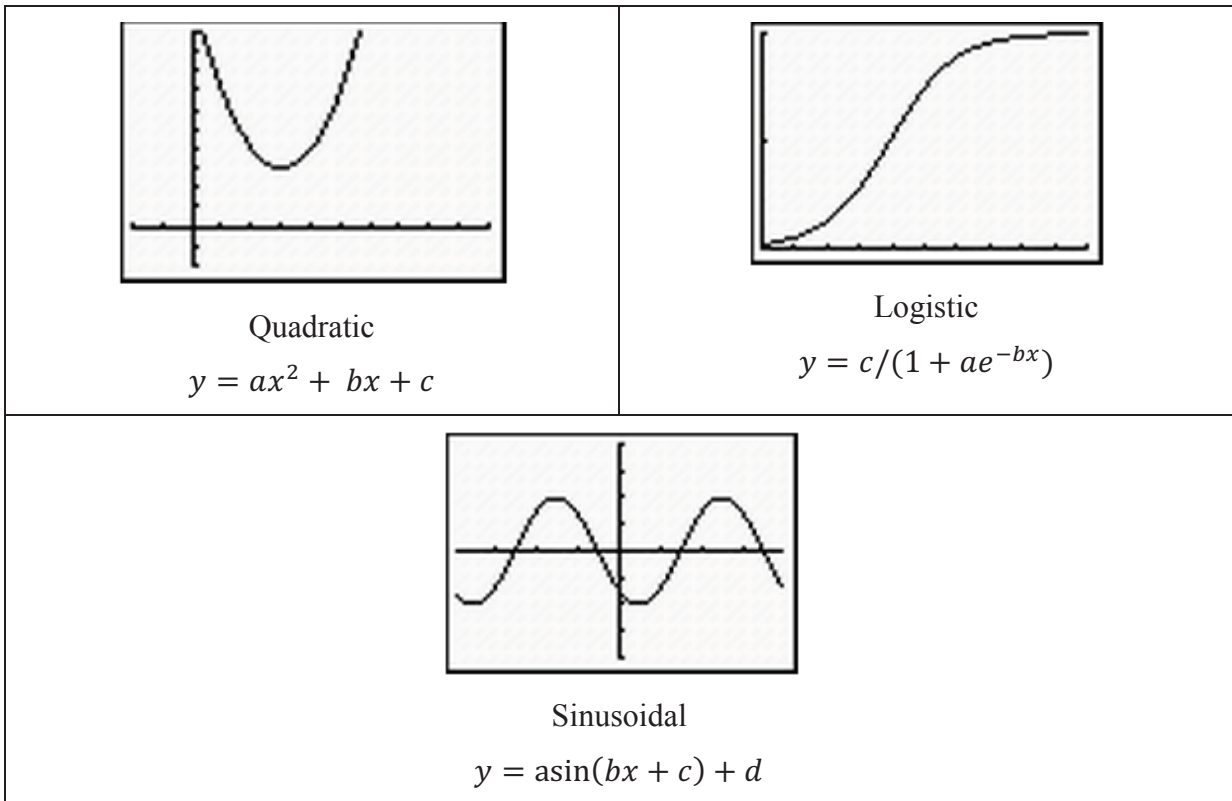
RULES FOR THE REGRESSION MODEL

A.1 SELECTION OF THE MODEL

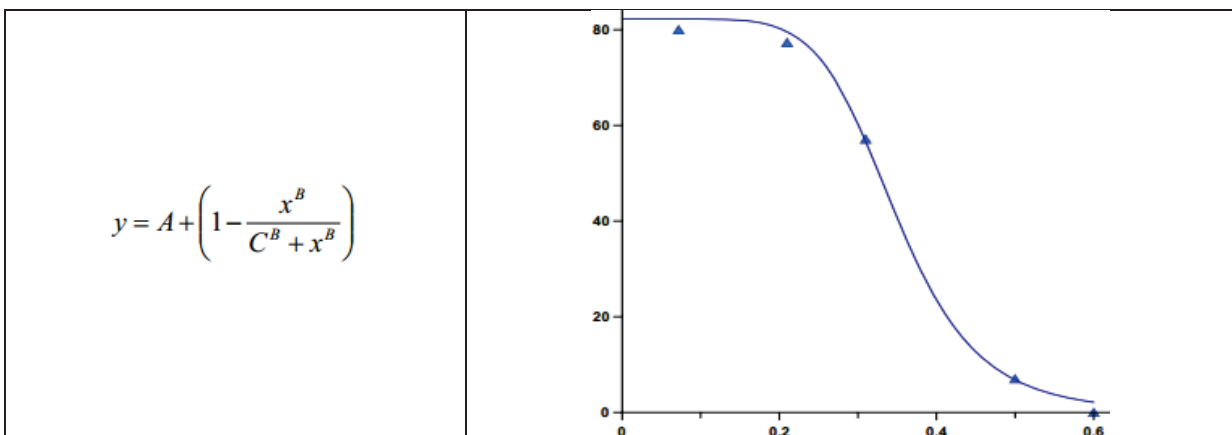
Prepare a scatter plot on excel and examine the graph. Look to see which regression model appears to best represent the scatter plot graph and determine the general shapes of the regression models. When trying to select a model, choose only those models that appear to fit the observed points reasonably well. Some common types of the plots and their governing equations are given in following sub sections

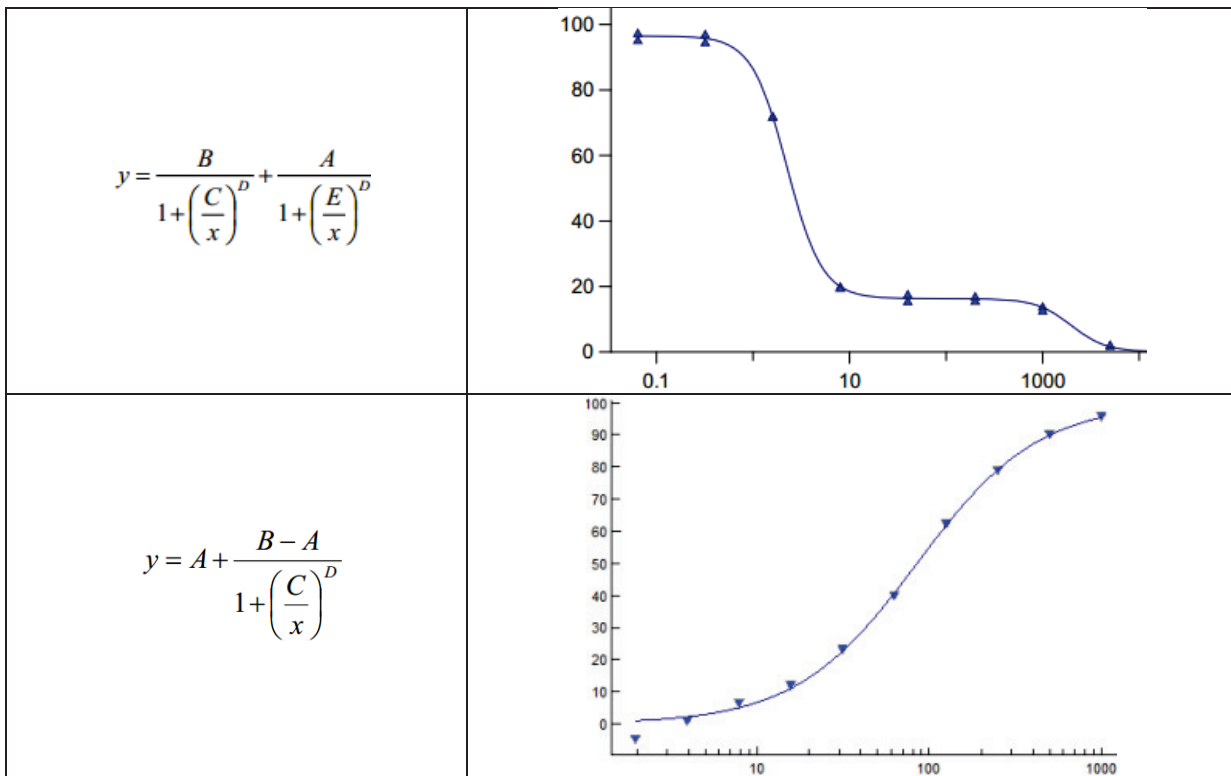
A.1.1 Types of the Basic Model

 <p style="text-align: center;">Linear $y = bx$</p>	 <p style="text-align: center;">Logarithmic $y = a + b.lnx$</p>
 <p style="text-align: center;">Exponential $y = ab^x$</p>	 <p style="text-align: center;">Power $y = ax^b$</p>



A.1.2 Types of the Logistic Model





A.2 CALCULATION OF CORRELATION COEFFICIENT

The correlation coefficient “R” exhibits the strength and direction of relationship between two variables. A higher value of |R| indicates a “good fit”

A.3 CALCULATION OF COEFFICIENT OF DETERMINATION

The coefficient of determination represents the percent of the data that is the closest to the line of best fit. For example, if $R = 0.922$, then $R^2 = 0.850$, which means that 85% of the total variation in y can be explained by the linear relationship between x and y (as described by the regression equation). The other 15% of the total variation in y remains unexplained.

A.4 EXAMINATION OF RESIDUAL

Examine the graph of the residuals, which depicts the measure of the signed distances between the actual data values and the outputs predicted by the model. A good model has residuals that are near zero and are randomly distributed.